Development of Environmentally Responsive Multifunctional Microgel Particles:

Synthesis, Characterization and Applications

by

Haobo Chen

A Dissertation Presented in Partial Fulfillment
of the Requirements for the Degree
Doctor of Philosophy

Approved October 2015 by the
Graduate Supervisory Committee:

Lenore L. Dai, Chair
Kangping Chen
Erica Forzani
Mary Laura Lind
Bin Mu

ARIZONA STATE UNIVERSITY

December 2015

ABSTRACT

Environmentally responsive microgels comprised of cross-linked polymer latex particles have drawn significant attention due to their intrinsic ability to rapidly change volume through various external stimuli such as pH, temperature, osmotic pressure, or electric and magnetic fields. Therefore, microgel dispersions have become a highly active topic of research as model colloids and for their potential in interdisciplinary scientific fields and applications such as enhanced oil recovery, biomaterials and catalysis. This work focuses on synthesis and characterization of environmentally responsive microgels and their composites, and encompasses methods of utilizing microgel systems as vehicles for the adsorption, retention, and targeted delivery of active species. Furthermore, ionic liquid (IL)-in-water emulsions are shown to be stabilized via responsive microgels.

This thesis first reports on the fundamental aspects of synthesis, functionalization, and characteristic properties of multifunctional environmentally responsive microgels derived from poly(N-isopropylacrylamide) (PNIPAm) and other functional comonomers. In particular, the uptake and release of active chemical species such as rheology modifiers into and from these ionic microgels is demonstrated. Moreover, a facile tunable method for the formation of organic-inorganic composites with Fe_3O_4-NPs adsorbed and embedded within ionic microgel particles is explored.

Additionally, the development of zwitterionic microgels (ZI-MG) is presented. These aqueous ZI-MG dispersions exhibit reversible parabolic swelling as a function of pH and display a minimum hydrodynamic diameter at a tunable isoelectric point (IEP). This study also elucidates the controlled uptake and release of surfactants from these particle systems. The extent of surfactant loading and the ensuing relative

swelling/deswelling behaviors within the colloidal polymer networks are explained in terms of their binding interactions.

In another component of this thesis, the versatility of fluorescently labeled composite microgel particles as stabilizers for IL-in-water Pickering emulsions was investigated. When the prepared particles form monolayers and equilibrate at the liquid-liquid interface on fully covered emulsion droplets, the colloidal lattice organization re-orders itself depending on the surface charge of these particles. Finally, it is shown that the spontaneously formed and densely packed layer of microgel particles can be employed for extraction applications, as the interface remains permeable to small active species.

ACKNOWLEDGMENTS

First and foremost I want to express my greatest gratitude to my advisor, Dr. Lenore L. Dai. I appreciate all her patience, flexibility and guidance to make my doctoral experience productive and stimulating. She has been a tremendous mentor for me throughout the course of my research. The joy and enthusiasm she has for teaching and research was motivational and contagious for me. She has taught me that research is not only for the attainment of new knowledge but also a test of one's own capability to learn. My profound gratitude also extends to all my doctoral committee members, Dr. Kangping Chen, Dr. Erica Forzani, Dr. Mary Laura Lind, and Dr. Bin Mu for providing me with their generous time and support to better my work.

Every result described in this thesis was accomplished with the help and support of fellow lab-mates and collaborators. I am grateful for having had the opportunity to work with a team of wonderful colleagues throughout this journey. In no particular order, these are Miranda Ngan, Wei Gao, Elizabeth Nofen, Prithwish Chatterjee, and Dr. Jin Zou. Special thanks to Morgan Kelley for her contributions to various parts of my research. Furthermore, I would like to acknowledge Dr. Jun Wu and Dr. Mingmeng Zhang for their help with TEM imaging, Dr. Konrad Rykaczewski for his expertise in Cyro-SEM microscopy. In addition, I would also like to acknowledge and thank Stella Nickerson and Mengbing Liang for their collaboration on the NASA MET project. Sincere thanks are given to our collaborators Dr. Jeffery Yarger and Chengchen Guo for their help with NMR analyses.

Moreover, I am grateful for financial support provided by The Gulf of Mexico Research Initiative (GoMRI), specifically from The Science and Technology of

Dispersants as Relevant to Deep Sea Oil Releases Consortium led by Dr. Vijay T. John. I am also appreciative for financial support provided by the National Aeronautics and Space Administration (NASA) through the award NASA-PICASSO-NNX14AI41G. Furthermore, I would like to acknowledge the use of facilities within the Magnetic Resonance Research Center (MRRC) and LeRoy Eyring Center for Solid State Science at Arizona State University.

My time at ASU was made enjoyable in large part due to the many friends that became an integral part of my life. In many ways, they have contributed immensely to my personal and professional growth. I am grateful for time spent with Shengke Zhang, Dr. Chengwei Wang, Weixiao Li, Benjamin Liu, Nathan Cao, Dr. Qiushi Fu, Jingxian Mao, Rouhan Zhang, Ting Yang, Qian Cheng at the SRC playing basketball, swimming, golfing, skiing or dining on campus, and for the many college buddies who visited me throughout the pursuit of my doctoral degree. A very special acknowledgement goes to my girlfriend, Krystal Shi, who has offered her companionship, love, and inspirations throughout my doctoral journey. I am so lucky to have met you here.

Finally, I would like to dedicate this thesis to my parents, Jianhui Wu and Dr. Baowei Chen, who instilled in me the importance of education from an early age. I am forever grateful for their unwavering support, encouragement, and unconditional love which has sustained me throughout my life. They have been constant cheerleaders through every academic and personal endeavor in my life. Thanks mom and dad for always believing in me and for teaching me to work diligently for the things that I aspire to achieve.

TABLE OF CONTENTS

Page

LIST OF TABLES vii
LIST OF FIGURES viii
CHAPTER
1. INTRODUCTION 1
2. BACKGROUND & MOTIVATIONS 6
2.1 Defining Microgels 6
2.2 Microgel Dispersion Preparation 8
2.3 Stimuli-Responsive Microgels 11
2.3.1 Fundamental Interactions 14
2.3.2 Responsive Microgel Particle Swelling: Experiments 18
2.4 Particle Assembly at Liquid-Liquid Interfaces 22
2.4.1 Pickering Emulsions 22
2.4.2 Packing at the Interface 24
2.4.3 Pickering Emulsions Stabilized via Microgels 25
2.4.4 Responsive Ionic Liquid Emulsions 31
2.5 Motivations and Applications Involving Multifunctional Microgels 33
2.5.1 Adsorption and Release of Active Species 33
2.5.2 Structure of Colloidal Lattices of Microgels at the IL-Water Interfaces 38
3. METHODOLGY 41
3.1 Materials 41
3.2 Particle Synthesis 42
3.2.1 Ionic Microgels 42
3.2.2 Zwitterionic Microgels 42
3.2.3 Composite Microgels 43
3.3 Uptake and Release of Active Species 45
3.3.1 Lecithin Uptake and Release within Ionic Microgel Particles 45
3.3.2 Uptake of Fe_3O_4-NPs with Ionic Microgel Particles 45
3.3.3 Surfactant Adsorption within Zwitterionic Microgel Dispersions 46

CHAPTER Page
3.4 IL-in-Water Emulsion Preparation 46
3.5 Characterization 47
3.5.1 Physical Particle Characterization 47
3.5.2 Spectroscopy Characterization 47
3.5.3 Interfacial Colloidal Characterization 48
4. RESULTS AND DISCUSSION 50
4.1 Development of Multifunctional Microgels 50
4.1.1 Synthesis and Characterization of Ionic Microgels 50
4.1.2 Synthesis and Characterization of Zwitterionic Microgels 56
4.1.3 Synthesis and Characterization of Composite Microgels 63
4.2 Uptake and Release of Active Species into and from Multifunctional Microgels . 65
4.2.1 Ionic Microgels 65
4.2.2 Zwitterionic Microgel Particles 72
4.3 Structure of Colloidal Lattices at IL-in-Water Interfaces 83
5. SUMMARY AND FUTURE WORK 92
5.1 Summary 92
5.2 Future Work 94
5.2.1 Impact of Microgel Cross-linking Density on Their Ability to Stabilize Pickering Emulsions 94
5.2.2 Magnetically Responsive Pickering Emulsions 97
REFERENCES 101
APPENDIX
A A COMBINED EXPERIMENTAL AND MOLECULAR DYNAMICS STUDY OF IODIDE-BASED IONIC LIQUID 124

LIST OF TABLES

Table Page

3.1 Monomer Compositions Used in the Preparation of Zwitterionic Microgel (ZI-MG) Particles. 43

4.1 The Avg. Hydrodynamic Size and Polydispersity Index (PDI) of Poly(NIPAm-*co*-DMAPMA) Microparticles at Different Temperatures Determined by DLS at pH 9. 51

4.2 Average Hydrodynamic Size and Polydispersity Index (PDI) of ZI-MG Microparticles at Various Temperatures Determined via DLS at the Isoelectric Point (IEP). 60

A1 Compositions of Simulation Systems. 129

A2 Simulated vs. Experimental Mixture Density at 300 K. 132

LIST OF FIGURES

Figure Page

2.1 Chemical Structures of the Monomers Widely Applied to Synthesis Stimuli-Responsive Microgel Particles. The Monomers are (a) Methylmethacrylate, (b) Methacrylic Acid, (c) Styrene, (d) Divinylbenzene, (e) Acrylics Acid, (f) N-Isopropylacrylamide, (g) N-N'-Methylene Bisacrylamide and (h) Ethyleneglycol Dimethacrylate. Adapted from [28]. 8

2.2 The Synthesis Mechanism of Microgel Dispersions Utilizing SFEP. Please Note, the Closed Circles Illustrate the Free-Radical Sites and the M and X^+ are the Vinyl Monomer and the Thermal Decomposition Product from the Cationic Initiator, Correspondingly. 9

2.3 Shows a Representation of the Generic PNIPAm-Based Microgel at Three Distance Scales. Adapted from [52]. 11

2.4 Shows a Snapshot of the Thermo-Induced Coil-to-Globule Transition of PNIPAm Polymer Chains. Adapted from [57]. 12

2.5 Illustrate the Schematic Depiction of the Thermally Induced Phase Transition in Linear PNIPAm and Gel Systems. Adapted from [31]..... 13

2.6 Illustrates a Schematic Representation of the Four Fundamental Interactions Acting in Various Microgel-Solvent Systems: (a) Hydrophobic, (b) Van der Waals, (c) Ionic/Electrostatic and (d) Hydrogen-Bonding Interactions. Adapted from [1]..... 14

2.7 Temperature Dependence of the Average Hydrodynamic Radii of Microgel Systems with Various Mol% of AAc Contents: (a) 0%; (b) 5%; (c) 10% and (d) 20%. Adapted from [3]..... 19

2.8 Lists Many of the Widely Used Monofunctional Monomers that are Anionic or Cationic. 20

2.9 Depicts the Interaction of Anionic Microgels with Oppositely Charged Cytochrome C (CytC). Adapted from [78]..... 21

2.10 Variation of ΔG of a Particle at the Planar Oil-Water Interface at Room Temperature with Respect to (a) Particle Radius and (b) Contact Angle. Adapted from [87] and [86], Respectively. 23

Figure Page

2.11 The Stabilizing Efficiency of the Prepared Microgel Particles for Octanol-in-Water Emulsions as a Function of pH and Temperature. Key: (Squares) Stable; (Circles) Unstable; and (Diamonds) Phase Separation. Adapted from [91]. 26

2.12 Graphic Representation of pH-Induced De-mulsification using the $P_4VP{-}SiO_2$ Particles as a "Pickering" Emulsifier. Oil-in-Water Emulsions were Prepared Using an Aqueous Dispersion of $P_4VP{-}SiO_2$ Particles: (a) After Centrifugal Purification; (b) Prior to Any Centrifugal Purification. Please Note Silica Sols are Around 20 nm. Adapted from [92]..... 27

2.13 Observations of Pickering Emulsions Obtained via Optical Microscopy. Toluene-in-Water Emulsion Stabilized by PNIPAm Microgel Particles (a-c). Toluene-in-Water Emulsion Stabilized by Hairy particles (d-f). (c) and (f) are Close Up Images of the Emulsion Surfaces. Adapted from [94]..... 28

2.14 Depicts Octanol/Water Emulsions Stabilized with Synthesis Product (A), the Supernatant (B), and the Purified Microgel (C). The pH of All Emulsions is ~9. Adapted from [95]..... 29

4.1 The Temperature Dependence of the Avg. Hydrodynamic Diameter of (a) Pure PNIPAm Microgels and (b) Poly(NIPAm-*co*-DMAPMA) Microgel Particles at pH 9 Obtained via DLS. Inset: The Thermally Induced Volume Phase Transition Temperature (VPPT) is Defined as the Temperature at Which the 1st Derivative of the Avg. Hydrodynamic Diameter Versus the Temperature Curve Reaches a Minimum Value. 50

4.2 The Dependence of Poly(NIPAm-*co*-DMAPMA) Microgels: (a) Reversibility of the Avg. Hydrodynamic Diameter via DLS and (b) Electrophoretic Mobility Results Measured by ELS on pH at Room Temperature. 52

4.3 The Temperature Dependence of the Avg. Hydrodynamic Diameter of Poly(NIPAm-*co*-DMAPMA) Microgels at pH 4, 7 and 10 Obtained via DLS. Inset: Shows the VPTT of the Prepared Sample at Various pH as a Function of Temperature..... 53

Figure Page

4.4 Confocal Microscopy Images of the Avg. Hydrodynamic Diameter of Stationary Swelled Poly(NIPAm-*co*-DMAPMA) Microgels Prepared in pH 5 and 10 Solution at Room Temperature. 55

4.5 Effect of pH on the Variation in Avg. Hydrodynamic Diameter (a-b) and ζ-Potential (c-d) for ZI-MG Particles Studied at Room Temperature: (a,c) ZI-MG (0.29); (b,d) ZI-MG (0.85). Dashed Lines are Applied as Indicators to Denote Both the IEP and the Zero Point of the ζ-Potential. 57

4.6. Temperature Dependence of the Average Hydrodynamic Diameter of ZI-MG Particles with Various Compositions Measured at the pH of Their Corresponding IEP. Inset: the Thermally Induced VPTT is Defined as the Temperature Which the First Derivative of the Hydrodynamic Diameter Versus the Temperature Curve Reaches a Minimum Value. 58

4.7. Temperature Dependence of the Average Hydrodynamic Diameter of ZI-MG (0.85) Particles Measured at pH 3 and 11 Obtained via DLS. Inset: Shows the VPTT of the Prepared Sample at Different pH as a Function of Temperature. 61

4.8. SEM Images of Dried Microgel Particles on Silicon Wafers for ZI-MG Particles Prepared with Various Mole Ratios: (a) ZI-MG (0.29) and (b) ZI-MG (0.85)..... 62

4.9 Illustrates the pH Dependence of the Average Hydrodynamic Diameter of the Composite Microgel Particles in an Aqueous Dispersion at Room Temperature. Inset: Displays the pH Dependence of the Electrophoretic Mobility of the Prepared Particles. 64

4.10 Temperature Dependence of the Average Hydrodynamic Diameter of the Composite Microgel Particles Measured at pH 3 and pH 10. Leftmost Inset: Shows the SEM Image of Dried Fluorescent Core Particles Along with the Average Hydrodynamic Diameter of Those Particles as a Function of Temperature. Right Insets: the Thermally Induced VPTT is Defined as the Temperature which the First Derivative of the Mean Hydrodynamic Diameter Versus the Temperature Curve Reaches a Minimum Value. 65

Figure Page

4.11 Snapshot Images of the Supernantants Collected from Lecitihin Uptake and Release via Poly(NIPAm-*co*-DMAPMA) Microgel Particles: (a) Uptake Supernatant Obtained from the Sample Initially Prepared at pH 5 and (b) Uptake Supernantant Obtained from the Sample Initially Prepared at pH 10 and (c) Release Supernatant Obtained from the Sample Initially Prepared at pH 5 and (d) Release Supernatant Obtained from the Sample Initially Prepared at pH 10..... 66

4.12 Normalized FTIR Measurements of the Collected Supernatants From Lecithin Uptake and Release via Poly(NIPAm-*co*-DMAPMA) Microgels: (a) Sample Initially Prepared at pH 5 and (b) the Sample Initially Prepared at pH 10..... 67

4.13 Rheology Measurements of the Obtained Supernatants from Lecithin Uptake and Release via Poly(NIPAm-*co*-DMAPMA) Microgels: (a) Sample Initially Prepared at pH 5 and (b) the Sample Initially Prepared at pH 10..... 68

4.14 TEM Images of Collapsed Organic-Inorganic Composites Composed of Ionic Microgels and Fe_3O_4-NPs Prepared at Various pH and the Zeta Potentials of the Poly(NIPAm-*co*-DMAPMA) Microparticles and the Pure Fe_3O_4-NPs Both as a Function of pH. 70

4.15 TEM Images of Reversible Formation of Organic-Inorganic Composites Composed of Ionic Microgels and Fe_3O_4-NPs: (a) the Sample was Tuned from pH 3 to 7 and (b) the Sample was Tuned from pH 11 to 7..... 71

4.16 SEM Images of Collapsed Microgels: (a) Pure Poly(NIPAm-*co*-DMAPMA) Microparticles Prepared at pH 7 and (b) Organic-Inorganic Composites Prepared at pH 7 with Fe_3O_4-NPs Adsorbed and Embedded within Poly(NIPAm-*co*-DMAPMA) Microgels. 72

4.17 Avg. Hydrodynamic Diameter (a) and the Electrophoretic Mobility (b) of ZI-MG (0.85) Particles as a Function of Added DOSS Concentration at pH 3 and 11 Studied at Room Temperature. 74

4.18 Avg. Hydrodynamic Diameter as a Function of the Equilibrium DOSS Concentration with pH Alterations at Room Temperature. 76

Figure Page
4.19 Normalized ^{1}H NMR Spectra: (a) DOSS Standard and Pure ZI-MG (0.85) Particles and (b) the Collected Supernatants from DOSS Uptake and Release via ZI-MG (0.85) Microgels at pH 3 and 11. Please Note the CMC of DOSS is ~2.66 mM. ... 77
4.20 Average Hydrodynamic Size (a) and Electrophoretic Mobility (b) and Adsorbed Amount of CPyCl Surfactant onto ZI-MG (0.85) Particles (c) as a Function of Equilibrium CPyCl Concentration at pH 3 and 11 Obtained at Room Temperature.79
4.21 Adsorbed Amount of CPyCl for the ZI-MG (0.85) Particles with a Fixed Initial CPyCl Concentration of 0.412 mM and 0.825 mM as a Function of pH Obtained at Room Temperature. 81
4.22 Avg. Hydrodynamic Size of ZI-MG (0.85) with Varying pH Measured at Room Temperature. 82
4.23 The Top Row Illustrates Confocal Microscope Images of Colloidal Lattices (a-d) at Droplet Surfaces at Varying pH and Temperatures. The Insets Show the FFT of the Associated Confocal Microscope Images. The Bottom Row Shows the Constructed Voroni Diagrams of the Colloidal Lattices at the Droplet Surfaces (e-h) at Varying pH and Temperatures. In e-h, the Cyan, Magenta, Lime Green, Yellow and Blue Fills Represent, Fourfold, Fivefold, Sixfold, Sevenfold, and Eightfold Sites, Respectively; the Gray Fills Represent Incomplete Cells at the Edge of the Lattice and were Not Taken into Account During Data Analyses. 84
4.24 Cyro-SEM Images of the Interface of IL-in-Water Emulsion Droplets Coverd by Composite Microgel Particles at pH 3 (a) and pH 10 (b) After Sublimation. 86

Figure Page

4.25 Influence of pH on the Interfacial Assembly of the Composite Microgel Particles at Varying Temperatures is as Follows: Scheme Illustrates the Particle Arrangement at the Interface and the Nearest Neighboring Distance (a), Normalized Pair Correlation Function $g(r)/g(r)_{\text{First Peak}}$ at pH 3 (b) and pH 10 (c), Histograms of Nearest Neighbor Distance on the Colloidal Lattices at pH 3 (d) and pH 10 (e), the Bar Charts Represent the Distribution of Four-to-Eight-Sided Polygons in the Colloidal Lattices at pH 3 (f) and pH 10 (g). All Analysis was Derived from the Voronoi Diagrams of Twenty Different Droplets. Inset: Shows the Normalized Pair Correlation Function $g(r)/g(r)_{\text{First Peak}}$ of a Theoretical 2-D Hexagonal Packed Lattice. 88

4.26 Macroscopic Pictures of IL-in-Water and IL-in-Water Emulsions Stabilized with Composite Microgel Particles at pH 3 and pH 10 (a), Immediately After the Addition of 0.02 mM Rhodamine B (b) and Upon Pigment Diffusion into the IL (c). 3-D Stacked Confocal Microcopy Images of the Successful Diffusion of Rhodamine B into the IL-in-Water Emulsions at pH 3 (d) and pH 10 (e); the IL is Colored Red and the Composite Particles are Yellow-Green. 90

5.1 Schematic Representation of the Adsorbed Microgel Particles and the Polymer Density Profile at the Fluid Interface for (a) Large and (b) Small Gel-Particles. In a Similar Way the Effect of the Cross-Linking Density may be Schematically Drawn (c and d) as Well as the Effect of Process Parameters Such as Initial Temperature or Energy (e and f). Please Note *z* is the Fistance From the Interface. Adapted from [166]. 95

5.2 Illustrates the Temperature Effect on the Formation of Fe_3O_4-MG Hybrid Colloids. 98

5.3 Represents the Hybrid Microgel Formation Mechanism (a) for Magnetic Cluster Bigger than the Nanogels and (b) for Magnet Cluster Smaller than the Nanogels. Adapted from [222]. 100

A1 (a) Density and (b) Melting Point of Binary Water/[BMIM][I] Mixtures by Mole Fraction Water (X_1). The Vertical Line at X_1=0.5 for Each Chart is Provided for Guidance. 131

Figure Page

A2 Representative Snapshots of MD Simulation Boxes for Mole Percentages of Water Ranging From 10-90%. Each Dot is an Atom, with Yellow Representing [BMIM], Red [I], and Blue Water. 133

A3 Comparison of the Conductivity (Black Squares) and Average Viscosity (Blue Circles) of Binary Water/[BMIM][I] Mixtures by Mole Fraction Water (X_1). 134

A4 BMIM (Yellow), Iodide (Red), and Water (Blue) From Simulation, Showing Hydrogen Bonds. 135

A5 Viscosity Deviation vs. Mole Fraction Water (X_1). The Line is a Redlich-Kister Polynomial [263] Fit to the Data by Least-Squares Regression. Redlich-Kister Polynomials Describe Excess Molar Quantities Such as Excess Molar Volume and Viscosity Deviation. It is the Form $Q_{ij} = x_i x_j \sum_{k=0}^{m} B_k (x_i - x_j)^k$ Where i and j are Any Two Components, B_k are Parameters Fit by Regression, and m is the Degree of the Polynomial Expansion. In This Case a Third Order Polynomial was Used. 137

A6 Radial Distribution Functions Around the Cation Head. "Head" Refers to the Imidazolium Ring within BMIM While "Tail" Refers to the Butyl Chain. 139

A7 Radial Distribution Functions of Iodide and Water Around the Iodide Anion..... 141

A8 Self-Diffusion Coefficients Versus Mole Fraction Water (X_1). 142

1. INTRODUCTION

Microgel particles are deformable and soft. They are typically comprised of a water-swollen crosslinked gel-network of colloidal dimensions. The microgel system is a dispersion solution as the composition within the microgel is thermodynamically balanced with the solvency conditions of the medium in which they are dispersed [1]. The equilibrium size of the microgel particle in dilute solution is determined by the intricate balancing between osmotic pressure within the gel-particle, derived from hydrated monomers and the possible incorporation of ionic functional groups, and the entropic elasticity arising from the crosslinked polymer chains. In recent years, microgel particles have drawn a significant amount of attention in multiple fields of research due to their intrinsic ability to rapidly change their volume (i.e. swell or deswell) through various external stimuli such as pH [2], temperature [3-5], osmotic pressure [6-8], or electric and magnetic fields [9-11]. They are currently used in a vast array of applications and consumer products, including surface coatings [12, 13], cosmetics [14, 15], and as promising controlled drug-delivering agents [16, 17].

The first part of the work reported herein describes the design and synthesis of multifunctional microgel particle systems with respect to various factors encompassing polymer composition, variation in temperature, pH, and solvent quality. In addition, the functional roles of environmentally responsive microgel systems potentially well suited as relevant vehicles for adsorption, retention, and targeted delivery for novel carrier applications of active species were investigated.

In addition, microgel particles have exhibited a remarkable duality with properties attributed both to colloidal and polymeric systems. Recent work has demonstrated that

the prepared gel-particles can be utilized to stabilize fluid interfaces leading to fascinating interfacial phenomena. This is due to liquid-liquid interfaces, which are able to provide 2-D templates for self-assembly of small particles. By virtue of inter-particle interactions alone, intricate patterns and structures spontaneously form and may be fused together to maintain their morphology in the absence of the interfacial template. Flat liquid-liquid interfaces can be used to make membrane-like structures whereas spherical interfaces (e.g. emulsion droplets) can be applied to make capsule-like structures. Such micro- and nano-structures may have potential impact especially for applications in biomedical, food, and petroleum fields.

In addition, this phenomenon manifests as Pickering emulsions, which have already seen wide application. Emulsions are stable mixtures of immiscible liquids, one liquid being dispersed as droplets in the other. To stabilize against coalescence and eventual separation, Pickering emulsion droplets are armored with solid particles. These emulsions offer many advantages over traditional surfactant stabilized emulsions. For example, Pickering emulsions impart enhanced stability against coalescence and, in many cases, are biologically attuned and environmentally-benign with easier handling. These characteristics open the door for their application in a variety of industries, spanning the recovery, separation and cleaning of crude oil [18-20], food [21-23], delivery of biomedicine [24-26], pharmaceuticals, and cosmetics. So far, particle self-assembly has been studied primarily at oil-water interfaces. Ionic liquids (ILs) are a novel class of liquids with a wealth of useful properties that can greatly enhance the applicability and tunability of self-assembly processes. Room temperature ILs are ionic materials which melt below 100˚C, many of at room temperature [27]. The remarkable advantage of ILs is

that their properties can be tuned for virtually any application simply by judicious choice of constituent ions. Consequently, they are also called "designer solvents." Such tunability would significantly augment the field of particle self-assembly. For example, self-assembly at liquid-liquid interface is usually governed by properties of the solid particles, which sometimes requires extensive functionalization. If instead this process could be tuned by the solvent, the cost of continuous production of self-assembled structures could be greatly reduced because there would be no need to repeatedly functionalize particles.

Pickering emulsions stabilized with solid particles already have wide applications and with the incorporation of ILs, their properties may be optimized for specific tasks. Understanding microgel particle behavior at IL-based liquid-liquid interfaces, however, has remained largely elusive. The latter part of the work has established the versatility of utilizing composite microgel particles in stabilizing ionic liquid-in-water emulsions. The details of their adsorption, conformation, and organization at the interfacial colloidal lattice of the spontaneously formed layer of adsorbed microgel particles at the liquid-liquid interface were explored and shown to have potential use in extraction processes as the interface remains permeable to active species. The corresponding presentation is organized as follows:

Chapter 2 of this thesis is divided into multiple sections dedicated to informing the reader with a fundamental understanding of the synthesis and functionalization properties of environmentally responsive microgel particles, the fundamental principles denoting particle self-assembly, and providing a brief introduction to ILs. The volume transitions of polymer gels resulting from the competition between attractive and

repulsive fundamental interactions within the polymer network are discussed in extended detail. Furthermore, the motivations for the work are identified and extensively described. Chapter 3 describes the materials and methodology utilized in all the thesis work. In Chapter 4, a detailed study focused on the development and characterization of multifunctional microgel systems for the controlled and targeted delivery of active chemical species is presented. Specifically, the results of the synthesis and characterization of multifunctional ionic and zwitterionic microgel systems which may undergo an extensive, reversible change in volume in response to environmental stimuli such as pH and temperature are further discussed. Additional studies have elucidated the effective uptake and release of rheology modifiers and molecular surfactants from these microgel particles owing to their unique environmental sensitivities. In another component of this work; it is explicitly shown that the prepared ionic microgel particles can demonstrate abilities to adsorb and repel nanometer-sized inorganic components, such as iron oxide nanoparticles (Fe_3O_4-NPs) upon pH variation. The extent of the loading of Fe_3O_4-NPs within the colloidal particles and morphology can be manipulated by tunable interactions between the Fe_3O_4-NPs and ionic microgel particles. The latter section of this chapter reports new evidence of the versatility of soft and environmentally responsive micron-sized colloidal gel particles as stabilizers for ionic liquid-water Pickering emulsions. These particles display a duality with properties ascribed typically both to polymeric and colloidal systems. The utilization of fluorescently labeled composite microgel particles allows in-situ and facile visualization without the necessity of invasive sample preparation procedures. When the prepared particles form monolayers equilibrated at the liquid-liquid interface on fully covered emulsion droplets, the colloidal

lattice organization re-orders itself depending on the surface charge of these particles. Moreover, it was demonstrated that the spontaneously formed and densely packed layer of microgel particles can be employed for extraction applications, as the interface remains permeable to small active species. Finally, Chapter 5 recaps the work for the characterization of the multifunctional properties of those prepared microgel particle systems as well as their applications. In the last section, future work is proposed to investigate the unique properties of microgel-stabilized responsive emulsions.

2. BACKGROUND & MOTIVATIONS

2.1 Defining Microgels

Microgels are dispersions of colloidal-scale particles, each comprised of a cross-linked polymer network [28]. Swollen microgels have a particle size within the range of 100 nanometers to several microns. Microgels can be made responsive owing to their ability to undergo rapid volume phase transitions. The extent of particle swelling is governed by the intrinsic nature of the polymer-solvent interaction, which is responsive to solution conditions. Thus, the particle size and the dispersion properties are responsive to external stimuli that affect the solvent including pH [29-32], temperature [33, 34], magnetic [35, 36] and electric fields [37, 38], or osmotic pressure [39].

Baker first introduced solvent-swellable microgel dispersions in 1956 when he prepared cross-linked polybutadiene latex particles and studied its swelling properties in a number of hydrophobic solvents [40]. Since that time, a large amount of work focused on microgel dispersions has also been reported. In 1986, Pelton and Chilante were the first to synthesized the most widely investigated water-swellable thermosensitive microgel dispersions based upon of poly(N-isopropylacrylamide) (PNIPAm) [41]. They found that the tunable nature of the physical properties and the intrinsic viscoelasticity of these microgel particles lead to a wide range of unique material properties.

In the recent years, advancements in multifunctional microgels have become a highly active research topic in both fundamental studies of soft matter as well as in interdisciplinary applied scientific fields. In particular, major areas of development include the use of microgels for the fabrication of photonic crystals [42-45], template-

based synthesis of inorganic nanoparticles with multifunctional properties [46-50], and as promising controlled drug delivery systems [51].

In general, microgels could be classified based on the physical or chemical nature of the cross-links that are responsible for their particle size and network structure. In microgels obtained by physical cross-linking, the network formation could be induced via non-covalent attractive forces such as hydrophobic bonding, and the more dominant ionic interactions [28]. Moreover, physically cross-linked microgel systems are sensitive and may lose colloidal stability upon exposure to various factors such as temperature, polymer composition, ionic strength (i.e. salt concentration), and the cross-linking densities. Applications of physically cross-linked microgels are often ideal for biodegradable systems. For example, these cross-linked microgels have been utilized for the uptake of drugs, which can be released upon dissolution of the polymer network. In contrast, microgels obtained via chemical cross-linking are more stable due to their covalent nature. These microgels are typically prepared by free-radical polymerization and retain a permanent gel-network structure derived from the addition of a crosslinking agent, which is imperative to prevent the microgels from dissolving in water during the copolymerization of the monomers.

Microgels could also be categorized based on their stimuli responsive properties, as attained by the types of functional groups composed within those particles. Non-responsive microgels are only swellable upon the absorption of water whereas environmentally stimulus-responsive microgels can rapidly change their volume through various external stimuli. The PNIPAm-based multifunctional microgel systems reported in this work are responsive to various environmental stimuli such as temperature and pH.

2.2 Microgel Dispersion Preparation

To accommodate the development of microgels, the objectives of microgel synthesis include regulating the particle size distribution, enhancing the colloidal stability, and controlling the distribution of functional groups. Figure 2.1 illustrates structures of the monomers frequently used to prepare microgel particles. The most widely studied approach to synthesizing microgel dispersions is via homogenous nucleation [28]. In homogenous nucleation, a solution of soluble monomer, including a cross-linking agent, is fed into the reactor and microgel particles are formed over the course of polymerization. An essential requirement for distinct particle formation is that the polymer formed must be insoluble under the polymerization conditions; monomers giving soluble polymers under the polymerization conditions will form a macrogel [52].

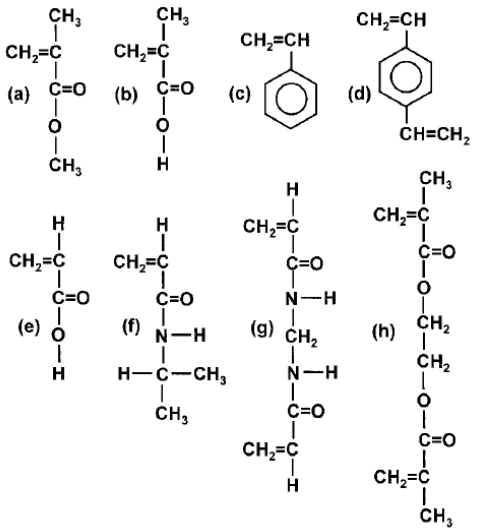

Figure 2.1 Chemical structures of the monomers widely applied to synthesis stimuli-responsive microgel particles. The monomers are (a) methylmethacrylate, (b) methacrylic acid, (c) styrene, (d) divinylbenzene, (e) acrylics acid, (f) N-isopropylacrylamide, (g) N-N'-methylene bisacrylamide and (h) ethyleneglycol dimethacrylate. Adapted from [28].

Four methods have been reported to describe the synthesis of microgel particles; anionic copolymerization [53], cross-linking of neighboring polymer chains [54], inverse micro-emulsion polymerization [55], and emulsion polymerization (EP) [52]. However, EP is the primary technique used for the preparation of multifunctional stimulus-responsive microgel dispersions involving homogeneous nucleation. In general, EP can be implemented in the presence of added surfactant (conventional EP) or with no employment of surfactant (surfactant-free emulsion polymerization, SFEP). In the first method, the presence of added surfactant provides stability through the polymerization and allows the microgel dispersions to be synthesized with higher total solid contents and a smaller particle size distribution (e.g. particles with hydrodynamic diameters less than ~150 nm). However, one major problem associated with the conventional EP approach is the difficulty of removing residual surfactant. In contrast, for the SFEP method, to avoid the contamination of residual surfactant, an anionic or cationic initiator is employed to charge the polymer chains formed during the polymerization stage to provide stability for

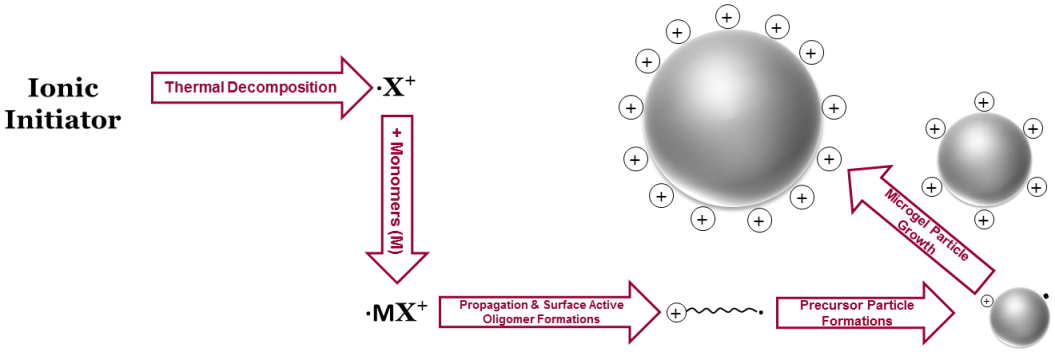

Figure 2.2 The synthesis mechanism of microgel dispersions utilizing SFEP. Please note, the closed circles illustrate the free-radical sites and the M and X^+ are the vinyl monomer and the thermal decomposition product from the cationic initiator, correspondingly.

the growing particles. Figure 2.2 depicts the general mechanism for preparation of microgel dispersions following SFEP.

The typical mechanism of an SFEP batch starts when all the monomer and ionic initiators are added at the beginning of the free-radical polymerization. During this process, the thermal decomposition of the ionic initiator initiates the surface-active oligomers to grow until they exceed the solubility limit of the solvent and reaches a critical chain length. Past this critical length, the growing chain collapses to form precursor particles. Further particle growth occurs as the precursors either aggregate with other precursor particles or deposit onto an existing, colloidally stable microgel particle. A termination step ensues within the particles once the radical species enters the growing particle.

A key feature of SFEP is that the duration of the nucleation stage is very short, thus a narrow final particle size distribution can be attained by increasing the electrolyte concentration and decreasing the initiator concentration [56]. In addition, SFEP method only applies to monomers with low water solubility, whereas most vinyl monomers used to produce specific environmentally responsive microgels are water-soluble. Therefore, the nomenclature surfactant-free “precipitation polymerization” denotes the preparation method of these microgel particles. Overall, this synthesis method is well suited for the preparation of PNIPAm-based microgel systems. Figure 2.3 shows a schematic illustration of a typical microgel particle at various distance scales upon successful synthesis.

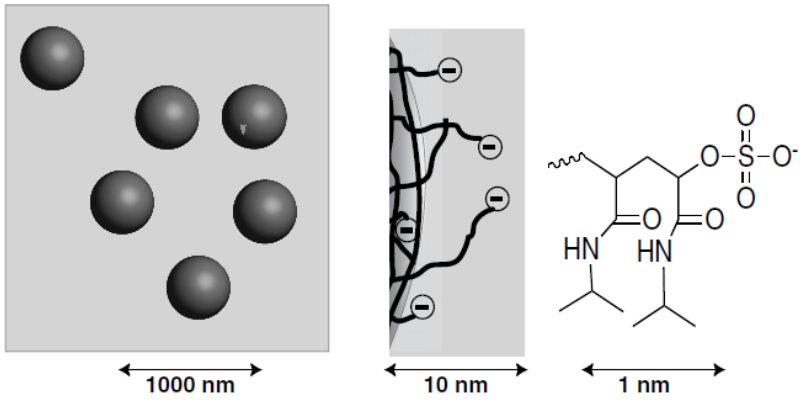

Figure 2.3 Shows a representation of the generic PNIPAm-based microgel at three distance scales. Adapted from [52].

2.3 Stimuli-Responsive Microgels

The tunable nature of the stimuli-responsive properties of microgels leads these dispersions to a broad range of versatile applications. The most investigated water-swellable thermosensitive microgels are derivatives of the thermosensitive monomer, NIPAm. The fundamental solution behaviors of PNIPAm in a solvent are contingent on various interactions such as solvent-solvent, polymer-polymer, and polymer-solvent. At low temperatures, linear PNIPAm chains are highly solvated due to the hydrogen-bonding between the amide residues on the polymer chains and the water molecules. Moreover, the water molecules are likely to form cage-like structures around the isopropyl groups on the polymer as the intensified hydrophobic effects dominant [57]. At low temperatures, PNIPAm exists in a random coil state induced by the stronger polymer-solvent interactions. However, once the temperature is elevated, the polymer-polymer interactions become more dominant, breaking the hydrogen-bonding between the water molecules and polymer, resulting in an entropy-driven phase separation as the polymer chains transition into a globule conformation. Figure 2.4 shows the thermo-

induced coil-to-globule transition of PNIPAm. The lower critical solution temperature (LCST) is termed as the temperature at which this phase transition occurs.

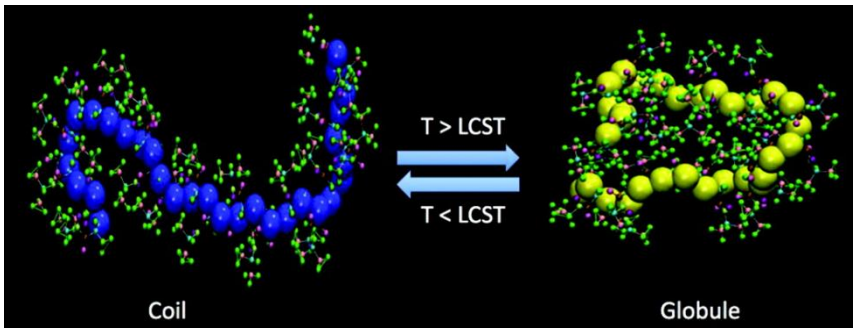

Figure 2.4 Shows a snapshot of the thermo-induced coil-to-globule transition of PNIPAm polymer chains. Adapted from [57].

For linear PNIPAm in water the LCST occurs at ~32˚C [5]. Please note that PNIPAm intrinsically possesses an inverse solubility upon heating. At the LCST, PNIPAm rapidly changes its hydrophilicity and hydrophobicity. Heskins and Guillet were the first to comprehensively investigate the entropy-favored thermodynamic origin of the LCST for linear PNIPAm [58]. The Gibbs free energy of this system can be described by the equation below.

$$\Delta G_{mix} = \Delta H_{mix} - T\Delta S_{mix} \qquad \text{(Equation 2.1)}$$

At lower temperatures, the free energy of mixing (ΔG_{mix}) is reduced. This is due to the dominating contribution of the negative enthalpy (ΔH_{mix}) in response to the hydrogen-bonding and decreased entropy (ΔS_{mix}) resultant from the reorientation of the water molecules around the nonpolar regions of the PNIPAm. At higher temperatures, the entropy dominates, inducing the free energy to grow in turn causing the PNIPAm to release the absorbed water and initiate the phase separation [59, 60].

Figure 2.5 depicts the thermosensitive phase transition demonstrated in PNIPAm chains and gels. In PNIPAm-based microgel systems, the LCST of the linear polymer manifests as the volume phase transition temperature (VPTT). The VPTT of the microgels is influenced via cross-linking density, solvent nature and composition, and the incorporation of the functional groups via copolymerization [61]. Below the VPTT, the microgels remain in their swollen, hydrophilic state. At temperatures above the VPTT, the gels deswell to the shrunken relatively hydrophobic state.

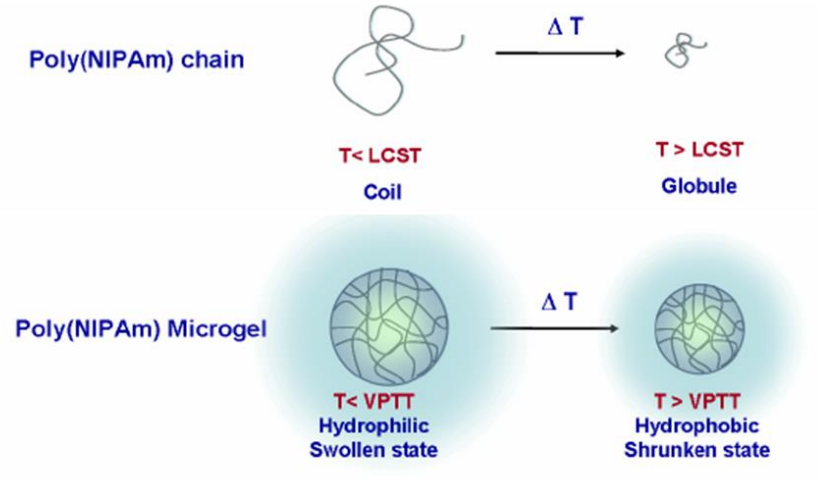

Figure 2.5 illustrate the schematic depiction of the thermally induced phase transition in linear PNIPAm and gel systems. Adapted from [31].

Overall, PNIPAm-based microgel systems feature higher surface area, diffusivity, and relatively faster stimuli-response kinetics in comparison with their bulk hydrogel counterparts [62-65]. Potentially, applications of PNIPAm-based microgels are well suited for the novel delivery of small active species.

2.3.1 Fundamental Interactions

The volume phase transition of colloidal polymer-gel ensues from the competition of pairwise attractive and repulsive interactions within the polymer-gel network and between the polymer-gel network and the solvent it is immersed in. In general, the presence of net attractive interactions may lead to particle aggregation. However, in the case of microgel particles, the net attraction is typically weak, so that any resulting coagulation is generally reversible. There is usually a combination of several fundamental intermolecular forces involved during the microgel swelling process, such as Van der Waals, hydrophobic, electrostatic, and hydrogen-bonding [66]. Figure 2.6 shows an illustration of the fundamental interactions governing in various gel-solvent systems.

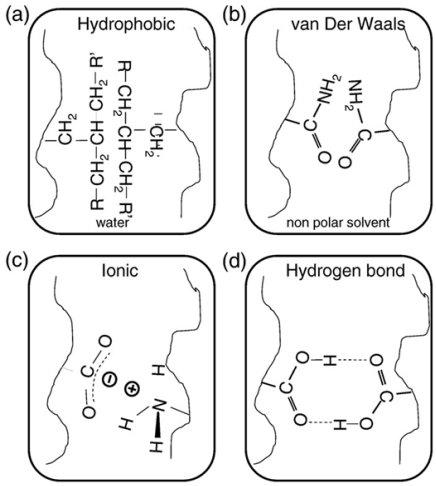

Figure 2.6 Illustrates a schematic representation of the four fundamental interactions acting in various microgel-solvent systems: (a) hydrophobic, (b) Van der Waals, (c) ionic/electrostatic and (d) hydrogen-bonding interactions. Adapted from [1].

The net balance that dictates the swelling of the gel-network can be influenced by the manipulation of these forces. To elaborate, if the net repulsive interactions governing the gel-network dominate the particles tend to swell. In contrast, the gel-network tends to

deswell if the net interactions become attractive. Thus, the net interaction balance within the gel-network can be fine-tuned via controlling the variables triggering the volume transitions of these microgels.

2.3.1.1 Hydrophobic Interactions

Hydrophobic interactions have an entropic origin and describe the strong attractive interactions occurring among the hydrophobic molecules in water. For linear polymers, in order to maximize the entropy, rearrangements of the water molecules must drive the polymer chains to aggregate. For gel-like network structures, such interaction can be generated by the variation of the side group of the polymer chains. In the case for PNIPAm-based microgels, by increasing the temperature above the thermally induced VPTT, the hydrophobic interactions dominate, resulting in a collapse of the polymer-gel network. Furthermore, the hydrophobic effect can be augmented via the addition of organic solvents such as alcohols. This effect is due to the ordered structural rearrangement of the encapsulated neighboring water molecules in the presence of hydrocarbon molecules [67, 68]. Other Studies with this type of solvents has been reported on poly[(methyl methacrylate)-*co*-(methacrylic acid)] gels [69].

2.3.1.2 Van der Waals Interactions

The pairwise potential between neutral microgels consists of a short-range repulsion that is analogous to the interaction among two polymer-coated surfaces, and the long-ranged van der Waal interactions which stems from the difference in the Hanmaker constants of the particle and the solvent [70]. Van deer Waals interactions are represented as dispersion forces derived from the orientation-dictated interactions between permanent dipoles, attractive instantaneous dipole-induced dipole, and induction forces. Since those

interactions extents from interatomic distances to nanometers between dipoles, their presence is more vital in non-polar solvents for macromolecules such as polymers and surfactants. Moreover, for gel-like systems, the addition of a non-polar solvent such as acetone may enhance the attractive Van der Waals interaction between polymer chains prompting the gel-network to collapse [71-73].

2.3.1.3 Electrostatic Interactions

Electrostatic interaction is defined as a long-range force that exists between charged molecules or ions. Those forces are considered to be the strongest among all intermolecular interactions for microgel dispersions that have been prepared using monomers containing ionic functional groups. The presence of electrostatic interactions is vital in the establishment of osmotic pressure via counterions as a resultant of ion-redistribution for the volume transition of ionic microgel systems. In addition, those forces also play an important role in the mechanism for direct Coulombic interactions. To further elaborate, when the microgel network carries a fixed charge (positive or negative) along its backbone, those charges will induce an imbalance among the ion distributed outside and inside the polymer-gel, thus leading it to swell or deswell. In addition, Coulomb repulsion screened by water due to the osmotic pressure exerted via counterions may also contribute to the volume phase transition [74, 75].

Experimentally, this phenomena can be found in the later discussed cationically charged poly(NIPAm-*co*-DMAPMA) microgel system. However, for multifunctional microgel systems which carry both cationic and anionic functional groups attached to the gel-network, such as a zwitterionic poly(NIPAm-*co*-AAc-*co*-DMAPMA) microgel

system, the polymer chains exert long-range electrostatic attractions while repelling each other over short ranges.

2.3.1.4 Hydrogen-Bonding

A hydrogen-bond is an attractive interaction between polar molecules that transpires when a hydrogen atom is bonded to a highly electronegative atom. The formation of attraction-driven hydrogen-bonds is directionally dependent as it requires an optimal orientation between the groups involved [76]. Thus, hydrogen-bond attractions can occur through intermolecular interactions between molecules or via intramolecular means. In the case of polymer gels, hydrogen-binding is a relevant interaction which greatly affects the swelling behavior of the prepared gel dispersions. To elaborate, the flexibility of the polymer chains allows the formation of inter-chain and intra-chain bounding. As temperature increases, in the presence of those attractive forces, the hydrogen-bonds are unable to withstand thermal agitation and break contributing to the collapse of the gel-network [70]. Similar to hydrophobic interactions, the addition of organic solvents, such as alcohols can also affect the hydrogen-bonding between water molecules [77].

For PNIPAm-based microgel systems, the volume phase transition is dominated via the hydrophobic interaction. However, at temperatures below the VPTT, hydrogen-bonds are formed among the amide groups of the PNIPAm as water molecules reorganizes around the alkyl groups of the polymer chains. Additionally, above the VPTT, these bonding interactions diminish and ultimately induce the collapse of the gel-network.

2.3.2 Responsive Microgel Particle Swelling: Experiments

2.3.2.1 Temperature-Responsive Particles

The origin of the thermosensitive properties of PNIPAm-based microgels was reviewed previously. At temperatures below the VPTT, the microgels are highly swollen and contain a large amount of water. Above this temperature, due to the expulsion of water content from the interior of the gel-network, the microgel is deswollen and has much smaller water content. Additional studies have shown that the VPTT of pure PNIPAm microgels is marginally higher when compared to the LCST of its linear polymer. This phenomenon is due to the increased heterogeneity of the polymeric subchain length within the microgels [78]. As hydrophobic interactions dominate above the VPTT, the regions with longer polymeric subchains collapse earlier than the regions with shorter subchains, thus leading the gel-network to undergo the phase transition at slightly different temperatures in contrast to its linear parent.

Furthermore, the VPTT of PNIPAm microgel systems can be finely tuned via copolymerization of other reactive functional monomers. This is due to the intricate balancing of the hydrophobic to hydrophilic interactions within the polymer-gel network. By the incorporation of hydrophilic moieties, VPTT can be increased. On the other hand, the incorporation of hydrophobic functional moieties decreases the VPTT.

Additionally, the VPTT can be heightened via increasing the co-monomer content. For example, Burmistrova and co-workers prepared anionic charged poly(NIPAm-*co*-AAc) particles and found that the VPTT increased with increasing the co-monomer content [3]. Figure 2.7 shows the dependence of the average hydrodynamic radius as a function of temperature for four types of microgels copolymerized with

various molar percentage of AAc. The growth in the hydrodynamic sizes of the particles with increasing co-monomer content is determined to be due to amplified electrostatic repulsion between the polymer chains and an increase in the osmotic pressure [7]. Interestingly, the incorporation high of AAc content also can lead to a two-step volume phase transition, shown in Figure 2.7*d*.

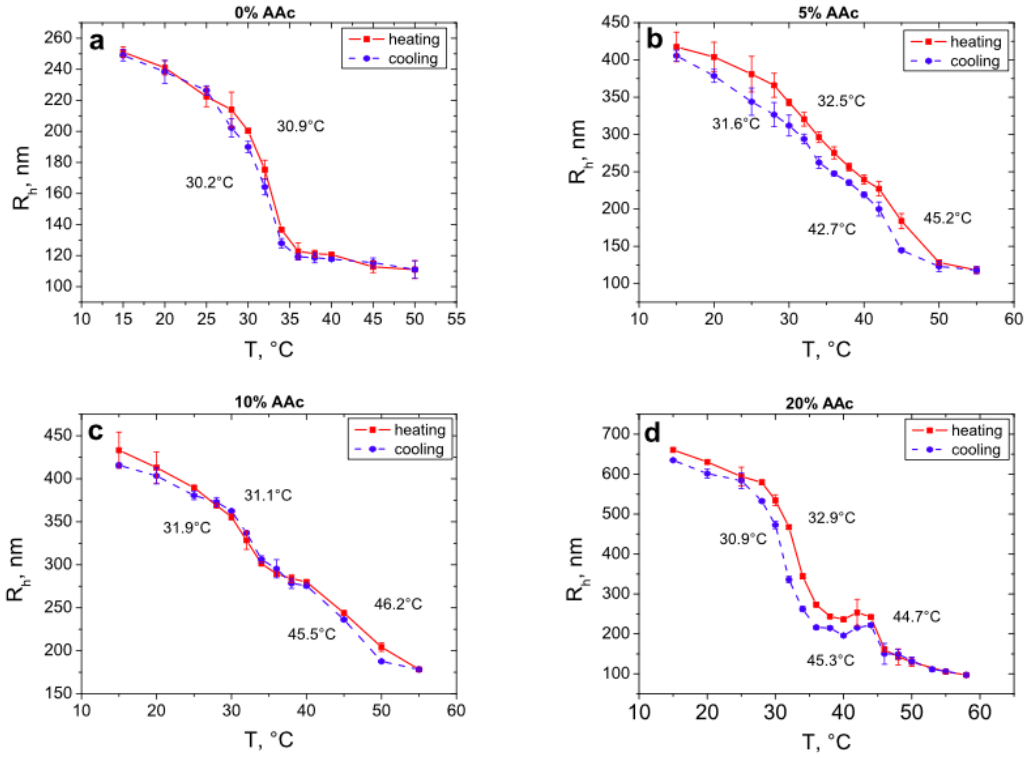

Figure 2.7 Temperature dependence of the average hydrodynamic radii of microgel systems with various mol% of AAc contents: (a) 0%; (b) 5%; (c) 10% and (d) 20%. Adapted from [3].

The first transition at 32 °C is induced by the dominant hydrophobic attraction derived from the dehydration of the PNIPAm gel-component. The additional transition beyond 32 °C is due to charge repulsion coupled with the augmentation of the generated osmotic pressure [79]. The effect of temperature is further reviewed in Chapter 4 for both the cationic and the more complicated zwitterionic microgel systems.

2.3.2.2 pH-Responsive Particles

The functionalization of PNIPAm microgels with the incorporation of anionic or cationic functional groups such as acrylic acid (AAc) [80], methacrylic acid [81], vinyl pyridine [82], and vinyl imidazole [83] yields the synthesis of multi-responsive microgels that undergo extensive volume transitions in response with tunable pH and temperature. Figure 2.8 lists several ionic monomers that have been used to prepare ionic and zwitterionic microgels.

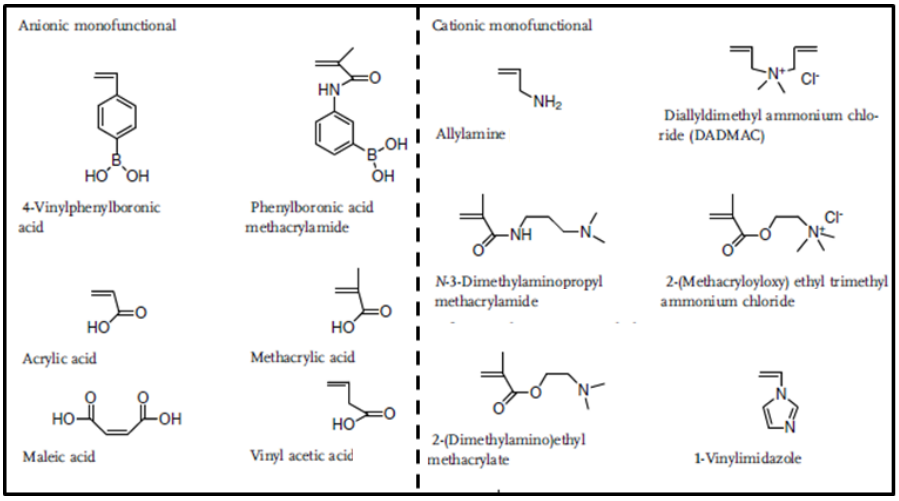

Figure 2.8 Lists many of the widely used monofunctional monomers that are anionic or cationic.

The dependence of swelling behavior on pH in ionic microgels largely derives from the long-range electrostatic interactions among the ionic functional groups. For example, Smith and Lyon have prepared anionic poly(NIPAm-*co*-AAc) microgel particles which undergo a sharp increase in hydrodynamic diameter at pH ~4.5 due to deprotonation of the carboxylic acids and the resultant strong electrostatic repulsion among the negatively charged carboxylate moieties (pKa of AAc ~4.25 [61]).

Moreover, their investigation elucidates the direct loading of protein, such as Cytochrome C (CytC) into the prepared anionic colloidal microgels. Figure 2.9 demonstrates the interaction of the prepared microgels with oppositely charged CytC via facile manipulation of the charge of the gel-network and the salinity of the medium. In addition, the modulation of AAc content was determined as the effective mean to tune the binding stoichiometry. For example, microgels with low charge content (10 mol% of AAc) encapsulated a smaller fraction of proteins due to the decreased swelling and low porosity of those networks. On the other hand, microgels prepared containing 30 mol% of AAc were capable of loading extremely high concentrations of CytC (~17 mM), which is beyond the solubility limit of the protein in aqueous media (~8 mM) at room temperature [78].

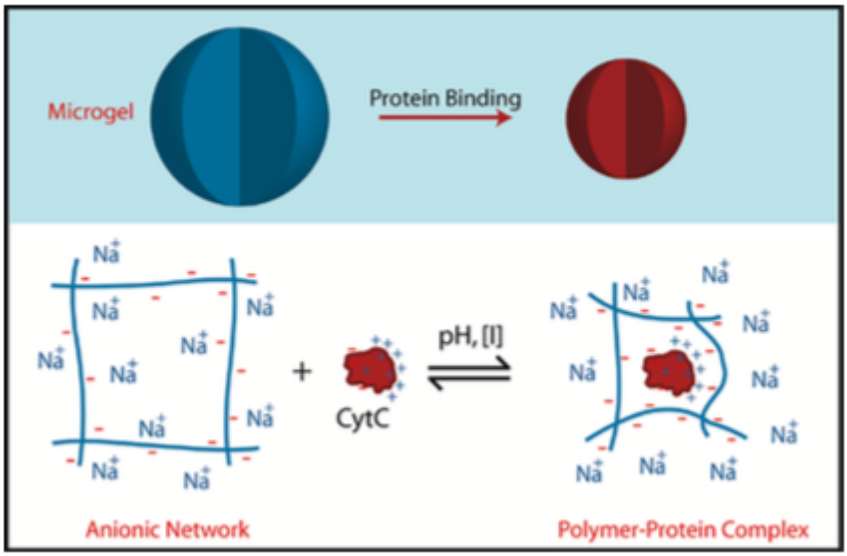

Figure 2.9 Depicts the interaction of anionic microgels with oppositely charged Cytochrome C (CytC). Adapted from [78].

The effect of pH and the utilization of the network swelling as a tunable variable for design of future delivery vehicles with specific encapsulation and release properties will be further reviewed for both cationic and the more complicated zwitterionic microgel systems in Chapter 4.

2.4 Particle Assembly at Liquid-Liquid Interfaces

2.4.1 Pickering Emulsions

Emulsions are a metastable mixture comprised of two immiscible fluids, such as oil and water. In general, conventional emulsions are obtained in the existence of various surface-active species, such as surfactants, amphiphilic proteins or polymers [84]. They have been widely applied for many industrial applications, such as cosmetics, foods, pharmaceutics and surface coatings and paintings. The utilization of solid particles as a new class of emulsion stabilizer, often termed Pickering emulsions is previously described by S.U. Pickering in 1997 [85, 86]. Studies have shown an extensive variety of synthetic organic or inorganic and even naturally occurring particles can be employed as the solid stabilizers.

In recent years, Pickering emulsions have received significant interest, not only from their importance in an assortment of applied studies but also because of their uniqueness in the stabilization mechanisms. In comparison, the main uniqueness of Pickering emulsions to the more conventional surfactant-stabilized emulsion is the absence of emulsifier exchange between the interface and the bulk [87]. To elaborate, the stabilization of Pickering emulsions is driven by thermodynamic requirements. The absorption of solid particles onto the liquid-liquid interface is a spontaneous process as it drives towards the preferable lower free energy state. The stability of solid particle

absorption via geometrical considerations on the phase interface can be quantified by desorption energy ΔG expressed through the following equation:

$$\Delta G = \gamma \pi r_p^2 \left(1 - \left|\cos(\alpha)\right|\right)^2 \qquad \text{(Equation 2.2)}$$

Where γ is the oil-water interfacial tension, r_p is the particle radius and α is the contact angle of the adsorbed particle; θ is defined as the angle towards the aqueous phase between the liquid interface and the tangent to the particle at the point where the three phases connect. Please note ΔG scales as the square of the particle size shown in Figure 2.10*a*. In addition, for particles selected with a size ranging from several nanometers to several microns and an intermediate hydrophobicity ($\theta = 90^\circ$), the estimated ΔG is many times of the thermal energy. Therefore, once adsorbed the particles anchoring may be considered as nearly-irreversible owing to the high ΔG. However, the adsorption of the particles only becomes reversible when very small particles ($r_p \leq 1$ nm) are employed as the ΔG becomes comparable to the thermal energy.

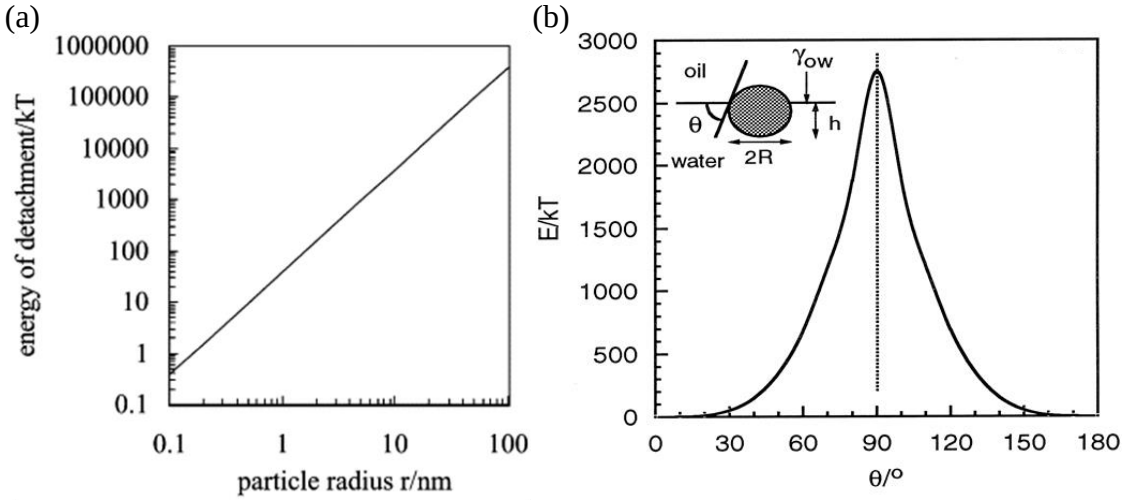

Figure 2.10 Variation of ΔG of a particle at the planar oil-water interface at room temperature with respect to (a) particle radius and (b) contact angle. Adapted from [87] and [86], respectively.

The wettability is another parameter to consider which has a vital effect on the adsorption of a particle at the interface. Figure 2.10*b* depicts the dependence of ΔG required to rip away a 10 nm particle from the oil-water interface. The greatest ΔG can be obtained when the particle is held at $\theta = 90^{\circ}$ as the particle is wetted equally at the interface.

The formation of Pickering emulsions with narrow size distributions could be simply attained via turbulent stirring through the limited coalescence process as result of irreversible particle anchoring [88]. This process consists of generating a large excess of oil-water interface compared to the area that can be covered by the solid particles. Upon cessation of stirring, insufficiently protected drops coalesce; decreasing the total amount of oil-water interface, and this coalescence ensues until the drops are adequately covered by the applied particles. The resulting emulsions are remarkably monodisperse as a consequence of this irreversible interfacial anchoring. In general, limited coalescence does not depend on nature of the applied stabilizers and has been observed for numerous Pickering emulsion systems.

2.4.2 Packing at the Interface

Pickering emulsion is an emulsion that is kinetically stabilized by solid particles which adsorb and partially wetted onto the interface between the two phases [85]. Owing to irreversible anchoring and total adsorption, equality between the final drop surface area and the ability of particle coverage yields a simple relationship among the reverse drop diameter D, the particle amount and their packing at the interface provided in the equation below.

$$\frac{1}{D} = \frac{n\pi d_p^2}{24CV_D} = \frac{S_{eq}}{6CV_D} \quad \text{(Equation 2.3)}$$

In Equation 2.3, *n* is denoted as the number of particles, d_p is the diameter and V_D is the dispersed phase volume. The coverage rate, *C*, is defined as surface covered by particles divided by the total interfacial area. This equation is extremely useful for the determination of the coverage rate *C*, as the drop size can be tuned via changing the amount of particles while keeping all other variables constant. Moreover, insight into the interfacial particle packing at the interface can be evaluated through the assessment of the coverage rate parameter. For a monolayer of solid particles densely and hexagonally packed at the interface, the coverage rate parameter *C* is equal to 0.9 [89]. For characterization of microgel adsorption through limited coalescence, the surface coverage characterizing the particle packing at the interface can directly be deduced from a drop size measurement in the low particle concentration regime where the average inverse droplet diameter is proportional to S_{eq}/V_D [90].

2.4.3 Pickering Emulsions Stabilized via Microgels

In recent years, advancements in microgels have become a highly attractive research topic in both fundamental studies of soft matter as well as in applied scientific fields. Swelling of microgel particles follows the same thermodynamic mandates as hydrogels. Intricate balancing between the inner and outer osmotic pressures of the gel-network must be achieved in order to reach the equilibrium gel-swelling volume. For the utilization of a non-ionic polymer, this swelling is dictated via polymer-solvent interactions, and the elasticity of the network. However, electrostatic contribution must be taken into account if the applied polymer is charged. In this case, the volume transition

is induced from the osmotic pressure exerted by free mobile counterions coupled with the Coulomb repulsions arose between the charges.

The first report of emulsion stabilized by microgels was attained with PNIPAm copolymerized with methacrylic acid (MAAc) [91]. These prepared responsive microgels demonstrated the ability to stabilize octanol-in-water emulsions under selective pH and temperature conditions. Moreover, the experimental observations regarding the stabilizing properties of the prepared microgel particles are illustrated in Figure 2.11. Stable emulsions were obtained at high pH and low temperature, whereas they were destabilized at low pH or high temperature [91]. It was postulate that under these specific conditions, the prepared soft particles became more hydrophobic, and partially drifted toward the octanol phase, therefore decreasing the interfacial particle packing density and triggering destabilization of the emulsion.

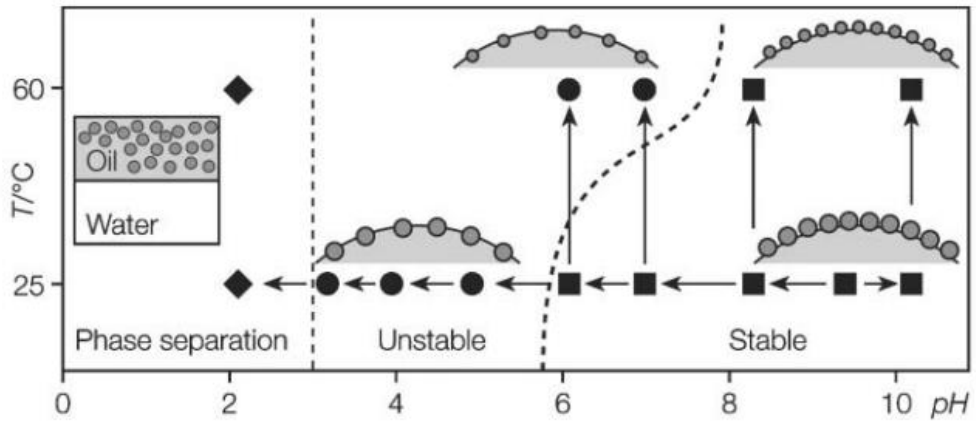

Figure 2.11 The stabilizing efficiency of the prepared microgel particles for octanol-in-water emulsions as a function of pH and temperature. Key: (squares) Stable; (circles) Unstable; and (diamonds) Phase separation. Adapted from [91].

Moreover, composite microgels composed of lightly cross-linked poly(4-vinylpyridine) (P4VP) with the integration of silica sols, were used as "Pickering" emulsifiers [92, 93]. Figure 2.12 shows the schematic representation of pH-induced de-mulsification utilizing the prepared P4VP-SiO_2 particles.

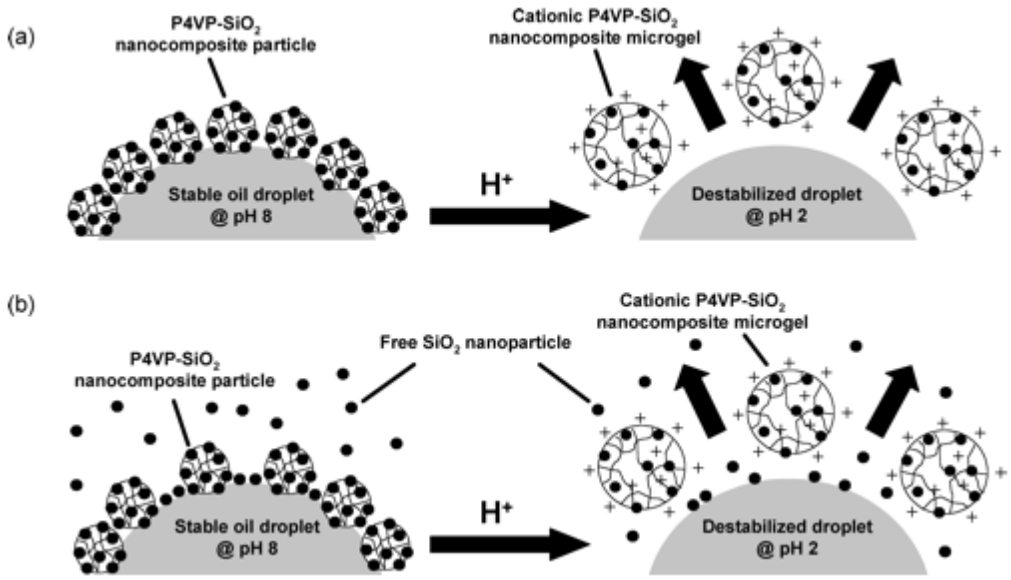

Figure 2.12 Graphic representation of pH-induced de-mulsification using the P4VP−SiO_2 particles as a "Pickering" emulsifier. Oil-in-water emulsions were prepared using an aqueous dispersion of P4VP−SiO_2 particles: (a) after centrifugal purification; (b) prior to any centrifugal purification. Please note silica sols are around 20 nm. Adapted from [92].

Please note both water-in-oil and oil-in-water emulsions were obtained, but only in high pH conditions, when the cationic microgels were fully collapsed due to the deprotonation of the vinylpyridine groups. Thus, Fujii and Armes concluded from this investigation that the fully swollen state facilitated the desorption of microgels from the interface [92].

The complexity of this research topic can be outlined by the two systems above exhibiting opposite stabilization behaviors upon swelling. However, the origin of emulsion stabilization was ambiguous as the role of the inorganic nanoparticles could not be well-defined from that of the organic polymer for the composite system. Additional studies were conducted to elucidate the de-mulsification phenomena. Tsuji and Kawagushi utilized pure PNIPAm microgels as emulsion stabilizers [94]. Figure 2.13 represents images of emulsions prepared from PNIPAm-carrying particles obtained via optical microscopy.

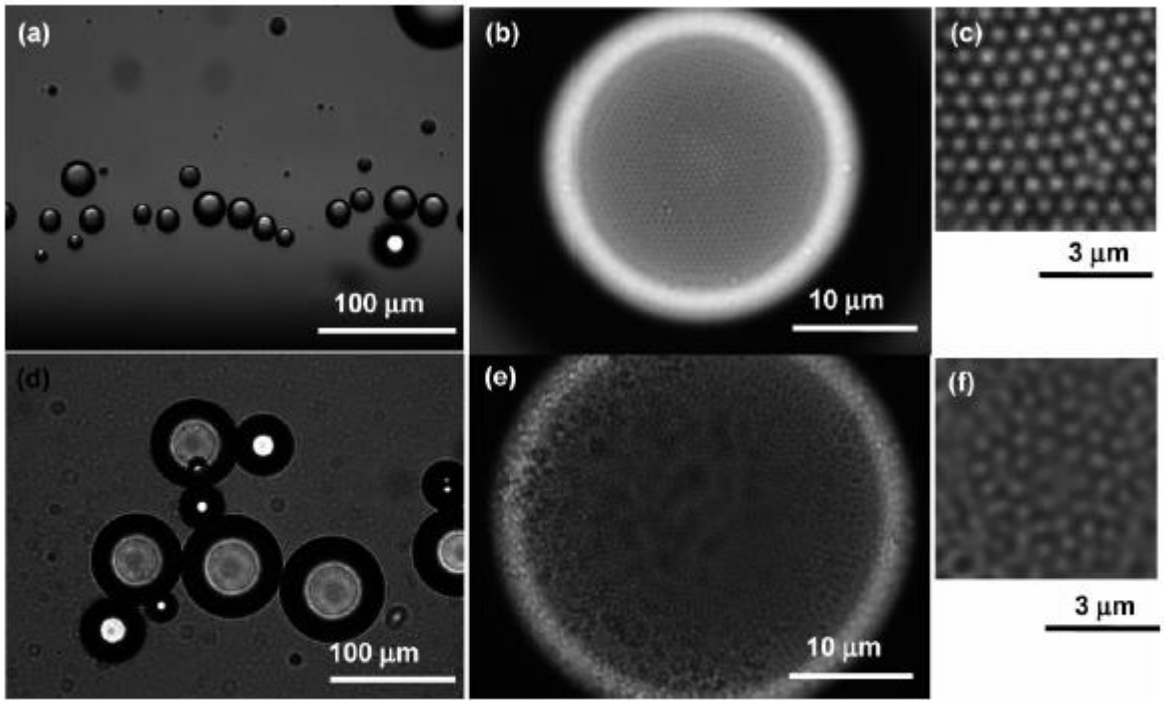

Figure 2.13 Observations of Pickering emulsions obtained via optical microscopy. (a-c) Toluene-in-water emulsion stabilized by PNIPAm microgel particles. (d-f) Toluene-in-water emulsion stabilized by hairy particles. (c) and (f) are close up images of the emulsion surfaces. Adapted from [94].

They have demonstrated that stable emulsions could be prepared from various non-polar oils. Additionally, phase separations occurred when those emulsions were heated above the VPTT. This de-mulsification process was described through

coalescence via the reduction of the surface coverage due to the shrinkage of the microgel.

In order to gain additional insights into the de-mulsification process of microgel-stabilized emulsions, Brugger and Richtering extensively reinvestigated the use of poly(NIPAm-*co*-MAA) microgels as stabilizers [95]. Their studies demonstrated that the pH during synthesis has a substantial influence on the composition and hence the properties of the microgel, including its capacity as a stabilizer for octanol-water emulsion. Figure 2.14 shows the microgel-stabilized octanol-water emulsions immediately after preparation.

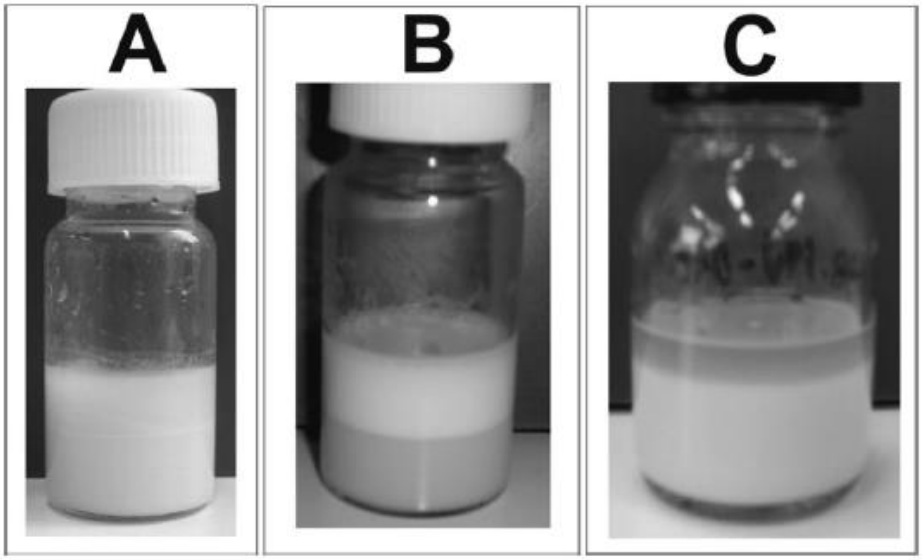

Figure 2.14 Depicts octanol/water emulsions stabilized with synthesis product (A), the supernatant (B), and the purified microgel (C). The pH of all emulsions is ~9. Adapted from [95].

In addition, they concluded that microgels can be applied as soft stabilizers for Pickering emulsions, only if the charges are integrated in the gel-network itself. Moreover, Brugger and Richtering located no evidence on desorption of microgel particles from the octanol-water interface throughout the destabilization process.

However, the formation of aggregated microgel chunks was spotted at the octanol-water interface in-turn prompting the postulation that emulsion destabilization was not a result of particle desorption but was principally caused by the variation of the interfacial mechanical properties [95]. Overall, the employment of microgels as stabilizers was revealed in initial studies. However, some of those conclusions regarding the effect of microgel swelling, the role of surface-active charges, and the mechanism of de-mulsification via desorption or interfacial modification seem to contradict with each other.

Therefore, as part of this work, we have investigated the application of the previously discussed stimuli-responsive microgels as an emulsifier. One major advantage of using responsive microgels for emulsification lies in the fact that PNIPAm-based microgels are thermosenitive, thus upon heating can lead to extensive variations in particle size, hydrophobicity, and surface charge density of the microgels. Also, the incorporation of amide moieties introduces pH-responsiveness, thus increasing functionality of the PNIPAm microgels. In general, we believe the study of this environmentally-responsive emulsifier that can evolve upon the effect of an external stimulus delivers extended emulsion control, in turn opening up a vast array of exciting applications.

2.4.4 Responsive Ionic Liquid Emulsions

The application of ionic liquids (ILs) as extraction solvents in chemical industries displays great potential, particularly for the extraction of chemically complex macromolecules such as proteins [96-98] and lipids [98]. Hence, the need to advance the use of ILs for large-scale separation processes are still desired. To improve the efficiency of extractions and reduce the time required to attain good separation, the application of emulsions is highly advantageous owing to their intrinsically large surface area [97]. Ideally, these emulsions must be designed to be stable against coarsening due to the effects of limited coalescence or Ostwald ripening. Also, the ability to collect and break to acquire the product-loaded ionic liquid phase is highly sought after. Furthermore, the stabilizer applied to produce these emulsions should not influence or interact with the desired product to be extracted.

The preparation of IL-water emulsions is challenging as the result of the low interfacial tension derived from the inherently large miscibility of the two phases. In contrast, to the oil-water interfaces, IL-water interfaces are highly structured due to charge hydration and correlations, result in only partial relevance of the general rules of emulsion preparation and stability [99]. Furthermore, while IL emulsions can be produced utilizing commercial surfactants, most of the previously stated design requirements are not met. For example, due to the inherent water solubility of most ionic liquids, Ostwald ripening leads to fast coarsening and emulsion destabilization. Additionally, surfactants often interact strongly with an assortment of amphiphilic macromolecules, which can lead to irreversible changes in the desired product such as

denaturation of proteins [98]. Overall, the exploration of a robust strategy to prepare IL emulsions meeting these desired requirements is highly favorable.

2.5 Motivations and Applications Involving Multifunctional Microgels

Recently, environmentally responsive colloidal microgel dispersions comprised of cross-linked polymer latex particles have garnered increasing attention in multiple interdisciplinary fields of research due to their particular ability to rapidly change volume (i.e. swell or deswell) through various external stimuli such as pH [2, 100, 101], temperature [3-5, 102], ionic strength [6-8, 103], or electric and magnetic fields [9-11, 35, 37]. With respect to this swelling phenomenon and the intrinsic "sponge-like" network structures of microgel particles in their expanded state, previous literatures have reviewed the potential for diffusive encapsulation and release of active species from thermosensitive poly(N-isopropylacrylamide)-based polyelectrolyte microgel systems [45, 104, 105]. They are found advantageous in a vast array of novel applications including sensing [106], separation technologies [107, 108], catalysis [109, 110], and as promising controlled drug delivering agents [111-113].

2.5.1 Adsorption and Release of Active Species

2.5.1.1 Ionic Microgel Particles

Much of previous research has focused on using environmental stimuli to vary the properties of the microgel network. For example, microgels synthesized through the copolymerization of N-isopropylacrylamide (NIPAm) with ionizable monomers have enabled the manipulation of the volume phase transition temperature of these particles [114, 115]. Recently, pH-responsive microgel dispersions have been the subject of significant interest for development of advanced drug delivery vehicles. For example, Zhang et al [116], have studied the "rational design" of chitosan-based microgel particles containing methotrexate that are responsive to pH changes. They have shown that the

encapsulated drug can be released when the microgel particles are exposed to low-pH environments that caused the chitosan to swell. Similar research was conducted for a series of drugs such as doxorubicin [16], dibucaine [113], and benzylamine [117]. However, aside from directly utilizing the responsiveness of the microgel particles for the uptake and release of therapeutic drugs, there has been little work reported on functionalized microgel particles for the environmental stimuli triggered uptake and release of active chemical species such as rheology modifiers and nanometer sized inorganic components. This work can be applied towards novel interfacial engineering by environmentally tailoring the release of rheology modifiers, such as lecithin, to equilibrate oil-water interfaces and subsequently vary the viscoelasticity of the targeted surrounding fluid. Potentially, this functionalized microgel carrier-system could be used for the magnetic separation via the tuned release of ferrous nanoparticles from microgels. Some tailored applications of this prepared system may lie in oil spill clean-up as well as in biomedical and microfluidic systems. There also remains interest and a need to explore new approaches to uptake magnetic nanoparticles into the organic network to form organic-inorganic microcomposites. Many previous studies involve using polymers synthesized by co-precipitation and emulsion polymerizations methods to uptake magnetic nanoparticles. For example, Kondo et al [118], synthesized PNIPAm microgels using aqueous ferrofluids as reaction media, which resulted in low magnetic nanoparticles concentration immobilized inside the prepared PNIPAM microgels. Furthermore, additional routes have been reported via Pichot et al [119, 120], where they have prepared core-shell magnetic microgels with polystyrene- PNIPAm as the shell. One drawback of this type of approach is that the organic-aqueous interface entailed for

polymerization requires organic solvents, surfactants, and stabilizers that can be environmentally challenging to remove [121-123]. Very recently López-Cabarcos and co-worker [124] prepared thermosensitive microgels covered with superparamagnetic iron oxide nanoparticles. In their simple chemical approach the iron oxide nanoparticles were incorporated on the surface by the co-precipitation method in the presence of the pre-synthesized microgels.

In this study, we synthesize ionic microgel dispersions in which the particles undergo large reversible volume phase transitions in response to environmental stimuli such as temperature and pH. We demonstrate that a rheology modifier is adsorbed into the microgel particles owing to the large swelling transitions based on their environmental sensitivities. The effective release of the rheology modifiers through "sponge-like" porous gel network structures of the ionic microgel particles is investigated. Finally, we explore a reproducible facile approach to obtain organic-inorganic composites through physical adsorption of iron oxide nanoparticles into the porous colloidal microgel network through facile reversible pH variation.

2.5.1.2 Zwitterionic Microgels

The development of advanced multi-responsive and stable zwitterionic microgel dispersions consisting of both cationic and anionic functionalized monomer units has been a subject of significant interest, stemming from their distinctive swelling properties and their ability to "trap" diffused solutes inside governed by complex intrachain electrostatic interactions. For example, Tam *et al*. recently reported the preparation of biocompatible zwitterionic microgel systems synthesized from chitosan, carboxymethyl cellulose, and modified methyl cellulose polymerized via an inverse microemulsion

technique for the fast response drug release of procaine hydrochloride [125]. Aside from directly utilizing the responsiveness of the prepared zwitterionic microgel particles for the uptake and release of therapeutic drugs [126], there has been less reported on their ability for the environmental stimuli triggered adsorption and desorption of active chemical solutes, such as macromolecular surfactants. Some earlier efforts have been made to examine the effect of varying surfactant concentrations during polyelectrolyte microgel synthesis [127, 128] as well as the interaction of surfactant molecules with microgel particles [129-131]. However, there also remains interest and need to explore the influence of the adsorption of surfactant on swelling properties of multifunctional zwitterionic microgel particle dispersions since they have the tunable ability to adsorb the surfactant when the two are oppositely charged and then release the surfactant when the charge of the microgels are manipulated to the same charge as the surfactant via a switchable pH.

In this study, we design and synthesize multifunctional zwitterionic microgel dispersions in which the particles undergo extensive reversible volume phase transitions in response to environmental stimuli such as temperature and pH. Potentially, a tailored application for the zwitterionic microgel system present in this work may lie in the uptake and release of active species for applications such as oil spill remediation technologies. More specifically, the prepared particles can be applied towards novel interfacial engineering by equilibrating at oil-water interfaces, subsequently varying the interfacial tension between the salt water and crude oil phases, and selectively uptaking or releasing oil dispersants, such as dioctyl sodium sulfosuccinate (DOSS) surfactant. We demonstrate here that an anionic surfactant, DOSS, can be adsorbed into and released

from the zwitterionic microgel particle dispersion owing to their unique environmental sensitivities. To further explore the interaction between surfactant molecules and the prepared zwitterionic particle dispersions, the binding of cationic surfactant cetylpyridinium chloride (CPyCl) and nonionic surfactant Triton X-100 (TX-100) with our microgels is also investigated.

2.5.2 Structure of Colloidal Lattices of Microgels at the IL-Water Interfaces

In recent years, ionic liquids (ILs) have drawn significant amount of attention as tunable "green solvents" used in the interdisciplinary fields of biotechnology and chemistry due to their high thermal stability [132-134], non-flammability [135-137], extensive electrochemical window [138, 139] and negligible vapor pressure properties [140-142]. They are currently utilized in a vast array of applications including catalysis [143, 144], CO_2 absorption [145-147], gas storage [27, 148], and as promising solvents for selective extraction processes [149-151]. While recent work has established the versatility of ILs as novel extraction media, their efficient use in the extraction of chemically sensitive active species still remains largely absent. Thus, the implementation of emulsions with intrinsically large surface area is highly advantageous for the tailored development of IL-based extraction system [97, 152]. These formulated emulsions must be able to remain stable against coarsening via Ostwald ripening while maintaining the ability to demulsify in order to obtain the extracted product absorbed into the IL-phase. The task to form IL-water emulsions is challenging due to low interfacial tension derived from the inherently large miscibility of the two phases along with the highly structured IL-in-water interfaces resultant of charge hydration and correlations [153, 154].

Traditionally, surfactants have taken the spotlight for the preparation of thermodynamically stable IL-water microemulsions. However, for the design of selective extraction processes, most of the desired requirements are not met due to the inherent water solubility of most ILs leading to Ostwald ripening and ultimately emulsion destabilization [155, 156]. The employment of surfactants may also interact adversely with a variety of biomolecules inducing irreversible changes to the targeted bioproducts,

especially for the extraction of compounds such as lipids [157, 158], organic acid [159, 160], and amphiphilic proteins from biological fluids [98, 161, 162]. Meeting these requirements to develop a robust approach to create IL-in-water emulsions is highly sought-after for the advancement of IL-based extraction applications. Particle-stabilized emulsions, also referred to as "Pickering emulsions [85]," are surfactant-free metastable dispersions of two non-miscible fluids like oil and water. These emulsions display high stability, which makes them very attractive for storage applications. Recently, there has been growing interest in utilizing soft particles like microgels as emulsifiers for the design of responsive Pickering emulsions, which evolve "on demand" via an external stimulus [99, 163]. While previous works have established the adaptability and versatility of microgel particles in stabilizing oil-water interfaces, the details of its adsorption mechanism at these liquid interfaces and their interfacial packing conformation still remains a matter of much debate [164-168].

In this work, we demonstrate that soft stimuli-responsive composite microgel particles can be effectively utilized as an emulsifier to fabricate IL-in-water emulsions. The microgel particles that we used in this investigation contain a fluorescent polystyrene core embedded in a thermosensitive and pH-responsive gel-shell composed of poly(N-isopropylacrylamide-*co*-acrylic acid). The rationale behind the design of this composite particle system is that it allows non-invasive in-situ visualization of the structure of microgel-laden IL-in-water interfaces, while preserving their interfacial and multi-responsive properties. We investigate the impact of the microgel particles' charge and hydrophobicity with their emulsification performance by varying solution temperature and pH for formulated emulsions. The morphology of the adsorbed soft gel-particles is

characterized via direct macroscopic visualization, confocal microscopy observations, and cryo-SEM studies of the emulsion droplet interfaces. To determine the main structural parameters of these colloidal lattices, we have constructed Vornoi diagrams and have statistically analyzed the defect number, concentration, and configuration of various possible scenarios for the adsorption mechanism of prepared particles at the interface. Moreover, the self-assembled and densely packed layer of composite microgel particles at the IL-in-water interface does not hinder their potential application in IL-based extraction processes, as the interface remains permeable.

3. METHODOLGY

3.1 Materials

For the microgel synthesis, co-monomers N-isopropylacrylamide (NIPAm, Acros), N-[3-(dimethylamino)propyl] methacrylamide (DMAPMA, Sigma-Aldrich), acrylic acid (AAc, Sigma-Aldrich), and styrene monomer (Sigma-Aldrich), cross-linking regent *N,N'*-methylene-bis-acrylamide (MBAm, MP), initiator potassium persulfate (KPS, Acros), 2,2'-azobis (2-amidinopropane) (V-50, Wako) and the particle steric stabilization agent sodium dodecyl sulfate (SDS, Sigma-Aldrich) were all used in the polymerization without further purification. For the uptake and release of active species, L-α-Phosphatidylcholine (lecithin, Arcos), superparamagnetic iron oxide nanoparticles (Fe_3O_4-NP, Sigma-Aldrich) with hydrodynamic diameter of 10±5 nm (no further surface modification) dispersed in water, laboratory grade anionic surfactant dioctyl sodium sulfosuccinate (DOSS, Sigma-Aldrich), cationic surfactant cetylpyridinium chloride (CPyCl, Fluka), and nonionic Trition^{TM} X-100 (TX-100, Sigma-Aldrich) was all used as received. Ionic liquid 1-butyl-3-methylimidazolium bis(trifluoromethanesulfonyl)imide ([BMIM][NTf2], IoLiTec Inc.), water (HPLC grade, Fisher Scientific), and fluorescent dyes Pyrromethene 556 (PM-556, Exciton), Rhodamine B (TCI America) were also used as received. All solutions were prepared with HPLC grade water (Fisher Chemical).

3.2 Particle Synthesis

3.2.1 Ionic Microgels

Ionic microgel particles were synthesized via surfactant free precipitation polymerization. The synthesis was carried out in a 3-necked (125 mL) round bottom reaction vessel, fitted with a reflux condenser, a magnetic stirrer, a thermocouple and a nitrogen inlet. NIPAm (0.45 g, 85 wt. % of total monomer), DMAPMA (0.05 g, 10 wt. %), and MBAm (0.025 g, 5 wt. %), were added into the reaction vessel along with 50 g of water. In a separate vial, a cationic free-radical initiator V-50 (0.015 g) was dissolved in 2 g water. Then, the monomer solution was immersed in a water bath set at 70 °C. The reaction mixture was purged with nitrogen for 45 min. After the temperature reached equilibrium and the purge stage was complete, the initiator solution was introduced. The polymerization reaction was left to proceed while being purged by nitrogen gas for 7 hours. The microgel dispersion was then allowed to cool and was purified against HPLC grade water at room temperature.

3.2.2 Zwitterionic Microgels

Zwitterionic microgel particles with assorted compositions were synthesized via free radical precipitation polymerization. The synthesis was carried out in a 3-necked (250 mL) round bottom reaction vessel along with 150 mL of water, fitted with a reflux condenser, a magnetic stirrer, a thermocouple and a nitrogen inlet. Overall, the concentrations of NIPAm in the reaction mixtures were controlled at 82.97±0.21 mol% while the molar ratios of DMAPMA/AAc were adjusted as shown in Table 1. The concentrations of crosslinker and initiator in the reaction mixtures were kept at 2.5-3.0 mol% and 0.8-1.2 mol%, respectively. In a separate vial, the free-radical initiator KPS

was dissolved in 5 g water. This initiator solution was slowly added after the monomer mixture was immersed in a water bath set at 70 °C and purged with nitrogen for 30 minutes. The polymerization was left to proceed under nitrogen gas for 8 hours. After polymerization was complete, the microgel dispersion was then allowed to cool to room temperature and was subsequently dialyzed (Spectra/Por Membrane, MWCO: 12-13 kD) against deionized water changed daily for one week at room temperature to remove any residual monomers from the resulting reaction mixture.

Table 3.1 Monomer compositions used in the preparation of zwitterionic microgel (ZI-MG) particles.

	DMAPMA [mol %]	**AA [mol %]**	**NIPAm [mol %]**
ZI-MG (0.29)	3.06 %	10.60 %	82.92 %
ZI-MG (0.85)	6.12 %	7.23 %	83.18 %

3.2.3 Composite Microgels

Composite gel-particles are prepared in a two-step procedure. Firstly, a fluorescent polystyrene core is synthesized through emulsion polymerization. This synthesis was carried out in a 3-necked (250 mL) round bottom reaction vessel along with 150 mL of water, fitted with a reflux condenser, a magnetic stirrer, a thermocouple and a nitrogen inlet. Overall, the concentrations of styrene monomers in the reaction mixtures were controlled at 90.19±0.37 mol% while the NIPAm monomers were adjusted to be 9.79±0.21 mol%. The concentrations of PM-556 and initiator in the reaction mixtures were kept at 0.02-0.04 mol% and 0.08-1.2 mol%, respectively. In a separate vial, the free-radical initiator KPS was dissolved in 5 g water. This initiator solution was slowly added after the monomer mixture was immersed in a water bath set at 70 °C and purged with nitrogen for 45 minutes. The synthesis was left to proceed under nitrogen gas

for 8 hours. After reaction was complete, the mixture was then allowed to cool to room temperature and was subsequently purified against deionized water via centrifugation (Eppendorf 5810-R), followed by decantation and re-dispersion in fresh water solvent at room temperature. Secondly, a non-fluorescent environmentally-responsive microgel shell is grown around the previously synthesized core via free radical precipitation copolymerization. This synthesis was carried out in a 3-necked (125 mL) round bottom reaction vessel, fitted with a reflux condenser, a magnetic stirrer, a thermocouple and a nitrogen inlet. Typically, 40.5±0.11 mol% NIPAm monomer, 58.42±0.14 mol% AAc monomers, and 1.15±0.08 mol% MBAm, were added into the reaction vessel along with 100 g of water and ~0.2 g (determined via freeze-drying) of the fluorescent core. In a separate vial, a varying amount of KPS was dissolved in 2 g water. Then, the monomer solution was immersed in a water bath set at 75 °C. The reaction mixture was purged with nitrogen for 45 min. After the temperature reached equilibrium and the purge stage was complete, the initiator solution was introduced. The polymerization reaction was left to proceed while being purged by nitrogen gas for 5 hours. After polymerization was complete, the particle dispersion was then allowed to cool to room temperature and was subsequently dialyzed (Spectra/Por Membrane, MWCO: 12-13 kD) against deionized water changed daily for one week at room temperature to remove any residual monomers from the resulting reaction mixture.

3.3 Uptake and Release of Active Species

3.3.1 Lecithin Uptake and Release within Ionic Microgel Particles

Microgel aliquots were purified in water via mild centrifugation (Eppendorf 5810-R) followed by redispersion in fresh water solvent. This process was repeated three times. Each sample was prepared by mixing 0.20 g of lecithin with 3 mL of purified microgel dispersion in acidic (~pH 5) and basic (~pH 10) medium. Next, these mixtures were sonicated (VWR Ultrasonic Cleaner) for 15 min and left overnight on a mild oscillation desktop shaker (PR-12) at room temperature to ensure complete lecithin dispersion and uptake into microgels. Subsequently, the samples were centrifuged (5,000 rpm for 15 min) to sufficiently sediment the microgel particles in the samples. Afterward, the supernatants were collected and centrifuged to remove any of the non-absorbing lecithin prior to further testing. Next, the remaining microgel particle sediment of both samples was redispersed in strong base (~pH 12) medium. Then, both mixtures were agitated and left to proceed one hour on a desktop shaker to release the absorbed lecithin. Finally, the mixtures were centrifuged and the aqueous supernatants were collected for additional qualifications.

3.3.2 Uptake of Fe_3O_4-NPs with Ionic Microgel Particles

Samples were prepared by mixing 2.00 mg of Fe_3O_4-NPs with 500 μL of purified microgel dispersion in pH 7 medium. Next, these mixtures were sonicated (VWR Ultrasonic Cleaner) for 15 min at room temperature to ensure complete mixing. Subsequently, the samples were vacuum filtered with 0.1 μm pore sized membrane filters to sufficiently remove any unattached Fe_3O_4-NPs. Next, the samples were collected off of the filter paper and redispersed in 3 mL of pH 7 HPLC grade water. Then, the mixture

was agitated for over 1 hour on a desktop shaker to ensure uniform solution. Four 500 μL aliquots of the mixture were taken out following the agitation to be modified to various solution pH via dilute 0.1 M HCl and KOH.

3.3.3 Surfactant Adsorption within Zwitterionic Microgel Dispersions

Zwitterionic microgel aliquots were purified in water via mild centrifugation (Eppendorf 5810-R), followed by decantation and re-dispersion in fresh water solvent to further remove any residual impurities. Each sample was prepared by mixing a known volume of targeted surfactant solution with 0.027±0.003 g of purified microgel particles dispersed in 3 mL of water in an acidic (~pH 3) or basic (~pH 11) medium. Next, these samples were sonicated (VWR Ultrasonic Cleaner) for 15 minutes and left overnight to equilibrate on a mild oscillation desktop shaker (PR-12) at room temperature. The aqueous samples were subsequently collected for additional qualifications.

3.4 IL-in-Water Emulsion Preparation

Stock solutions of prepared composite microgel particles at the desired solid content were prepared via dilution. When required, the pH was adjusted via the gradual addition of 0.1 M HCl or KOH. The background electrolyte added was 10 mM KCl. In a typical batch, emulsions were prepared using an ultrasonic processor, Ultra Turrax T25, at constant speed (8500 rpm), sonicating the dispersion of composite microgel particles in water with [BMIM][NTf2] (weight ratio 8:2) for 45 seconds at room temperature. The total weight of each emulsion was ~5 g. Moreover, facile dilution tests and visual inspections of the creaming or sedimentation behavior due to the density mismatch between IL and water were applied to determine the emulsion type. Prior to qualifications all emulsions were left to equilibrate overnight at room temperature.

3.5 Characterization

3.5.1 Physical Particle Characterization

The mean hydrodynamic diameter, electrophoretic mobility, and ζ-potential of the particles were determined via dynamic light scattering (DLS) and electrophoretic light scattering techniques using PSS NICOMP 380 ZLS. When required, the pH was adjusted via the gradual addition of 0.1 M HCl or KOH. Scanning electron microscopy (SEM) images of the particles were obtained using FEI/Philips XL30 Environmental FEG SEM. Confocal microscopy of the stationary swelled and deswelled microgel particles dyed with Alexa Fluor 488 (Invitrogen) were imaged and processed utilizing Leica TCS SP5 and ImageJ software, respectively. A TA Instruments AR-G2 rheometer equipped with a 60 mm, 1° cone was used to measure the viscosity and other rheological properties of all solutions. Transmissions electron microscopy (TEM) images of composite microgels were obtained via Tecnai F20 (FEI).

3.5.2 Spectroscopy Characterization

The lecithin uptake and release detection analyses were attained by Fourier transform infrared spectroscopy (FTIR) employing a Bruker IFS 66v/S apparatus, mounted with Harrick ATR-GATR sample accessory.

To detect DOSS adsorption, ^{1}H nuclear magnetic resonance spectroscopy was used. All solution samples were centrifuged at 10,000 rpm for 45 min to sufficiently sediment the microgel particles in the samples. Afterward, the aqueous supernatants were collected for ^{1}H NMR analysis to quantify residual DOSS amounts. For the preparation of each individual NMR sample, 600 μL supernatant fluid was mixed with 30 μL (4.36 mM) 4,4-dimehtyl-4-silapentane-1-sulfonic acid (DSS) solution and 70 μL D_2O in a 5.0

mm NMR tube, giving a total sample volume of 700 μL. All ^{1}H NMR experiments were performed on Varian VNMRS 500 MHz instrument with a triple-resonance probe operating in triple-resonance ($^{1}H/^{13}C/^{15}N$). Standard water suppression was used and all spectra were collected with spectral width of 16.0 ppm, an acquisition time of 3.0 seconds, a relaxation delay of 3.0 seconds, and 64 scans with the ^{1}H resonance of DSS peak (0 ppm) as reference.

Solution depletion method was utilized to quantify the CPyCl adsorption. Each sample was prepared by following the previously described method. Upon reaching the binding equilibrium CPyCl concentration, the microgel particles were separated from solution by centrifugation at 10,000 rpm for 45 min. The equilibrium surfactant concentrations of the collected supernatants were then obtained from a calibration curve of absorbance versus surfactant concentration performed via Perkin Elmer Lambda 18 UV-Vis spectrometer. The wavelength used was 258 nm [169], which corresponds to the maximum absorbance peak for CPyCl. When required, the pH was adjusted via gradual addition of 0.1 M HCl or KOH.

3.5.3 Interfacial Colloidal Characterization

The interfacial colloidal arrangement was imaged using confocal laser scanning microscope Leica TCS SP5 under controlled temperature conditions. The fluorescence intensity spectra were acquired via a wavelength scan over the range of 500-599 nm for the composite microgel particles and dye adsorption under excitation at 488 nm. The spectra for the aqueous phases after the emulsification were obtained under the same laser intensity and at nearly the same depth within the prepared samples. The particle

coordinate center positions, the fast Fourier transform (FFT) pattern, and the Voronoi diagrams were analyzed and constructed via ImageJ and Fiji software.

The cryo-SEM experiments were conducted using FEI Nova 200 Focused Ion Beam and SEM equipped with Gatan Alto 2500 cryogenic cooling stage and vacuum transfer chamber. About 0.5 μL drop of the emulsion was placed on top of a 1 mm diameter copper cylinder that was mounted to the cryo-shuttle that was attached to the end of the transfer rod. The whole assembly was plunge frozen in liquid nitrogen slush, which was made by partially evacuating a chamber with liquid nitrogen. The sample was held in the liquid nitrogen slush until bubbling around the rod ceased (about 30 seconds). Subsequently, the freezing chamber was evacuated and sample was moved to the cooled and evacuated transfer chamber. To reveal inside of the IL-in-water emulation, the top of the frozen drop kept at about -140 to -160°C was fractured off using a cooled blade. To provide a better view of microgel particles at the drop-water interface, a layer of water was selectively sublimated by raising temperature of the sample within the evacuated transfer chamber to -90°C for 30 minutes. Afterwards, the sample temperature was again decreased to -140 to -160°C and sample was in situ sputtered coated with a thin grounding gold-palladium layer. The grounded samples were transferred to the cooling stage mounted within the SEM chamber and kept at -140 to -160°C for the remainder of the experiment. SEM imaging was performed with energy of 2 to 5 keV and current of 0.21 to 0.4 nA with a working distance of 5 mm.

4. RESULTS AND DISCUSSION

4.1 Development of Multifunctional Microgels

4.1.1 Synthesis and Characterization of Ionic Microgels

Figure 4.1*a* exhibits the temperature dependence of the average hydrodynamic diameter of the pure PNIPAm microgel particles at pH 9. The proposed fundamental mechanism which governs this thermally induced volume phase transition temperature (VPTT) can be attributed to the hydrophobic force associated to the dehydration of the PNIPAm gel at higher temperatures [5, 170]. In the analysis, VPTT is defined as the temperature at which the first derivative of the hydrodynamic diameter versus temperature curve reaches a peak value. The VPTT for the pure PNIPAm microgels have demonstrated a temperature transition at 32 °C, which is in good concurrence with the literature [5, 41, 91]. Furthermore, the incorporation of an ionic co-monomer, DMAPMA, was validated in order to synthesize thermosensitive microgels with pH-

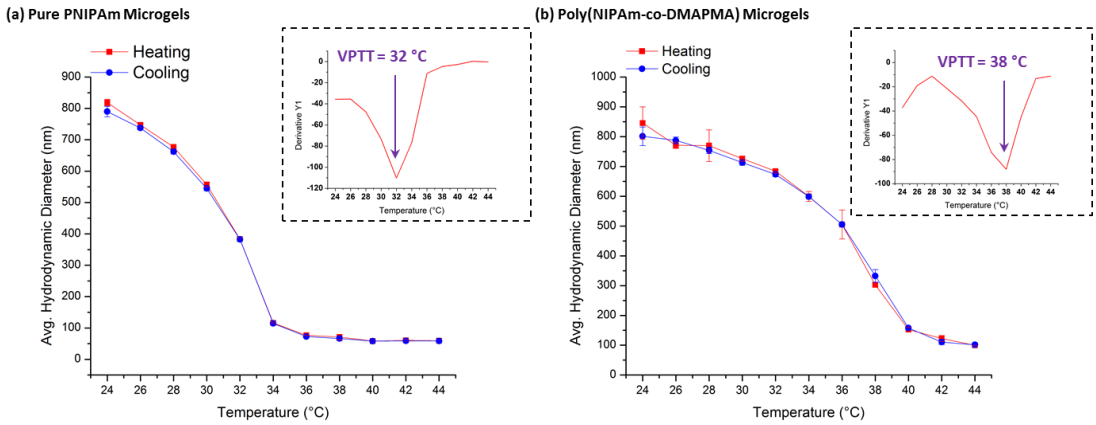

Figure 4.1 The temperature dependence of the avg. hydrodynamic diameter of (a) pure PNIPAm microgels and (b) poly(NIPAm-*co*-DMAPMA) microgel particles at pH 9 obtained via DLS. Inset: The thermally induced volume phase transition temperature (VPPT) is defined as the temperature at which the 1st derivative of the avg. hydrodynamic diameter versus the temperature curve reaches a minimum value.

responsiveness. Figure 4.1*b* demonstrates the dependence of the average hydrodynamic diameter for the prepared ionic poly(NIPAm-*co*-DMAPMA) microgel particles as a function of temperature at pH 9.

The apparent shift to 38 °C in the VPTT for the ionic microgel particles was postulated to be due to an increase in both the electrostatic interaction between the polymer chains and the osmotic pressure generated through the addition of DMAPMA. This aligns with similar research conducted by Kratz and co-workers [69], which focused on the influence of acrylic acid content on the swelling behavior of poly(NIPAm-*co*-acrylic acid) microgels. Thus, the addition of carboxyl groups distributed throughout the PNIPAm network could possibly cause the charge repulsion and osmotic pressure to counteract and suppress the collapse ability of PNIPAm at 32 °C.

Table 4.1 The avg. hydrodynamic size and polydispersity index (PDI) of poly(NIPAm-*co*-DMAPMA) microparticles at different temperatures determined by DLS at pH 9.

Temperature [°C]	Hydrodynamic Size [nm]	PDI
24	823	0.128
28	762	0.101
32	679	0.094
36	505	0.118
40	155	0.099
44	101	0.172

However, as the temperature increases the hydrophobic interactions can still overcome the electrostatic repulsion caused by the addition of DMAPMA and the polymer network can reach its final collapsed particle size above 38 °C. Furthermore, we observed that over the temperature range from 24 °C to 44 °C, the size distribution measured as

polydispersity index (PDI) does not vary considerably even though the average hydrodynamic size of ionic poly(NIPAm-*co*-DMAPMA) microgels at 44 °C reduced to 1/8 of their average size at 24 °C (Table 4.1).

Figure 4.2*a* represents the overall measured swelling-deswelling hydrodynamic diameter trend of the ionic microgel dispersions as a function of pH at room temperature. It was determined that these microgels exhibit sensitivity to pH variations and show near reversible swelling-deswelling behavior.Under the pH range of 2 to 7, it was proposed that the amine groups contained within the microgel dispersions were fully protonated and thus the electrostatic repulsion between the polymer chains and osmotic pressure mainly governs the extent of particles swelling [171]. The decline in the hydrodynamic diameter between pH 7 to 12 was postulated to be the loss of positive charge within the gel networks, thus internally rendered the microgel particles neutral to slightly negative. The corresponding electrophoretic mobility results were also gathered to further authenticate the above data, shown in Figure 4.2*b*.

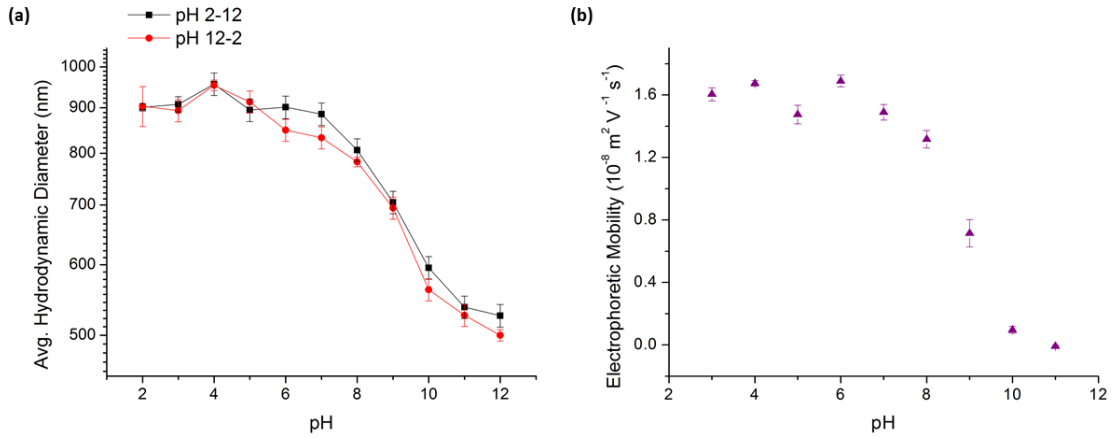

Figure 4.2 The dependence of poly(NIPAm-*co*-DMAPMA) microgels: (a) reversibility of the avg. hydrodynamic diameter via DLS and (b) electrophoretic mobility results measured by ELS on pH at room temperature.

These measurements serve, as an indication of the ionic microgel particle surface charge, thus justifying the surge in mobility was resultant from the protonation of the amine groups contained in the particles between pH 2 to 7. Figure 4.3 shows the effect of pH on the VPTT of the prepared ionic poly(NIPAm-*co*-DMAPMA) microgel particles. At constant temperature, the relatively higher average hydrodynamic size values of the prepared ionic microgels at pH 4 should be induced by the protonation of dimethylamino groups within the colloidal microparticles. Therefore, the decrease of the average hydrodynamic diameter for the prepared ionic poly(NIPAm-*co*-DMAPMA) microgels at pH 4 was noticeably slower, corresponding to a higher VPTT.

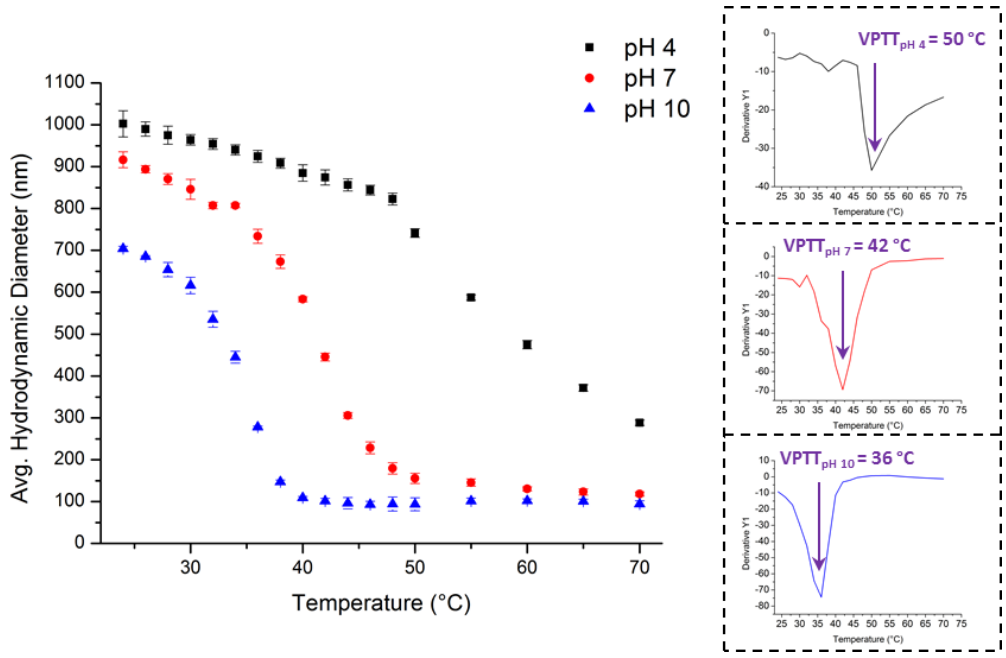

Figure 4.3 The temperature dependence of the avg. hydrodynamic diameter of poly(NIPAm-*co*-DMAPMA) microgels at pH 4, 7 and 10 obtained via DLS. Inset: Shows the VPTT of the prepared sample at various pH as a function of temperature.

To further investigate the influence of the copolymer concentration on the VPTT of the prepared charged particles, a series of monodisperse poly(NIPAm-*co*-DMAPMA) microgels were synthesized with varying DMAPMA content (5%, 10%, and 15 wt. % of the total monomer) with identical amount of MBAm (5 wt. %). In order to achieve the desired total monomer content, the concentrations of NIPAm monomer were adjusted accordingly. The determined VPTT at pH 9 of the colloidal microgels prepared with 5%, 10% and 15 wt. % of DMAPMA were observed to be 34 °C, 38 °C, and 44 °C, respectively. This phenomenon is likely due to the intricate balancing between hydrophobic attractions of the NIPAm and the repulsive electrostatic interactions contributed by the increasing amount of amino group derived from the DMAPMA moieties happening during the particle shrinking process.

Confocal microscopy was used to further verify the above DLS findings of dispersed ionic microgel particles. Figure 4.4 shows the confocal images of the microgel particles modified to solution pH 5 and 10 at room temperature, with the presence of Alexa Fluor-488 (AF 488) dyes.

The determined particle size via post-image processing correlated well with the DLS experimental results. Additionally, the dependence of swelling behavior in response to pH variation was accompanied by an observed reduced fluorescent intensity of the stationary microgel particles when changing from pH 5 to 10. One hypothesized explanation for this phenomenon is that the microgel particles will become increasingly hydrophobic with an increase in pH. Thus, at pH 10, the strongly hydrophilic AF 488 dyes [172, 173] are less likely to be absorbed into the hydrophobic microgel particles corresponding to the observation of decreased fluorescence intensity from within.

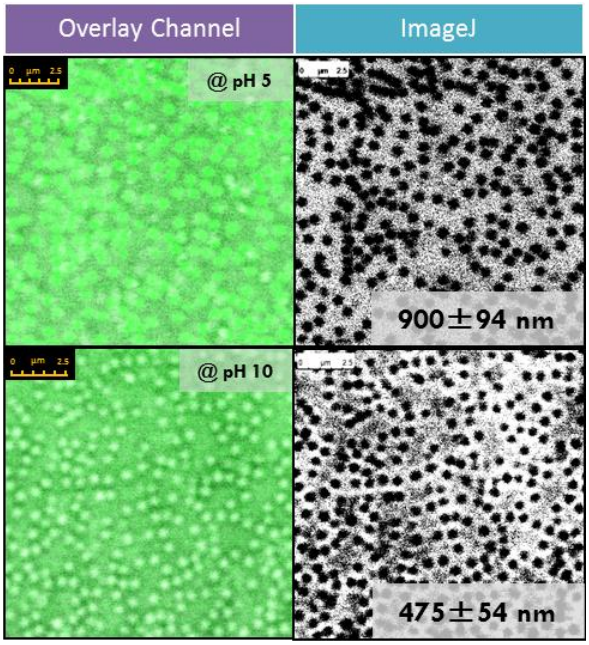

Figure 4.4 Confocal microscopy images of the avg. hydrodynamic diameter of stationary swelled poly(NIPAm-*co*-DMAPMA) microgels prepared in pH 5 and 10 solution at room temperature.

Overall, the pH-responsive swelling-deswelling trends of these prepared microgel particles agree with the observations of ionic microgel particles reported by Amalvy et al [2]. The main difference being that, in the earlier work, they employed emulsion polymerization of 2-(diethylamino) ethyl methacrylate (DEA) with the incorporation of surfactant, rather than the utilization of DMAPMA and PNIPAm via surfactant-free precipitation polymerization. Furthermore, other work on DMAPMA-based bulk hydrogels has presented analogous swelling trends with pH variations [174, 175]. Therefore, microgel particle dispersions containing DMAPMA can be proposed as an attractive alternative compared to the more commonly reported DEA copolymerized microgel particles [103, 176] and DMAPMA-based bulk hydrogels.

4.1.2 Synthesis and Characterization of Zwitterionic Microgels

Poly(DMAPMA) and poly(AAc) have been widely used as hydrophilic building blocks in multifunctional polymers [177-179]. In order to integrate cationic and anionic microgel functionalities, DMAPMA and AAc monomers have been copolymerized with NIPAm successfully to synthesize zwitterionic microgel (ZI-MG) dispersions. Figure 4.5 represents the overall normalized swelling-deswelling hydrodynamic diameter trends (*left*) of the poly(NIPAm-*co*-DMAPMA-*co*-AAc) microgel particles with varying fractions of anionic and cationic functional groups and their corresponding electro-kinetic potential (*right*) as a function of pH at room temperature. It is observed that a steep swelling transition occurred for the ZI-MG particle dispersions with increasing acidity between the isoelectric point (IEP) to pH 3. This swelling segment is ascribed to strong electrostatic repulsion generated among the polymer chains due to the presence of fully protonated amine groups (the pk_a of DMAPMA polymer is 8.8 [180]) synthesized within the prepared microgels. Alternately, the deprotonation of the residual carboxyl groups (the pk_a of AAc polymer is 4.25 [181]) distributed within the gel network is postulated as the primary mechanism responsible for the increase in particle size with rising basicity past the IEP. To elaborate, the electrostatic repulsion generated between the negatively charged carboxylic groups leads to an increase in the hydrophilicity among the gel network in turn triggering the prepared microgel particles to be capable of uptaking larger amounts of polar solvent [61].

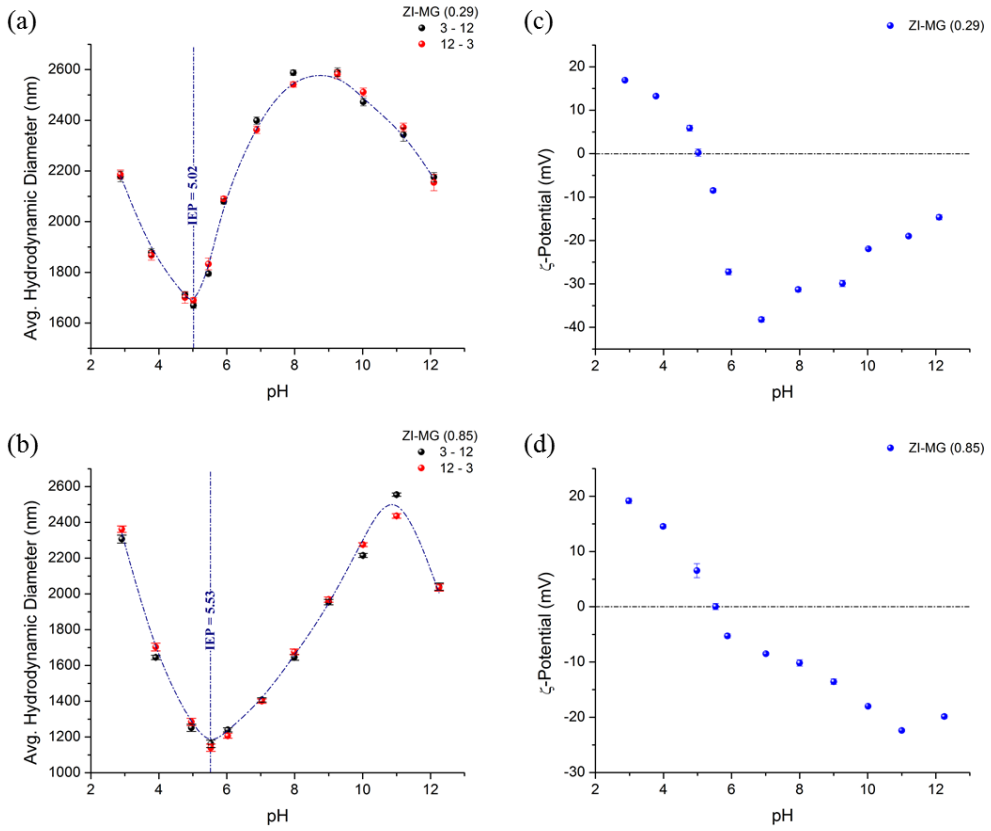

Figure 4.5 Effect of pH on the variation in avg. hydrodynamic diameter (a-b) and ζ-potential (c-d) for ZI-MG particles studied at room temperature: (a,c) ZI-MG (0.29); (b,d) ZI-MG (0.85). Dashed lines are applied as indicators to denote both the IEP and the zero point of the ζ-potential.

Furthermore, these prepared ZI-MG particles exhibit the sharpest average hydrodynamic diameter contraction around the IEP. This is attributed to charge

neutralization, which leads to semi-collapsed particles in the aqueous medium causing the microgels to shrink to a minimum size at the IEP [125]. Intriguingly, the IEP can be engineered to shift towards lower pH values (from 5.5 to 5.0) via facile reduction of the molar ratio between DMAPMA and AAc monomers (from 0.29 to 0.85) within the prepared ZI-MG particles. This IEP manipulation effect is possibly due to the excessive number of deprotonated carboxylate moieties (supplied by AAc content) compared to the number of protonated amine moieties (supplied by high DMAPMA content) within the prepared ZI-MG particles. Therefore, the IEP is reached by protonating excess carboxylate functional groups not previously neutralized by the amine functional groups via increasing acidity. The obtained electro-kinetic potential measurements, as displayed in Figure 4.5*c-d*, correlated well with the results determined for the variation in

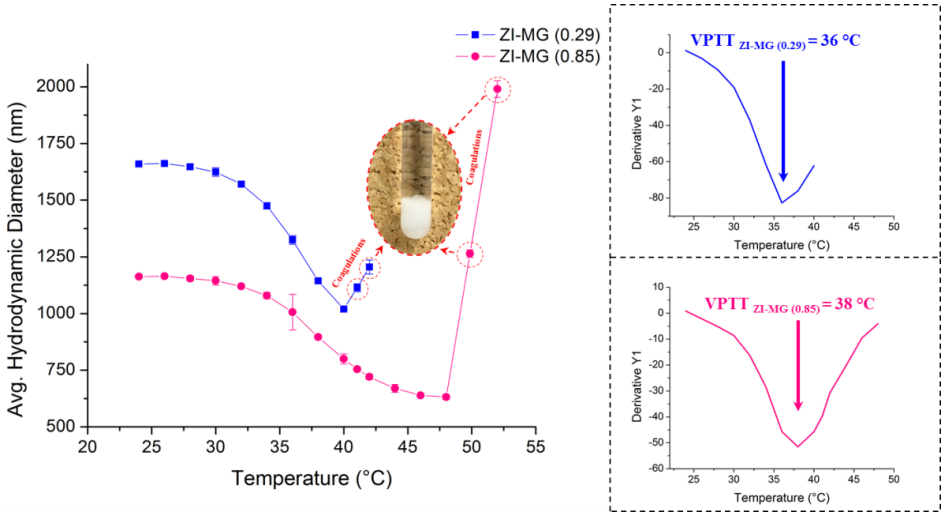

Figure 4.6. Temperature dependence of the average hydrodynamic diameter of ZI-MG particles with various compositions measured at the pH of their corresponding IEP. Inset: the thermally induced VPTT is defined as the temperature which the first derivative of the hydrodynamic diameter versus the temperature curve reaches a minimum value.

hydrodynamic diameter size as a function of pH. As expected, the net charge of the prepared particles is zero at the IEP and the particles demonstrate gradual zwitterionic swelling behaviors on either side of the IEP while carrying an excess net positive or negative charge due to the electrostatic repulsions and the osmotic pressure generated within the microgels via the counter ions. To further investigate the influence of the copolymer concentrations on the prepared ZI-MG particles, the temperature-induced phase transition of cross-linked microgel systems was evaluated. Figure 4.6 displays the temperature dependence of the average hydrodynamic diameter of ZI-MG with varying compositions obtained at their corresponding IEP.

Under these established experimental conditions, the synthesized ZI-MG (0.29) and ZI-MG (0.85) particles demonstrated gradual deswelling as a function of temperature in the absence of extensive particle coagulations below 40 °C and 48 °C, correspondingly. In addition, we found that the size distributions measured as polydispersity indices (PDI) do not vary substantially even though the mean hydrodynamic size of the ZI-MG (0.29) and ZI-MG (0.85) at 40 °C and 48 °C were reduced to $^{3}/_{5}$ and $^{1}/_{2}$ of their average size at 24 °C, respectively when heated (Table 2).

Table 4.2 Average hydrodynamic size and polydispersity index (PDI) of ZI-MG microparticles at various temperatures determined via DLS at the isoelectric point (IEP).

Temperature [°C]	**ZI-MG (0.29)**		**ZI-MG (0.85)**	
	d(h) [nm]	**PDI**	**d(h) [nm]**	**PDI**
24	1659 ± 3	0.067	1163 ± 8	0.048
28	1647 ± 11	0.101	1155 ± 10	0.011
32	1571 ± 9	0.125	1120 ± 9	0.055
36	1324 ± 18	0.172	1006 ± 68	0.147
40	1020 ± 5	0.138	800 ± 22	0.131
44			670 ± 14	0.155
48			631 ± 12	0.185

The proposed fundamental mechanism that governs this thermally induced gel collapse is the intraparticle hydrophobic interaction among the cross-linked amphoteric chains due to the incorporation of NIPAm monomer units, which upon polymerization, have a volume phase transition temperature (VPTT) of 32 °C [91].

Furthermore, the formation of ion pairs in the presence of hydrophilic segments, consisting of ionic co-monomers, such as DMAPMA and AAc monomer units, should

trigger an increase in the VPTT [182]. To confirm the above assertions, the VPTT's of all ZI-MG were determined by attaining the peak values of the first derivative of the hydrodynamic diameter versus temperature curve. The insets on Figure 4.7 illustrate the VPTT of ZI-MG (0.85) and ZI-MG (0.29). The slight shift to 38 °C in the VPTT for the more symmetrically composed ZI-MG (0.85) particles is assumed to be predominantly influenced by the increased formation of ion pairs. However, the variation in the magnitude of the mean hydrodynamic diameter for ZI-MG (0.85) is smaller in comparison to ZI-MG (0.29) due to having a higher effective cross-linking density, which consequently reduces its flexibility and swelling potential. Figure 3 shows the effect of pH on the VPTT of the prepared ZI-MG (0.85) particles. The average hydrodynamic size values at pH 11 are substantially larger than those at pH 3 as a function of temperature. In addition, the decrease of the mean hydrodynamic diameter for the prepared ZI-MG (0.85)

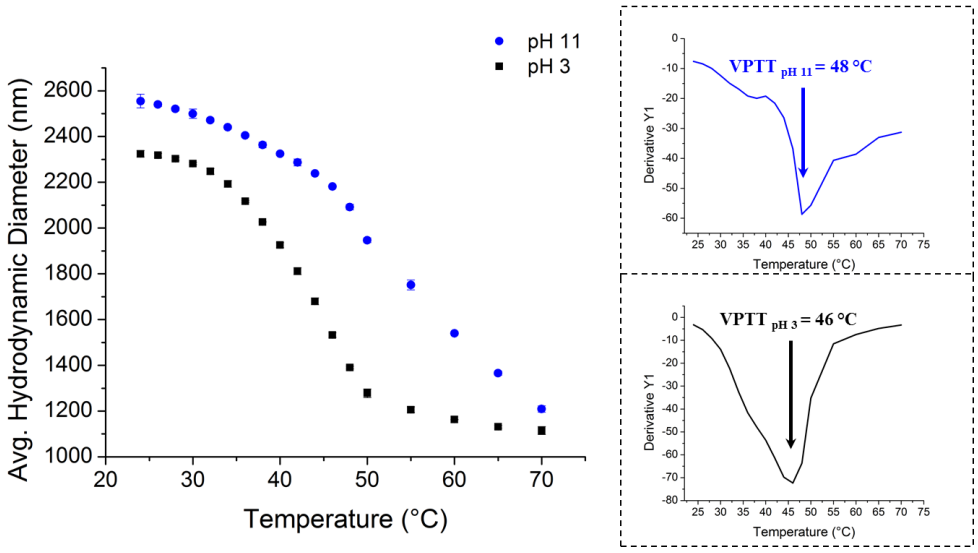

Figure 4.7. Temperature dependence of the average hydrodynamic diameter of ZI-MG (0.85) particles measured at pH 3 and 11 obtained via DLS. Inset: shows the VPTT of the prepared sample at different pH as a function of temperature.

at pH 11 was noticeably more gradual, resultant in a slightly higher VPTT.

This phenomenon is likely due to the intricate balancing between hydrophobic attractions of the NIPAm and the strong electrostatic repulsion contributed by the relatively higher concentration of anionic functional groups resulting from the AAc moieties within the colloidal microparticles throughout the particle shrinking process. Overall, the thermo-responsive swelling-deswelling trends of those prepared ZI-MG particles agree with the observations of zwitterionic nanogels reported by Kokufuta et al [183]. The main difference being that, in the aforementioned work, they synthesized nano-sized gel particles by aqueous redox polymerization of AAc and 1-vinylimidazole (VI) in the presence of sodium dodecylbenzene sulfonate (SDBS) as a surfactant.

Additionally, SEM imaging was utilized to capture the surface topography of dried microgels on mica substrates shown in Figure 4.8. The average dried particle sizes for ZI-MG (0.29) and ZI-MG (0.85) processed via ImageJ software are estimated to be 151.1±2.3 nm and 154.9±5.7 nm, respectively.

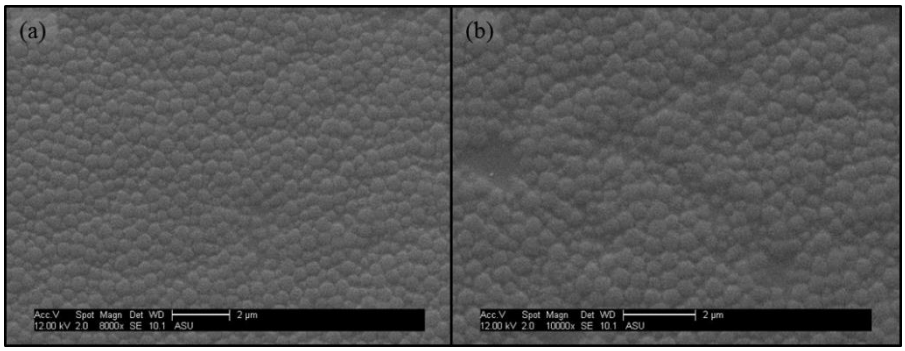

Figure 4.8. SEM images of dried microgel particles on silicon wafers for ZI-MG particles prepared with various mole ratios: (a) ZI-MG (0.29) and (b) ZI-MG (0.85).

4.1.3 Synthesis and Characterization of Composite Microgels

To verify the environmental-responsiveness of the prepared composite particles, the average hydrodynamic diameter of these particles as a function of both pH and temperature was characterized via dynamic light scattering. Figure 1 illustrates that at room temperature, the size of the composite microgel particles swell continuously from pH 4 to higher pH. This steep swelling transition originates from the deprotonation of the residual carboxyl groups distributed within the gel network of the composite shell. As expected, at pH values less than 4 (pka of AAc polymer is 4.25 [184]), the prepared composite particles are largely uncharged as an equilibrium size of the particles is set through the intricate balance among the elasticity of the crosslinked gel-network and the internal osmotic pressure of the hydrated acrylic acid monomers [45, 185, 186]. On the other hand, at pH values greater than 4 the electrostatic repulsion generated between the negatively charged carboxylic groups leads to an increase in the hydrophilicity among the gel network in turn triggering the prepared composite particles to be capable of uptaking larger amounts of polar solvent [187] and a larger equilibrium hydrodynamic size results. The correspondingly electrophoretic mobility results were also obtained to illustrate the charging of the composite microgel particles as residual carboxyl moieties are ionized at higher pH, shown in the inset of Figure 4.9.

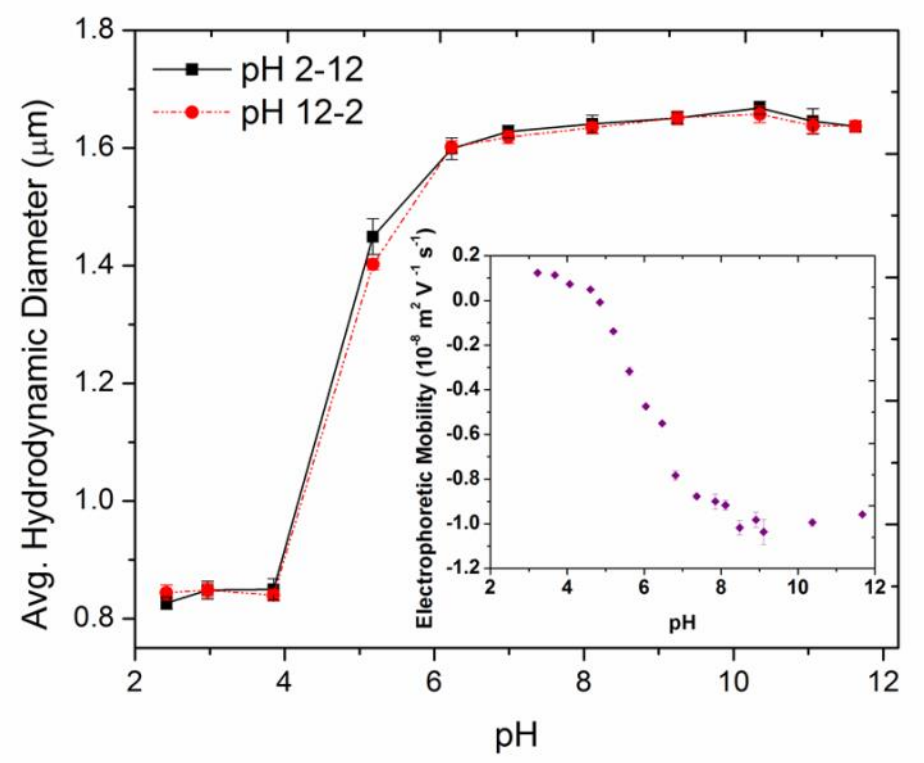

Figure 4.9 Illustrates the pH dependence of the average hydrodynamic diameter of the composite microgel particles in an aqueous dispersion at room temperature. Inset: displays the pH dependence of the electrophoretic mobility of the prepared particles.

We also investigated the temperature-induced phase transition of composite microgel particle systems. For neutrally charged composite particles, at pH 3, we found a volume phase transition temperature (VPTT) of 33 °C, which shifts to a higher temperature and broadens with increasing pH, displayed in Figure 4.10. These characterization measurements indicate the incorporation of a fluorescent polystyrene core does not alter the environmentally responsiveness of the prepared composite gel-particles.

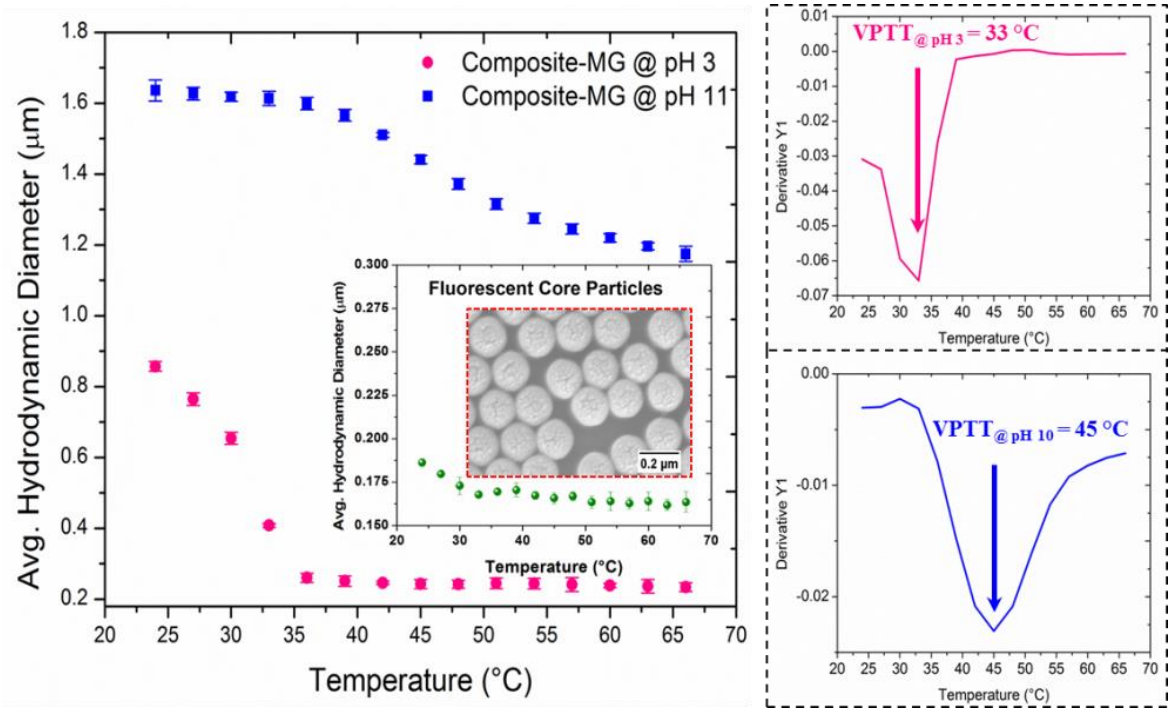

Figure 4.10 Temperature dependence of the average hydrodynamic diameter of the composite microgel particles measured at pH 3 and pH 10. Leftmost inset: shows the SEM image of dried fluorescent core particles along with the average hydrodynamic diameter of those particles as a function of temperature. Right insets: the thermally induced VPTT is defined as the temperature which the first derivative of the mean hydrodynamic diameter versus the temperature curve reaches a minimum value.

4.2 Uptake and Release of Active Species into and from Multifunctional Microgels

4.2.1 Ionic Microgels

4.2.1.1 Uptake and Release of Lecithin

The gel network structure of the prepared particles and their ability to endure large swelling-deswelling transitions allows small molecules, such as lecithin, to be incorporated and later released from the microgel interior. The release of lecithin can potentially be applied towards modifying the viscoelasticity of a targeted fluid which equilibrates at the oil-water interface. Figure 4.11 displays the snapshot images of the supernatants collected from the lecithin uptake and release.

For the uptake of lecithin, the presence of clear supernatant was observed for the sample prepared at pH 5 prior to the strong base-wash elution process (Fig. 4.11*a*), whereas a hazy supernatant was witnessed for the sample prepared at pH 10 (Fig. 4.11*b*). Furthermore, for the release of lecithin post strong base-wash, the presence of a milky supernatant was attained for the sample initially prepared at pH 5 (Fig. 4.11*c*), while a mostly lucid supernatant was obtained for the sample initially prepared at pH 10 (Fig. 4.11*d*).

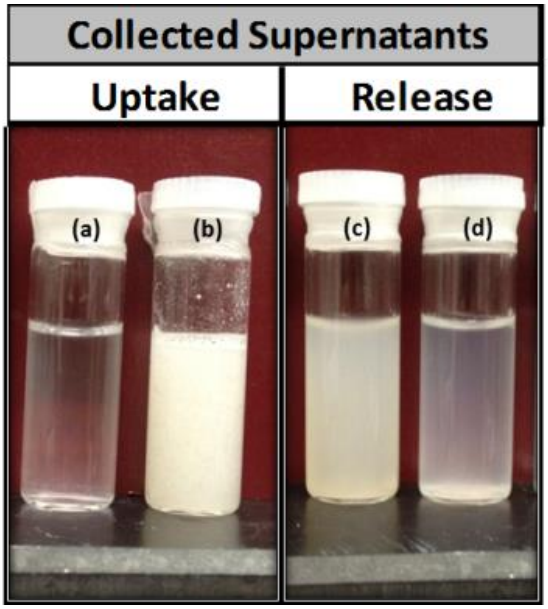

Figure 4.11 Snapshot images of the supernantants collected from lecitihin uptake and release via poly(NIPAm-*co*-DMAPMA) microgel particles: (a) uptake supernatant obtained from the sample initially prepared at pH 5 and (b) uptake supernantant obtained from the sample initially prepared at pH 10 and (c) release supernatant obtained from the sample initially prepared at pH 5 and (d) release supernatant obtained from the sample initially prepared at pH 10.

FTIR measurements were utilized to validate the uptake of the lecithin from those collected supernatants. Figure 4.12*a-b* depicts the FTIR absorption results of the supernatants via the designed uptake and release experiment. It was interpreted from the results that the incorporation and release of lecithin was successful for the microgel

dispersions initially modified to be pH 5, evidenced by the distinct infrared spectra which corresponded with known literature [188].

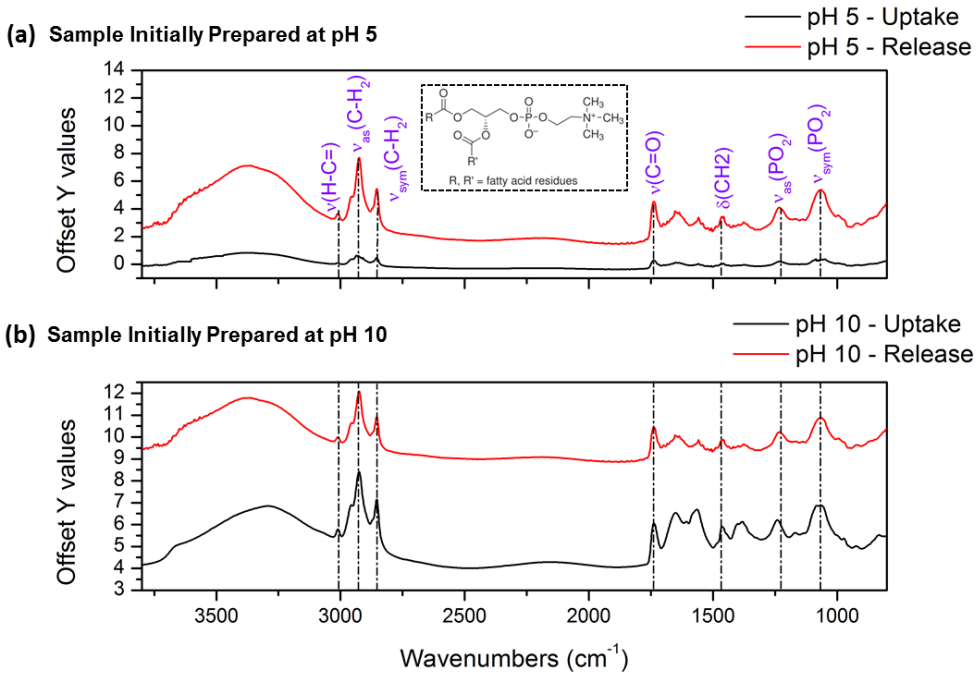

Figure 4.12 Normalized FTIR measurements of the collected supernatants from lecithin uptake and release via poly(NIPAm-*co*-DMAPMA) microgels: (a) sample initially prepared at pH 5 and (b) the sample initially prepared at pH 10.

To further authenticate the previous FTIR results, rheology measurements of those supernatants were also performed. It was noted, in the presence of lecithin, shear-thinning behaviors were observed on the viscosity of a water-based fluid as shear rate increases. Figure 4.13*a-b*, displays the fluid viscosity as a function of shear rate for the collected supernatants from the lecithin uptake and release. The supernatant viscosity of the sample initially altered to pH 5 was efficient for the lecithin uptake due to dramatic increases in shear-thinning documented prior and following of the strong base-wash. In contrast, the adverse rheological behaviors were established from the supernatants of the microgel samples adjusted to be initially at pH 10.

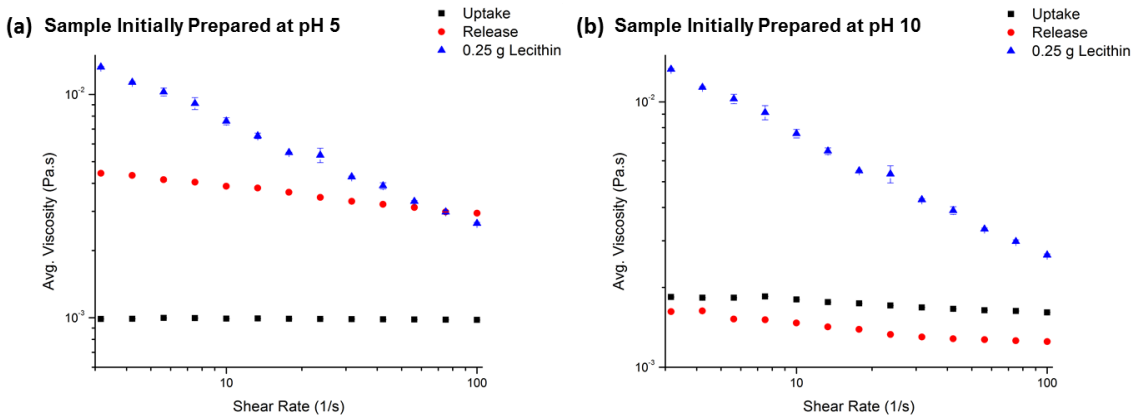

Figure 4.13 Rheology measurements of the obtained supernatants from lecithin uptake and release via poly(NIPAm-*co*-DMAPMA) microgels: (a) sample initially prepared at pH 5 and (b) the sample initially prepared at pH 10.

Possible mechanism that dictates this absorption process can be related to the dominant "driving forces" derived from the ionic properties and the associated fundamental interactions of the prepared microgels coupled with osmotic pressure balancing. To further elaborate, lecithin molecule is amphoteric in nature, hence it has both amine and carboxylic acid groups that can either donate or accept a proton based on its isoelectric point of 3.3-4.6 [189, 190]. Therefore, from pH 4 to 7, during the designed entrapment process, the lecithin molecules carry a negative charge as result of being above the aforementioned isoelectric point. This is vital to note, since in this pH range the amine groups contained within the prepared ionic particles are fully protonated and the long-range electrostatic interaction becomes highly attractive to the negatively charged lecithin molecules. Moreover, the presence of the counterions can establish an osmotic pressure balancing between the interior and exterior of the microgels contributing to particle swelling with water upon uptake [28]. Thus, the extent of swelling was hypothesized to be dependent on the concentration of fixed ionic groups within the gel network, the degree of ionization of the charged groups, as well as the electrolyte

concentration in the continuous phase. In addition, when the latter is more dominant, the ionic osmotic pressure difference between the particle interior and exterior would become relatively small, and the swelling would be dictated via the osmotic pressure affiliated with the neutral part of the network [129, 191]. In the highly basic pH range, the microgel network is internally rendered slightly negative which in turn acts to repulse the encapsulated negatively charged lecithin resulting in a "squeezing" release process.

4.2.1.2 Formation of Composites based on Ionic Microgel Particles and Fe_3O_4-NPs

In this study we explored a facile approach to obtain polymer-inorganic composites that do not require organic solvents, surfactants or stabilizers entailed by emulsion polymerization to encapsulate inorganic or metallic nanoparticles. Organic-inorganic composites were prepared with Fe_3O_4-NPs adsorbed and embedded within microgel particles of the cross-linked, environmentally responsive polymer. The presence of Fe_3O_4-NPs covered and partially covered composite particles were observed for the sample prepared at pH 7 and 5, whereas uncovered microgels were attained at pH 3 and 10. Figure 4.14 shows representative TEM images of composite microgel particles fabricated at various pH along with the zeta potentials data of the prepared ionic microgel particles and pure Fe_3O_4-NPs as a function pH.

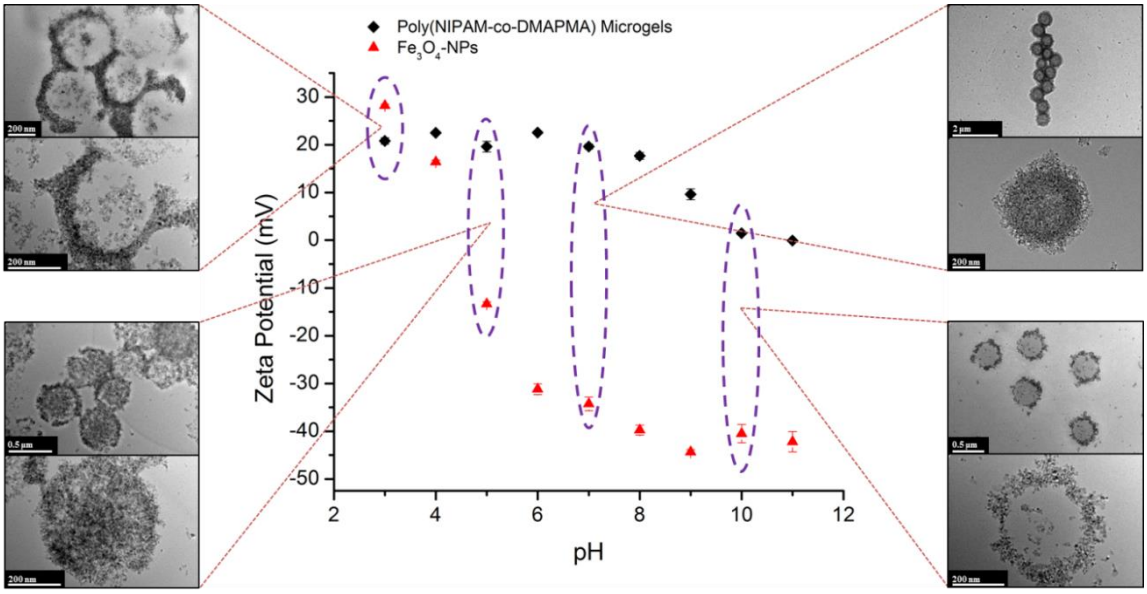

Figure 4.14 TEM images of collapsed organic-inorganic composites composed of ionic microgels and Fe_3O_4-NPs prepared at various pH and the Zeta potentials of the poly(NIPAm-*co*-DMAPMA) microparticles and the pure Fe_3O_4-NPs both as a function of pH.

Strong electrostatic interaction was assumed as the primary "driving force" dominating the uptake and adsorption of the Fe_3O_4-NPs to the ionic microgels at pH 5 and 7. In addition, charged groups were present at the periphery of the prepared microgel particles since they were synthesized in the deswollen state via precipitation polymerization [70]. These positive surface-charge groups likely arose from the cationic initiator residues at the end of the constituent polymer chains within the particles, and helped to stabilize the microgel particles against coagulation in their deswollen state [192]. Thus, at pH 5-7, the formations of composite dispersions were possibly caused by the governing electrostatic attraction pulling the strongly negative Fe_3O_4-NPs to the net positive microgel particles. On the other hand, at pH 10, where the prepared ionic microgel particles were neutral to slightly negatively charged, the uptake and adsorption of the negatively charged Fe_3O_4-NPs did not fully transpire, as the electrostatic

interaction between the two types of particles was then unattractive or slightly repulsive. Furthermore, at pH 3, the formation of Fe_3O_4-NPs fully covered composite particles was also nonexistent, likely due to the presence of both positively charged Fe_3O_4-NPs and microgel particles. Figure 4.15*a-d* illustrates the nearly reversible formations of the aforementioned composite colloids upon pH tuning.

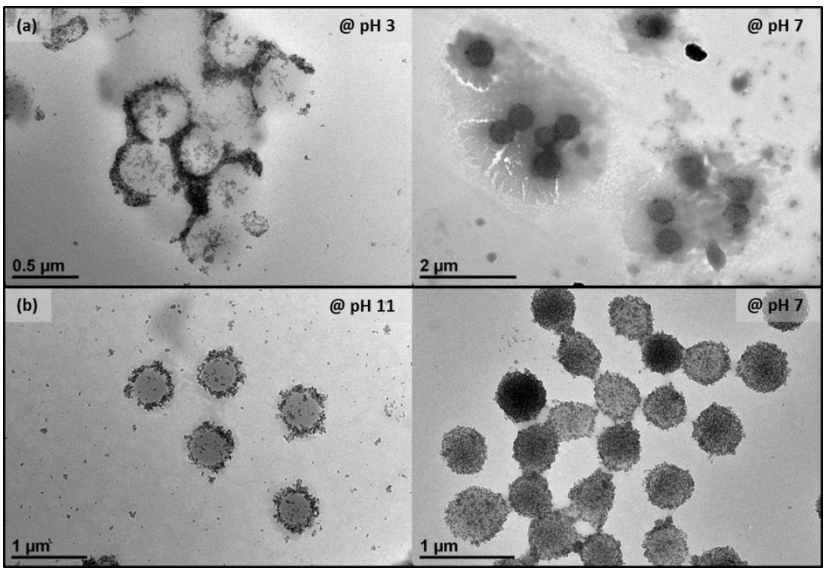

Figure 4.15 TEM images of reversible formation of organic-inorganic composites composed of ionic microgels and Fe_3O_4-NPs: (a) the sample was tuned from pH 3 to 7 and (b) the sample was tuned from pH 11 to 7.

Additionally, SEM imaging was utilized to capture the surface topography and thus the change in hydrodynamic diameter at pH 7 between the dried microgel and the microgel with organic-inorganic composites adsorbed onto its surface as shown in Figure 4.16*a-b*. Intriguingly, it seems plausible for the adsorbed and embedded Fe_3O_4-NPs at pH 5-7, to be released by inducing strongly repulsive electrostatic interactions between the microgel particles and the Fe_3O_4-NPs via altering the solution pH. This postulate was founded on the basis that the loading efficiency of the Fe_3O_4-NPs encapsulated within the

gel network was dictated by the tunable electrostatic interactions, which were strongly influenced from the protonation of the contained amine groups within the prepared ionic microgel particles.

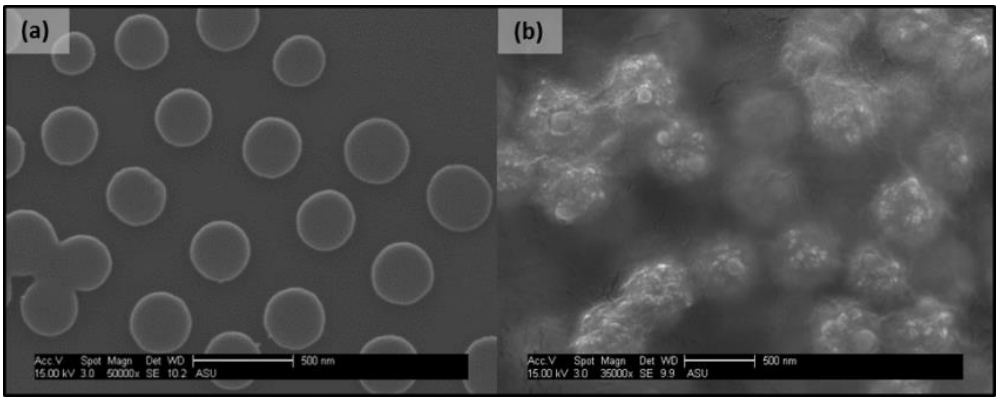

Figure 4.16 SEM images of collapsed microgels: (a) pure poly(NIPAm-*co*-DMAPMA) microparticles prepared at pH 7 and (b) organic-inorganic composites prepared at pH 7 with Fe_3O_4-NPs adsorbed and embedded within poly(NIPAm-*co*-DMAPMA) microgels.

4.2.2 Zwitterionic Microgel Particles

4.2.2.1 Adsorption of Anionic DOSS Surfactant

DOSS is an anionic organic sulfonic acid salt surfactant contained in Corexit 9500 and is commonly applied as a synthetic chemical dispersant used to modify and disrupt the interfacial tension between the water-oil interfaces [193]. Relevance in adsorbing and releasing DOSS offers potential for applications in chemical processing and oil spill remediation. Figure 4.17*a* illustrates the average hydrodynamic diameter of the ZI-MG (0.85) as a function of added DOSS concentrations at pH 3 and 11 measured at room temperature. At pH 3, where the amine groups of the DMAPMA are fully protonated and the prepared particles convey a net positive charge, the average hydrodynamic diameter of the microgel particles declines progressively with increasing DOSS concentrations. Thus, it is postulated that the dominant mechanism for the adsorption of DOSS into the

gel network is derived from the strong electrostatic attraction present between the negatively charged head groups of DOSS to the positively charged DMAPMA moieties within the prepared particles. In contrast, at pH 11, where the prepared particles exhibit strong anionic characteristics, the mean hydrodynamic diameter initially decreased and subsequently remained nearly unvarying, implying that if there is any substantial adsorption of DOSS, then no extensive deswelling occurs with rising DOSS concentration. Due to this lack of deswelling, a non-electrostatic mechanism is assumed for the initial shrinking of the ZI-MG particles at pH 11, which leads to the slight adsorption of DOSS molecules. Thus, it is hypothesized that the "driving force" for this initial particle deswelling is the high affinity nature of the hydrophobic interaction among the hydrocarbon tail groups of the DOSS surfactant to the partially hydrophobic moieties across the prepared gel network.

Overall, with respect to the corresponding differences in the mean hydrodynamic diameter with increasing DOSS concentration, the effect of ZI-MG composition is less apparent when examined at both pH values. However, the ZI-MG (0.85) particles are comprised by a greater fraction of amine groups in comparison to the ZI-MG (0.29) particles and consequently demonstrated marginally greater adsorption characteristics when measured in the degrees of deswelling as a function of added DOSS concentrations.

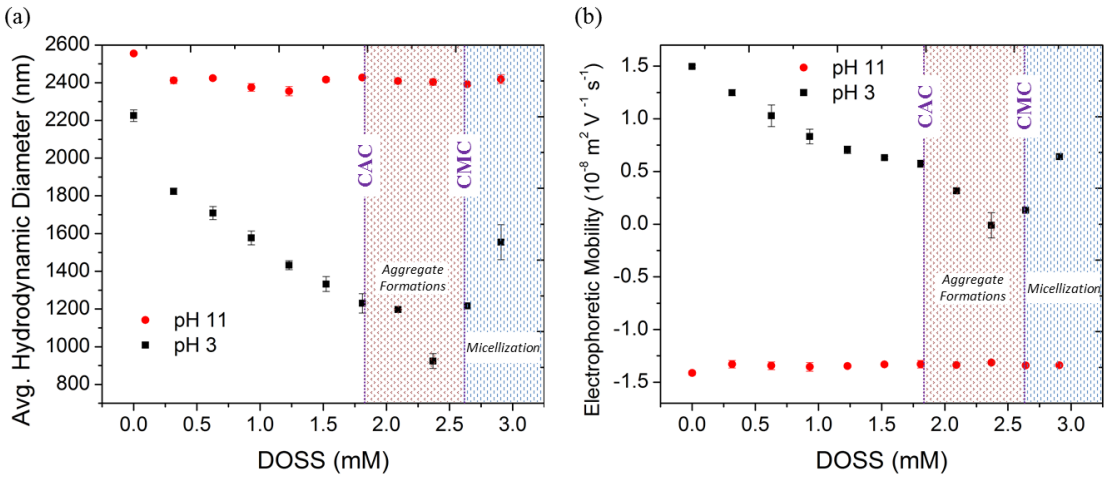

Figure 4.17 Avg. hydrodynamic diameter (a) and the electrophoretic mobility (b) of ZI-MG (0.85) particles as a function of added DOSS concentration at pH 3 and 11 studied at room temperature.

Additionally, it is vital to note that there is an inflection point on the adsorption curve, where the average hydrodynamic diameter of the ZI-MG particles reaches a minimum value just below the critical micelle concentration (CMC) of DOSS (~2.6 mM [194]) at room temperature. A probable explanation for the apparent reswelling of microgels prior to the solution CMC may be attributed to the interactions between the polyelectrolyte chains encompassed within the prepared particles to the oppositely charged surfactants applied in this system. To further elucidate, in the oppositely charged mixed solution, the dominant electrostatic attraction among the charged groups can lead to a bulk complexation above a surfactant concentration defined as the critical aggregation concentration (CAC). Upon exceeding the CAC of DOSS (~1.8 mM [195]) at room temperature, the formation of surfactant aggregates within the gel network may ensue. Thus, at surfactant concentrations beyond the CAC, strong internal electrostatic repulsion between the formed aggregates within the microgel particles could induce a rapid increase in the adsorption amount and consequently result in their reswelling with water.

This behavior is directly akin to that investigated via Langevin *et al.*, in which they examine the cationic surfactants and anionic polyelectrolytes interaction in mixed aqueous solution with various techniques [196].

The electrophoretic mobility measurements displayed in Figure 4.17*b* are also in concurrence with the mean hydrodynamic diameter data previously discussed. At pH 11, the electrophoretic mobility of the particles is invariant with added DOSS concentration, whereas at pH 3 the electrophoretic mobility of the prepared particles becomes more negative with rising DOSS concentration prior to the CAC. This further implies that DOSS molecules can be uptaken into the microgel bulk. At pH 3 with added DOSS concentrations above the CAC, the electrophoretic mobility is more positive, alluding that more DOSS molecules can be absorbed within the microgel particles. Moreover, other work has presented analogous mobility profiles with the uptake of sodium dodecylbenzenesulfonate (SDBS) into cationically charged PNIPAm-based core-shell microgel particles [129].

One interesting application derived from the presented microgel system is that DOSS can be uptaken and released from the ZI-MG particles by utilizing an environmental trigger: tuning the pH from 3 to 11. This is evident in Figure 4.18; there is a noticeable decrease in the adsorbed amount of DOSS investigated below the CMC concentration upon increasing pH indicated from the extensive variations in the measured hydrodynamic diameter of the particles. This phenomenon is resultant of the inversion of ZI-MG particle charge properties from positive to negative through modifying the solution pH to 11. It is postulated that when the pH is raised to 11, ionization renders carboxylate groups of the AAc moieties negative and the amine groups of the DMAPMA

moieties re-protonate, becoming neutral, resulting in a net negative charge. Thus, the release of the anionic DOSS molecules via electrostatic repulsion between the negative charges springs from the anionic surfactant and the ZI-MG gel network. Furthermore, based on the initially added DOSS concentration, the surfactant desorbs back into solution corresponding to an estimated 70% hydrodynamic size increase at 2.092 mM DOSS prior to the CMC. We presume that the release of DOSS could be further augmented in conjunction with rising temperature through a squeezing release process

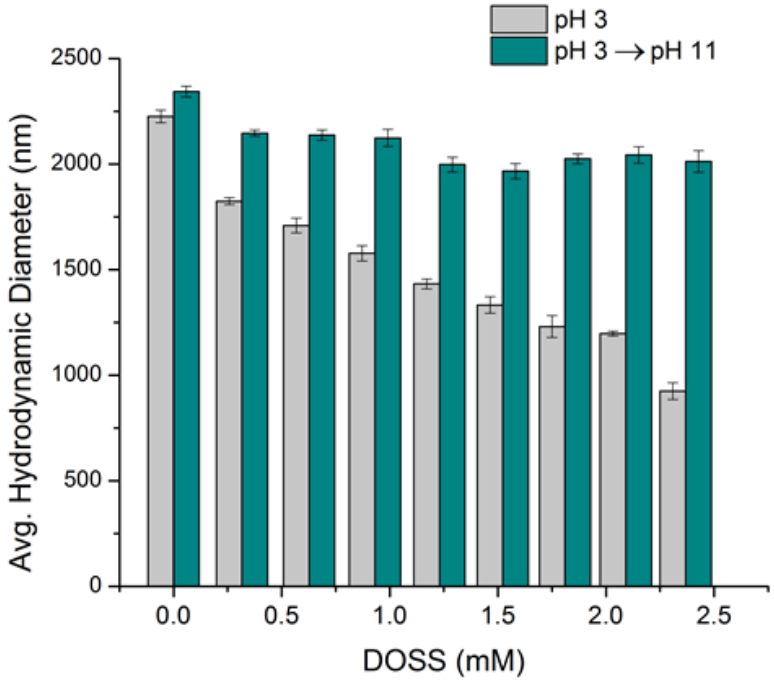

Figure 4.18 Avg. hydrodynamic diameter as a function of the equilibrium DOSS concentration with pH alterations at room temperature.

due to the temperature responsiveness of the prepared ZI-MG particle dispersions.

Surfactant molecules are amphipathic and have complicated solution chemistry. In order to further validate and quantify the adsorption of DOSS, ^{1}H NMR was utilized for the collected supernatants obtained during the uptake and release studies at pH 3 and

11. Figure 4.19 depicts the ^{1}H NMR results of the gathered supernatants. It is interpreted that DOSS was successfully adsorbed onto the prepared ZI-MG dispersions modified to be pH 3 at concentrations below the CMC, this is made evident by the reduced DOSS methylene and methyl resonances at 1.29 ppm and 0.85 ppm, respectively [197]. In contrast, the obtained supernatants for the samples modified to be pH 11 demonstrated relatively higher intensity for methylene and methyl resonances (at all concentrations of DOSS) signifying less adsorption of DOSS.

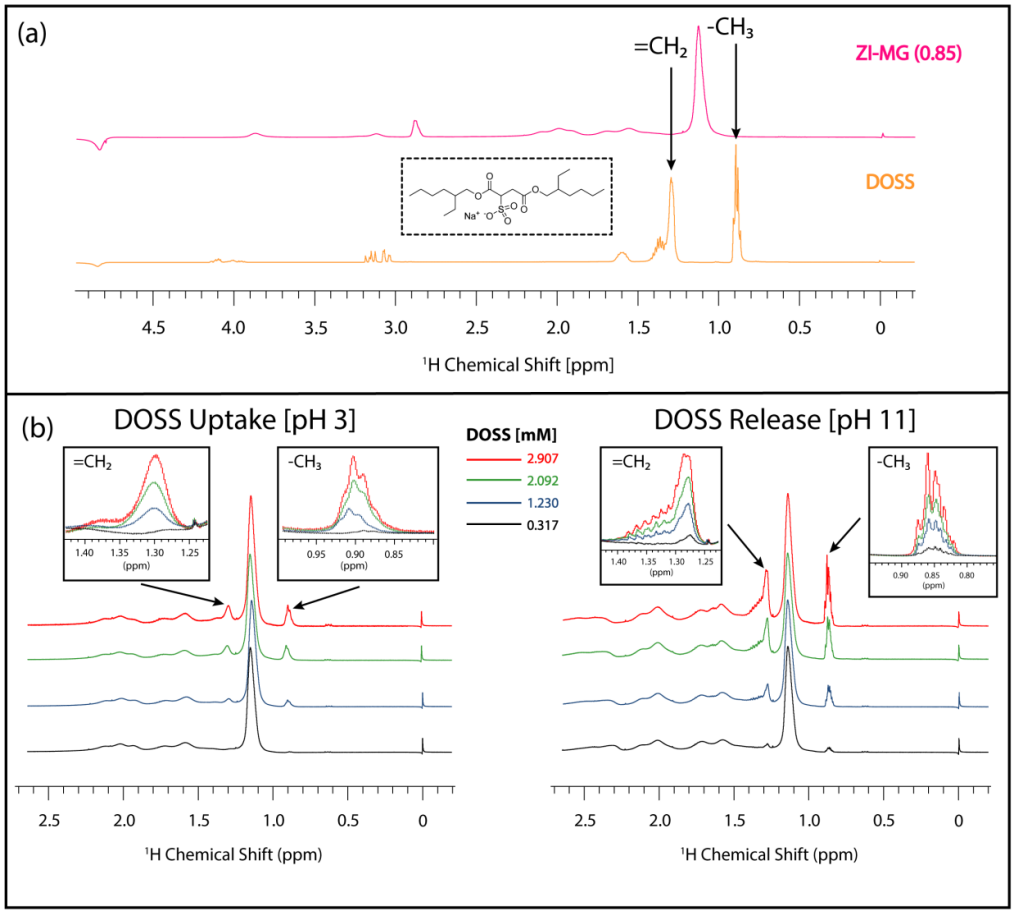

Figure 4.19 Normalized ^{1}H NMR spectra: (a) DOSS standard and pure ZI-MG (0.85) particles and (b) the collected supernatants from DOSS uptake and release via ZI-MG (0.85) microgels at pH 3 and 11. Please note the CMC of DOSS is ~2.66 mM.

4.2.2.2 Adsorption of Cationic CPyCl Surfactant

CPyCl is a versatile cationic surfactant which can be widely applied for multiple antiseptic applications [198, 199]. The average hydrodynamic diameter of the ZI-MG (0.85) particles, as a function of added CPyCl concentrations at pH 3 and 11 obtained at room temperature is shown in Figure 4.20*a*. At pH 3, where the ZI-MG are strongly cationic, the hydrodynamic diameter remains nearly invariant with increasing CPyCl concentration, signifying that if there is any uptake of the cationic surfactant, then no extensive deswelling occurs. In contrast, at pH 11, where the carboxyl groups of the AAc moieties are fully ionized, the prepared particles carry a net negative charge, the mean hydrodynamic diameter of the microgel particles decreases steadily as a function of increasing CPyCl concentration. Thus, it is hypothesized that governing mechanism for CPyCl adsorption into the microgel network is an electrostatic interaction at pH 11.

Figure 4.20*b* illustrates that the measured electrophoretic mobility data are in good accordance with regard to the corresponding variations in the hydrodynamic diameter with increasing CPyCl concentrations over the concentration range studied (the maximum CPyCl equilibrium concentration investigated is less than the CMC of ~0.9 mM [200] at room temperature). At pH 3, the mobility of the prepared particles is independent of CPyCl concentration, whereas at pH 11 the electrophoretic mobility of the ZI-MG becomes less negative with increasing CPyCl concentration due to the adsorption of CPyCl molecules onto the gel-bulk. It was postulated at higher CPyCl concentrations the electrophoretic mobility might become more positive with the formation of surfactant aggregates within the gel network.

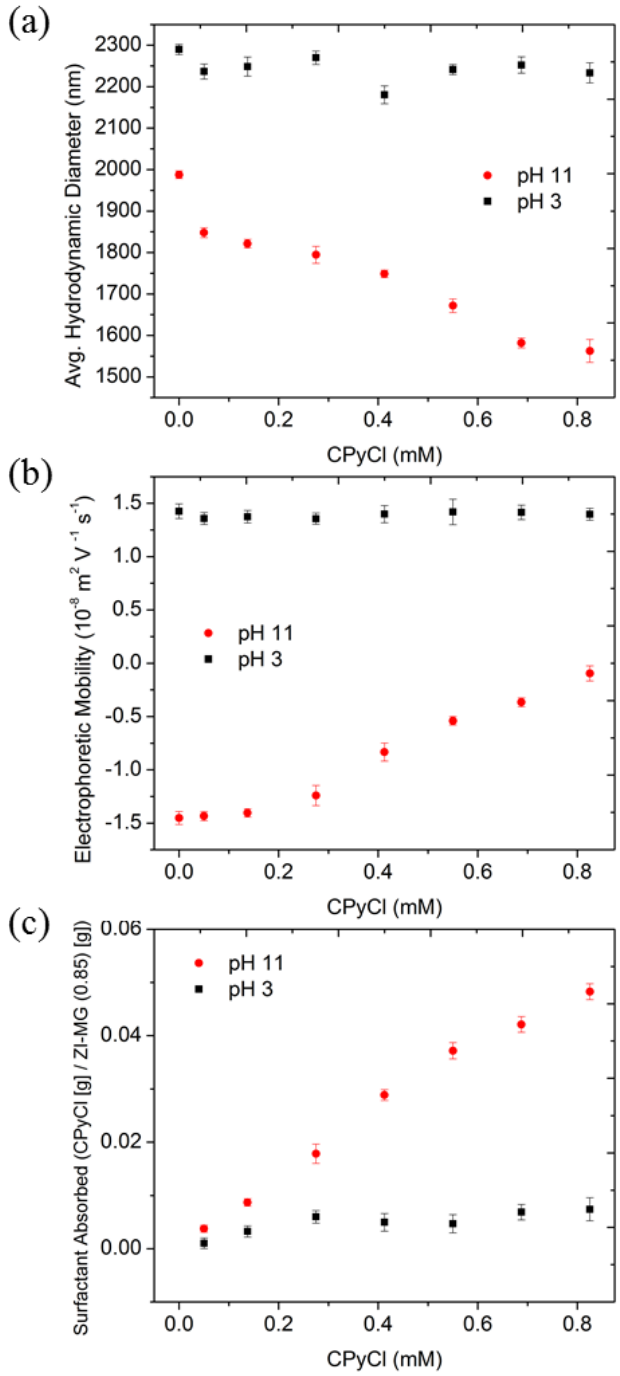

Figure 4.20 Average hydrodynamic size (a) and electrophoretic mobility (b) and adsorbed amount of CPyCl surfactant onto ZI-MG (0.85) particles (c) as a function of equilibrium CPyCl concentration at pH 3 and 11 obtained at room temperature.

The effect of pH on the adsorbed amounts of CPyCl for the dispersed ZI-MG particles is shown in Figure 4.20*c*. At pH 3, where the prepared ZI-MG particles exhibited strong cationic characteristics, there appear to be only a slight adsorption of the CPyCl molecules with greater CPyCl concentration. This is most likely governed by hydrophobic interactions between the tails of the surfactant molecules to the presence of fully protonated amine groups within the polymer network comprising the ZI-MG particles. In comparison, at pH 11, the adsorbed amount at any given CPyCl concentration is substantially greater than at pH 3. This is postulated to be due to the strong electrostatic attraction among the cationic surfactant head groups to the anionic sites within the gel-network, analogous to the adsorption of DOSS at pH 3, as discussed earlier.

Figure 4.21 shows the variation with pH in the amount of CPyCl adsorbed via ZI-MG (0.85) when the initial concentration of added CPyCl is kept constant at ~0.412 mM and ~0.825 mM. It is evident from Figure 9 at either fixed concentration that the amount of adsorbed CPyCl does decrease strongly with pH. It is also significant that there is a sharp increase in the adsorbed amount across the IEP of the prepared particles between pH 5 and 6. This implies tunable uptake and release potentials where the required variation in pH application is relatively small.

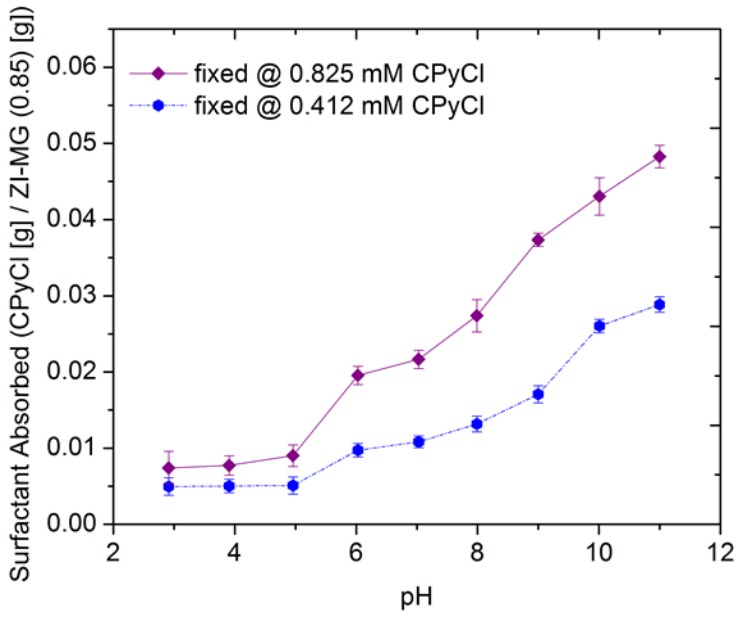

Figure 4.21 Adsorbed amount of CPyCl for the ZI-MG (0.85) particles with a fixed initial CPyCl concentration of 0.412 mM and 0.825 mM as a function of pH obtained at room temperature.

4.2.2.3 Adsorption of Nonionic TX-100 Surfactant

In this study we explore the uptake of a nonionic surfactant into the zwitterionically charged microgel particles. The average hydrodynamic diameter of ZI-MG (0.86) particle dispersions as a function of added nonionic TX-100 surfactant concentration is illustrated in Figure 4.22. At pH 3 and 11, the overall swelling profiles are analogous when compared. The slight particle deswelling prior to the CMC (~0.24 mM [201]) is proposed to be due to the binding of nonionic surfactant with the prepared microgels at room temperature. At pH 3, the ether oxygens in the bulky ethylene oxide head groups of the nonionic surfactant molecules interact with the hydrogen on the neutral carboxylic residues within the microgel particles. However, at pH 11, with the presence of deprotonated carboxyl moieties, the adsorption mechanism is proposed to be

due to hydrophobic attraction among the nonionic surfactant's tail groups to the DMAPMA groups with diminished polarity within the ZI-MG particles.

This aligns with the notion that with the absence of electrostatic attraction between the ionized groups and the targeted surfactant at both pH values, the surfactant uptake may occur via hydrogen-bonding or hydrophobic interaction. Moreover, at both pH values and as a function of TX-100 concentrations, the mean hydrodynamic diameter has a slight increase in the measured particle size above the CMC. This small increase in size of the prepared microgels at concentrations above the CMC is hypothesized to be due to the accumulation of free TX-100 within the bulk, where the formation of surfactant aggregates within the gel network can occur upon exceeding the CAC, thus creating an internal electrostatic repulsion to dictate particle swelling.

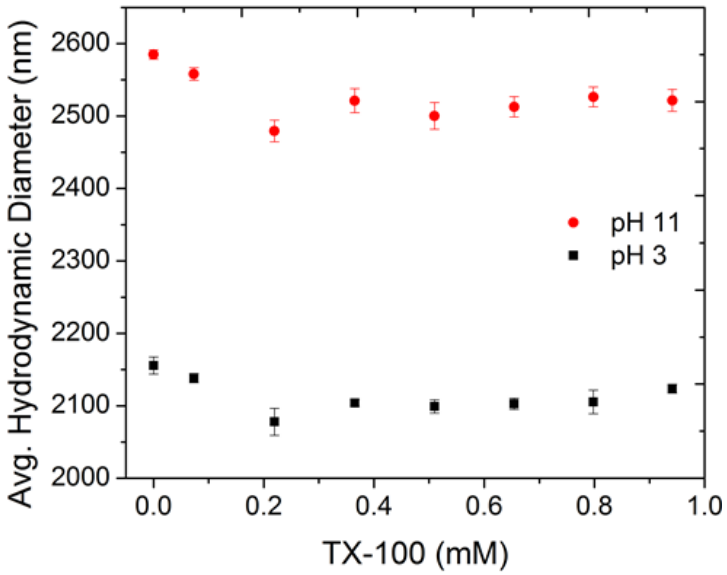

Figure 4.22 Avg. hydrodynamic size of ZI-MG (0.85) with varying pH measured at room temperature.

4.3 Structure of Colloidal Lattices at IL-in-Water Interfaces

Figure 4.23*a-d* shows representative confocal microscope images obtained at under high magnification of IL-in-water Pickering emulsion droplets containing the prepared composite microgel particles at various pH and temperatures. We observed that the surface coverage is independent of the droplet size and that the interface appears highly fluorescent whereas the continuous phase is very dark, signifying that most of the prepared particles are located in the vicinity of the interface. In addition, the imaged microdomains of the droplets show that the adsorbed microgel particles appear not to be in close contact. This observation of inhomogeneous spatial distribution of the fluorescent intensities is evident of integration of fluorescently-labeled cores within the composite particles which allows accurate detection of the particle center-of-mass. Clearly, composite microgel particles are able to effectively stabilize an IL-in-water interface through their spontaneous adsorption at the liquid interface. While the mechanism with which microgel particles adsorb remains uncertain, it has been established that it is different from classical Pickering stabilization, and embodies features of both particle-like anchoring and polymer-like adsorption [202]. While we observe adsorption of our soft microgel particles at all IL-in-water interfaces investigated, fine-tuning of the chemistry is required for solid colloid particles. This is achieved by altering the hydrophobicity, the charge density, or the surface functional groups.

Figure 4.23*a* represents confocal microscope images of the colloidal lattice at pH 3 at 24 °C. The inset FFTs of the images show six distinct first-order peaks with multiple higher-ordered reflections. This pattern is similar to those observed on polystyrene-polyvinylpyridine block copolymer films with very ordered colloidal lattice and can be

interpreted as an indication of the close-packed-ordered structure [203, 204]. Moreover, the colloidal microgel particles within the lattice oscillate around their equilibrium positions, hypothesized as the result of constrained motion due to the underlying lattice constraint and thermal fluctuation. Figure 4.23*b* illustrates representative confocal microscope images of the colloidal lattice at pH 10 at 24 °C.

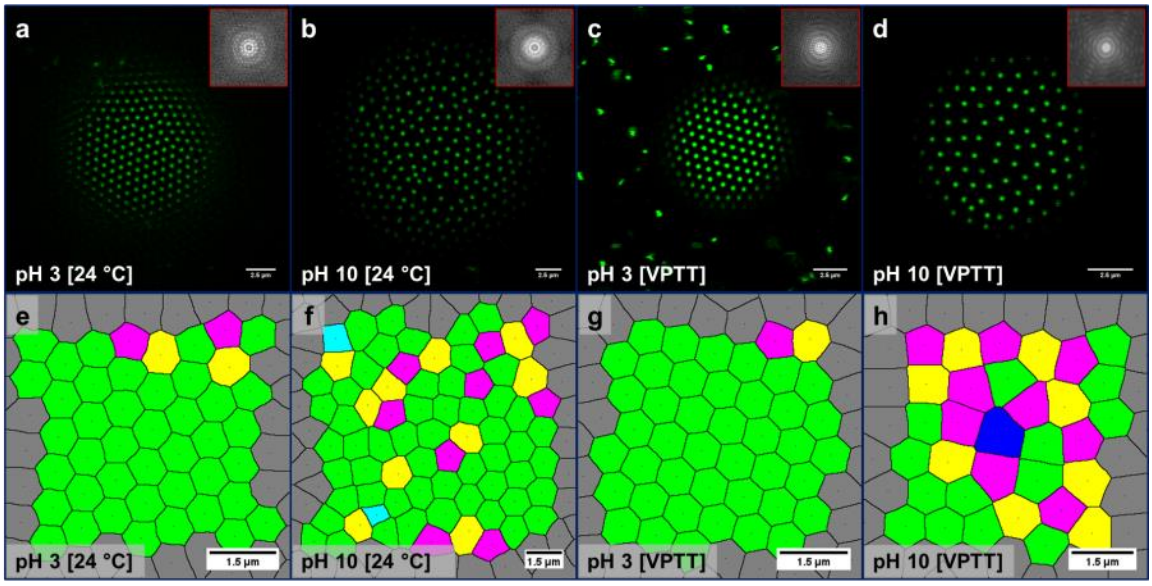

Figure 4.23 The top row illustrates confocal microscope images of colloidal lattices (a-d) at droplet surfaces at varying pH and temperatures. The insets show the FFT of the associated confocal microscope images. The bottom row shows the constructed Voroni diagrams of the colloidal lattices at the droplet surfaces (e-h) at varying pH and temperatures. In e-h, the cyan, magenta, lime green, yellow and blue fills represent, fourfold, fivefold, sixfold, sevenfold, and eightfold sites, respectively; the gray fills represent incomplete cells at the edge of the lattice and were not taken into account during data analyses.

The FTTs display a diffuse ring, which is similarly observed on poly(dimethylsiloxane)-in-water Pickering emulsions containing sulfate-treated and aldehyde-sulfate-treated polystyrene particles when assembled into less ordered microdomains and was inferred to the presence of a large fraction of defects [204]. From

FFT analysis and the visual inspection, the colloidal lattices of the prepared pH 10 samples is less ordered than the pH 3 samples at various temperatures.

The differences in the colloidal lattice organizations are postulated to be due to the effect of surface charge of the microgel particles at the IL-in-water interfaces. At pH 3, the particles are neutrally charged and thus oscillate around their equilibrium positions in an ordered, closely-packed lattice. In contrast, at pH 10, where the carboxyl groups of the AAc moieties are fully ionized, the prepared particles carry a net negative charge thus oscillate outside equilibrium within the lattice and spread further apart, influenced by strong interparticle electrostatic repulsion. Remarkably, upon elevating the temperature to their respective VPTT, the caliber of colloidal lattice organization was visually maintained at both pH 3 and 10, illustrated in Figure 4.23*c,d*.

To further characterize the structure of these colloidal lattices, we have constructed Voroni diagrams and evaluated the defect number and configurations. Voroni diagrams divide the space into polygons with shared sides having equal distances to the two adjacent particle center locations [205]. For this study, they were constructed via the particle centers in snapshots of the confocal microscope images to assist in visualizing lattice topology. Please note, the number of polygon sides reflects the coordination number of a particle, in turn yielding the number of nearest neighbors [206]. For an ideal triangular lattice, all particles should have a coordination number of 6. Fourfold, fivefold, sevenfold, and eightfold coordinated sites observed in this investigation are defined as defects, akin to previous defect analyses focused on experimentally observed colloidal lattices [207, 208]. Figure 4.23*e-h*, shows the color-coded Voronoi diagrams of the IL-in-water Pickering emulsion droplets containing the prepared composite microgel particles

at various pH and temperatures. The distorted hexagonal cells designate low local hexagonal symmetry of the lattice. In fact, organized semi-perfect hexagonal symmetry was more readily observed in emulsion droplets stabilized by the microgel particles at pH 3. This is hypothesized to be a result of localized minimum oscillation of these particles, displayed in Figure 4.23*e,g*. The number of defect sites was more prevalent at pH 10 where the continuous oscillation was augmented via electrostatic repulsion, shown in Figure 4.23*f,h*. Upon rapid tuning of the pH, either from pH 3 to pH 10 or vice versa, no variations in emulsion stability are detected. However, colloidal packing pattern changes are observed.

Additionally, Cyro-SEM imaging was utilized to capture the surface topography of these emulsions prepared at pH 3 and pH 10, shown in Figure 4.24. As the micrographs suggest, self-assembly of the swollen microgel particles at the IL-in-water interface under these conditions leads to distinctive densely packed coverage of the IL droplets with the stabilizing composite microgel particles.

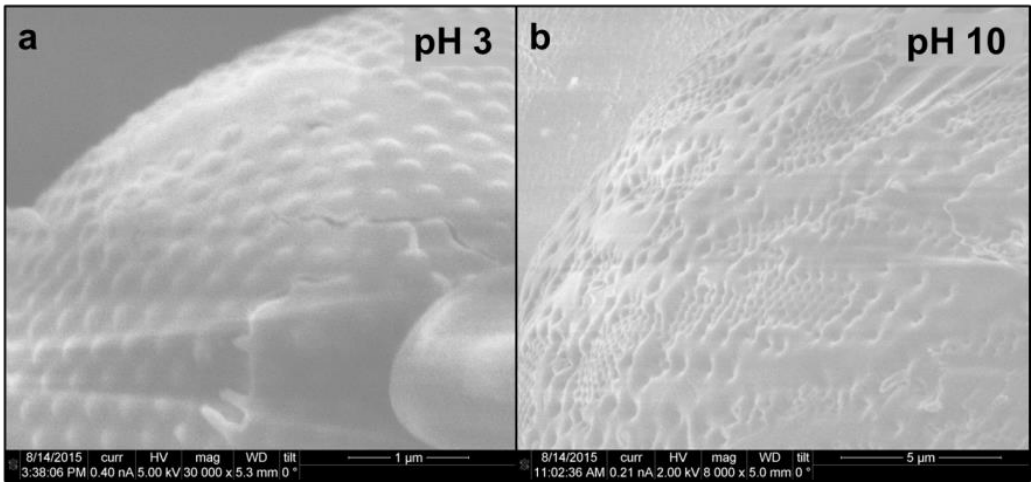

Figure 4.24 Cyro-SEM images of the interface of IL-in-Water emulsion droplets coverd by composite microgel particles at pH 3 (a) and pH 10 (b) after sublimation.

To quantify the impact of pH and temperature on the interfacial packing, we carried out additional interfacial structural analysis. Through in-situ and non-invasive visual inspection without the requirement for sample treatments such as vitrification and freeze-fracturing utilized in prior studies [209-211], we have confirmed there is indeed an increase in the interparticle separation distance (defined also as the nearest neighbor distance, shown in Figure 4.25*a* scheme) upon increasing pH. To evaluate this, the normalized radial distribution functions of the composite microgel particle positions g(r) were generated from twenty different droplets. As expected, the colloidal lattice structure at pH 3 demonstrated the distinctive pattern for 2-D hexagonal packing, with characteristic peaks at a, $a\sqrt{3}$, 2a, $a\sqrt{8}$, and 3a, where a is the nearest neighboring distance, shown in Figure 4.25*b*. In contrast, at pH 10, we assessed more disorder in the characteristic peaks, which denotes a more random packing-structure. In addition, upon increasing the pH to 10, the interparticle distances increase as evidenced from the corresponding peak shift to larger values of r. To characterize the colloidal lattice packing organization and particle spread at the interface, we normalized g(r) with the average hydrodynamic diameter, Dh, of the prepared particle dispersion of the same pH via dynamic light scattering. This method collapses the nearest-neighbor peaks of all pair correlation functions into a single peak at a normalized distance r/Dh ~0.95 and r/Dh ~0.66 at room temperature for pH 3 and 10, respectively. These ratios suggest that our composite microgels shrink when adsorbed at the IL-in-water interface. Prior work has demonstrated that microgel particles can spread, remain un-deformed, or shrink, at an oil-in-water interface reliant on a variety of factors such as interfacial tension [8, 90], shear history [212, 213], and charge density [214]. Please note that previous observation for

homogenous microgel particles are made with potentially invasive techniques in which the sample, containing thermo-responsive particles, is first cooled and then freeze-fractured, while our observations are made in-situ. Others have investigated the packing

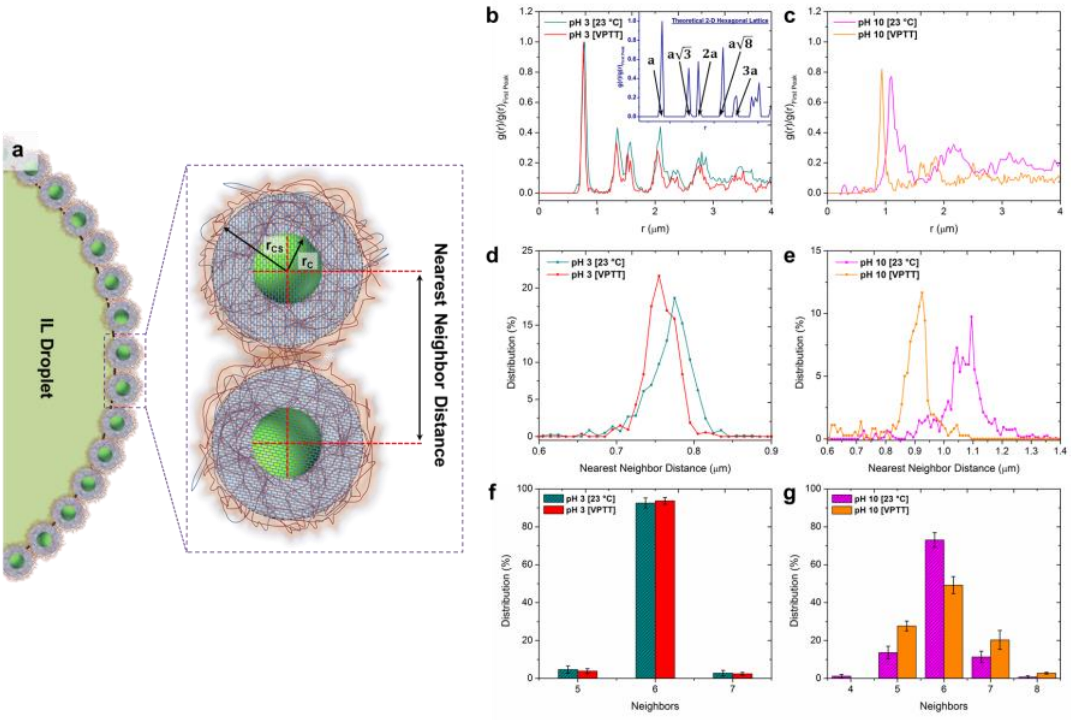

Figure 4.25 Influence of pH on the interfacial assembly of the composite microgel particles at varying temperatures is as follows: scheme illustrates the particle arrangement at the interface and the nearest neighboring distance (a), normalized pair correlation function $g(r)/g(r)_{\text{First Peak}}$ at pH 3 (b) and pH 10 (c), histograms of nearest neighbor distance on the colloidal lattices at pH 3 (d) and pH 10 (e), the bar charts represent the distribution of four-to-eight-sided polygons in the colloidal lattices at pH 3 (f) and pH 10 (g). All analysis was derived from the Voronoi diagrams of twenty different droplets. Inset: shows the normalized pair correlation function $g(r)/g(r)_{\text{First Peak}}$ of a theoretical 2-D hexagonal packed lattice.

of similar core-shell particles, with a silica core, using scanning force microscopy. In this case, the imaging occurs under artificial conditions, requiring drying of the sample inducing changes to the surface structure [].

To investigate the effect of temperature on interfacial structure, we introduced in-situ localized heating during confocal microscopy imaging. It appears that the colloidal

lattices at pH 10 have a wider particle spacing distribution than the studied colloidal lattices at pH 3. The histograms of nearest neighboring distance of over 400 counts in approximately twenty droplets for each system at room and elevated temperatures are shown in Figure 4.25*d,e*. The distribution histograms of the pH 3 systems show similar peak width, while the histograms of the pH 10 system demonstrate a much broader peak. When we focus on the increased temperature effect of both systems and sort the nearest neighboring distance, we find that on the same droplet the interparticle distance between adjacent composite microgel particles at pH 3 and pH 10 are always larger at room temperature than at their respective VPTT. To further elucidate the effect of temperature on the lattice structure, we present a bar chart of the counts (distribution %) of the number of nearest neighbors for the adsorbed composite microgel particles for pH 3 and 10 at both room and elevated temperatures. Interestingly, the distribution of the number of neighbors was not impacted by increasing the temperature for both systems, as depicted in Figure 4.25*f,g*. Upon increasing the temperature to the VPTT, there was an in-situ decrease in droplet size, and the interparticle distance between adjacent adsorbed particles reduced without changes in organization of the colloidal lattice. However, when we later heated both systems significantly over the VPTT (~70 °C), the emulsion became unstable and effectively de-mixed to two macroscopic phases (see macroscopic images in the supporting information). Upon increasing the temperature substantially higher than the VPTT for both of the microgel particle stabilized emulsions, the particles deswell and become adhesive. While this thermo-induced destabilization mechanism remains undefined, we tentatively postulate the following: the surface coverage decreases and the two interfaces, divided by a thin film of water, become attractive. This attraction removes

both the thermodynamic and kinetic barriers inhibiting coalescence, akin to the studies conducted for microgel particle behavior at the oil-in-water interface.

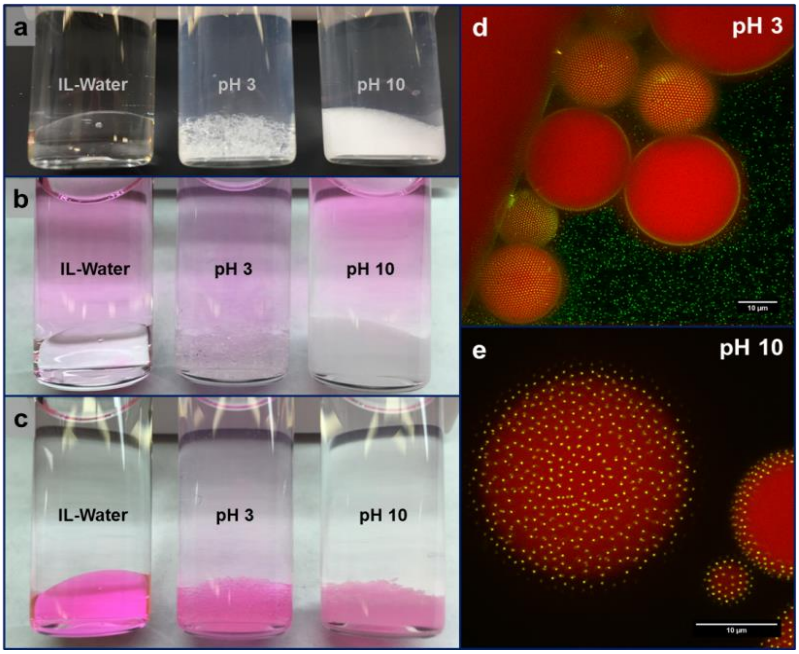

Figure 4.26 Macroscopic pictures of IL-in-water and IL-in-water emulsions stabilized with composite microgel particles at pH 3 and pH 10 (a), immediately after the addition of 0.02 mM Rhodamine B (b) and upon pigment diffusion into the IL (c). 3-D Stacked confocal microcopy images of the successful diffusion of Rhodamine B into the IL-in-water emulsions at pH 3 (d) and pH 10 (e); the IL is colored red and the composite particles are yellow-green.

A significant requirement for extraction is that the interface between IL and water remains permeable. To investigate this, we add fluorescent dye, rhodamine B, to the continuous phase of an IL-in-water emulsion stabilized with prepared microgel particles illustrated in Figure 4.26. Immediately upon the addition of the dye, the pigment is found in the IL phase (Fig. 4.26*c*). To better visualize the uptake of small molecules across a microgel-laden interface for both pH systems, we utilized confocal microscopy at room temperature. Intriguingly, we found that all of the dye is located in the IL droplets and

none remains in the water phase (Fig. 4.26*d,e*). This shows that despite the densely packed interface, small molecules can easily permeate across the porous adsorbed gel-particle layer.

5. SUMMARY AND FUTURE WORK

5.1 Summary

In this work, we assessed a method to synthesize multifunctional environmentally responsive ionic microgel particles. More importantly, we have elucidated the effective uptake and release of active chemical species such as rheology modifiers into and from these ionic microgels to alter the bulk viscosity of a targeted surrounding fluid. Additionally, we explored an approach that leads to controlled formation of organic-inorganic composites with Fe_3O_4-NPs adsorbed and embedded within ionic microgel particles. Overall we have shown that the adsorption and loading of Fe_3O_4-NPs within the ionic microgel particles can be easily manipulated using the ionization and swelling of the particle-gel-network as a facile tunable variable.

Furthermore, we reported a method to synthesize micrometer-sized multifunctional environmentally responsive ZI-MG particles. These aqueous ZI-MG dispersions exhibit large reversible parabolic swelling as a function of pH and displayed a minimum hydrodynamic diameter value at a tunable IEP. In addition, we explored an approach that leads to controlled adsorption of surfactant molecules within dispersed ZI-MG particles via facile pH manipulation. It was demonstrated that the adsorption and desorption of the surfactant from the prepared particles could be predominantly governed by electrostatic attraction, hydrogen-bonding, and hydrophobic interaction depending on the mixture pH and surfactant type.

Overall, our investigations of the prepared charged microgel systems revealed the exciting effects of gel-network structure on active macromolecule encapsulation. Thus, we believe those systems are potentially well suited as a relevant vehicle for the

adsorption, retention, and targeted delivery for novel carrier applications of active species.

In another component of this thesis, we report the self-assembly of composite microgel particles in IL-in-water Pickering emulsions. When spontaneously adsorbed at the liquid-liquid interface, these soft and environmentally responsive particles display an interesting duality in their interfacial behavior attributed to both a Pickering-like anchoring and a polymer-like adsorption. The incorporation of a fluorescently labeled core into the microgel particle allows non-invasive and in-situ visualization of an unanticipated correlation between the gel-stabilizer's charge and interfacial colloidal lattice packing in response to external stimuli such as pH and temperature. Moreover, de-emulsification can be triggered at high solution temperature due to the removal of both the kinetic and thermodynamic barriers preventing coalescence. Additionally, we demonstrated that the densely packed layer of gel-particles remains permeable at the IL-in-water interface for absorption of active species. Thus, through the utilization of stimuli-responsive microgel particles as emulsifiers we are able to create highly tunable systems, which may open up novel extraction applications.

5.2 Future Work

5.2.1 Impact of Microgel Cross-linking Density on Their Ability to Stabilize Pickering Emulsions

Previously we have successfully established the versatility of microgels in stabilizing IL-in-water interfaces. However, the extensive details of their adsorption, conformation, and organization still remain largely indefinable. Additionally, how their compressibility and deformability interplay with other forces that act on microgels at a liquid interface is unknown. Such deformation plays in important roles in microgels' adsorption and conformation at the oil-water interface and, as a result, on their final emulsion properties [215, 216].

We propose utilization of the scaling theory developed by Vilgis and Stapper [217], which will enable the prediction of microgels' fractal structures along with their mechanical properties at the interfaces. This study will focus on the influence of the soft nature of the gel-particles (based on particle compositions) to deform at the interface and interconnect. To elaborate, initially spherical in dispersion, the microgel particles flattened once at the emulsion drop surface, exhibiting a "fried-egg-like" morphology attributed to their structure [166]. The peripheral part of the microgel particles overlapped and interpenetrated, inducing interfacial elasticity, postulated to be responsible for emulsion stability. When the deformability is lost, either by increasing the microgel cross-linking density or via increasing the emulsion temperature, the stabilization efficacy should be reduced. Thus, the cross-linking density of the microgels has been found to govern not only the emulsion stability but also their flocculation state [216]. A similar study focused on the influence of the particle size on the ability of PNIPAm

microgels to stabilize oil-in-water Pickering emulsion has been recently conducted by Schmitt et al [90]. Figure 5.1 illustrate the schematic representation of the adsorbed microgels and the polymer density profile, ρ(*z*), at the oil-in-water interface for varying particle size, cross-linking degree, emulsion temperature, and stirring shear energy. In their study, when cross-linking density was increased, the drops became adhesive, leading to highly flocculated emulsions that were fragile against mechanical stirring.

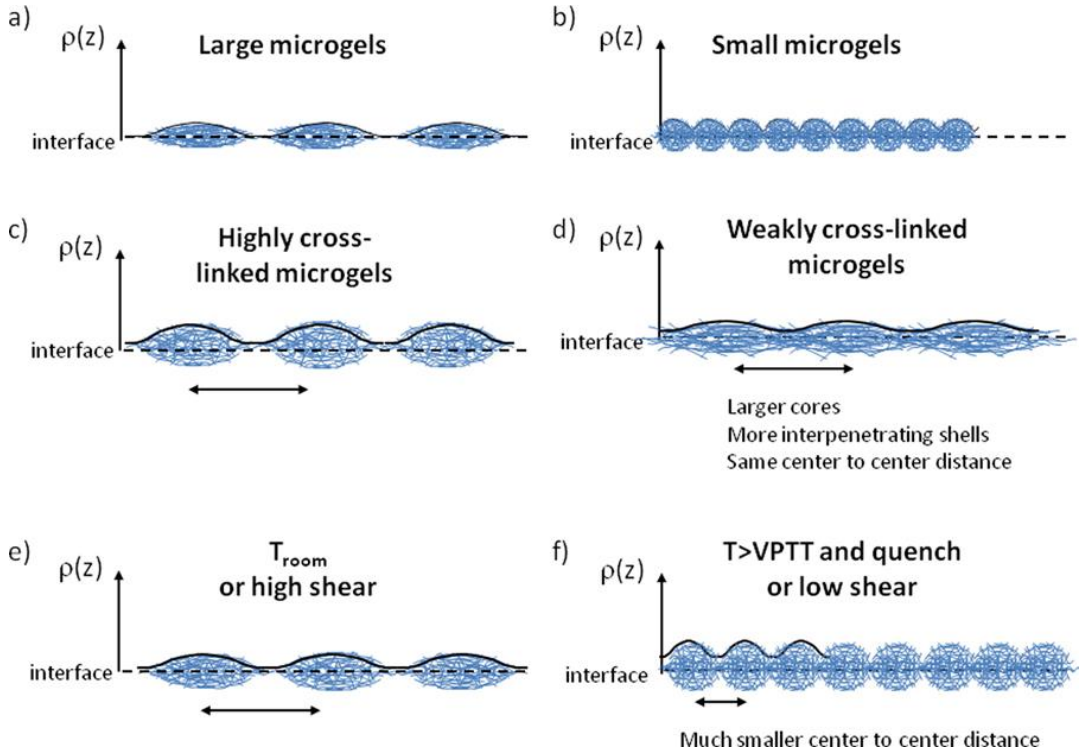

Figure 5.1 Schematic representation of the adsorbed microgel particles and the polymer density profile at the fluid interface for (a) large and (b) small gel-particles. In a similar way the effect of the cross-linking density may be schematically drawn (c and d) as well as the effect of process parameters such as initial temperature or energy (e and f). Please note *z* is the distance from the interface. Adapted from [166].

Therefore, through the utilization of the cryo-SEM technique, we will be able to demonstrate that the drop adhesion was due to microgels bridging opposite interfaces. To create bridges, microgels already adsorbed at one interface have to access the free

interface on the opposite drop already covered by gel-particles. The bridging probability is then related to the microgels' mobility at the interface and the tendency of the drop to create a new interface during the adhesive film formation. We hypothesize that one of the consequences of the microgel deformability loss is the reduction of their lateral overlapping and interpenetration at interface, triggering a more liquid mechanical behavior of the interface-favoring bridging. This study would be similar to the work done by previous group members focused on understanding droplet bridging in ionic liquid-based Pickering emulsions [218]. We further propose that highly deformed microgels (with a lower cross-linking density) induce high surface coverage and high interfacial connectivity (due to shell interpenetration) resulting in a more elastic interface able to resist bridging as microgels prepared with low number of cross-links should adsorb much better than microgels prepared with higher cross-linking densities as they are more likely to interpenetrate each other.

In order to confirm the above postulate, we plan to conduct a systematic study of the interfacial deformation by synthesizing fluorescently labelled composite microgels with varying cross-linking densities and measuring surface tension throughout their adsorption process in IL-water emulsions.

5.2.2 Magnetically Responsive Pickering Emulsions

Emulsions are often applied as a tool to organize matter. This can be accomplished either by the immobilization of particles in a capsule configuration at the interface or through the adsorption of the particles at the interface. Therefore, novel applications can be developed through the "tunable" destabilization of responsive emulsions under external stimuli. For example, the utilization of microgel-stabilized emulsions as biocatalysts was recently reported [219-221]. In this case, biocatalysis allows the production of enantiopure substances via enzymes [110]. However, many substrates are poorly water-soluble, while enzymes require aqueous environments. As a result, enzyme-catalyzed reactions are often implemented in biphasic aqueous-organic systems. The approach of using microgel-stabilized emulsions offers a facile method to attain high substrate concentration. In addition, the emulsion may be broken just by increasing the temperature above the VPTT to recover the reaction product in the organic phase and to recycle the microgels and the enzyme in the aqueous phase.

Derived from the above concept, we aim to develop responsive organic-inorganic hybrid microgels that can equilibrate at fluid interfaces, and in turn temporarily "thicken/solidify" the targeted fluid layer which then can be removed via "skimming" upon tunable destabilization of the responsive emulsions under external stimuli. To accomplish this, we plan to prepare multi-responsive emulsifiers with the incorporation of magnetic nanoparticles into the thermosensitive and pH-responsive microgels. We expect that the targeted droplets will be stabilized by such particles. In addition, we postulate that through the application and manipulation of a static magnetic field the stabilized droplets can be isolated from the continuous phase. Furthermore, we

hypothesize that the localized heating induced through the use of a high frequency magnetic field can lead to targeted emulsion destruction via drop coalescence above the VPTT.

Our previous work has demonstrated a facile approach to obtain polymer-inorganic composites through the physical interactions between microgel particles and inorganic nanoparticles. Figure 5.2 illustrates the effect of heating on the formation of hybrid microgels consisting of Fe_3O_4-NPs prepared in the work described in Chapter 4.2.

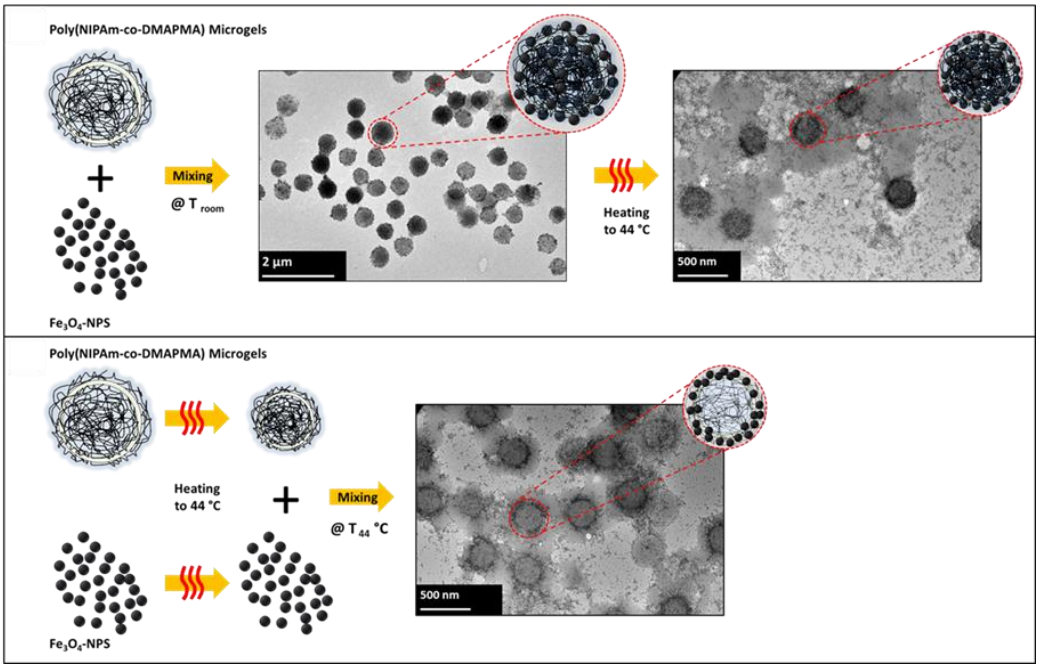

Figure 5.2 Illustrates the temperature effect on the formation of Fe_3O_4-MG hybrid colloids.

Those hybrid microgels were formed due to the governing electrostatic attraction pulling the strongly negative Fe_3O_4-NPs to the net positive microgel particles at pH 7. However, previous results indicated that the effect of heating enables the collapse of those particles and thus frees the adsorbed Fe_3O_4-NPs from the surface. Therefore, an alternative preparation method must be utilized to prepare hybrid magnetic microgels

which can withstand structural damages upon pH and temperature variations. To accomplish this set objective, we propose the following synthesis method presented by Laurenti et al [222]. In this method, PNIPAm microgels are prepared by the previously described surfactant free radical polymerization. However, right after starting the reaction, we will introduce sodium acrylate (0.01 M, 35 mg) with the aim of enriching the microgels with carboxylic groups distributed on the surface. In turn, this will create a carboxylic group-rich shell in which the iron nanoparticles could be deposited. After the addition of the acrylate monomer the mixture will be refluxed for 7 hours under N_2 atmosphere, and subsequently, the particles will be filtered and dialyzed. Finally, the magnetic hybrids will be prepared by the co-precipitation method in the presence of the previously synthesized microgels. For this synthesis experiment, 0.1 g of previously prepared microgels will be dispersed in 50 mL of NaOH (0.1 M) aqueous solution. Afterward, 50 mL of a HCl solution (0.1 M) in which has been previously dissolved 32.5 mg (0.18 mmol) of $FeCl_3 \cdot 6H_2O$ and 12 mg (0.09 mmol) of $FeCl_2 \cdot 4H_2O$ will be slowly added dropwise to the microgel dispersion under continuous stirring at 25 °C. Figure 5.3 outlines the preparation of monodisperse and thermosensitive microgels with magnetic cores. Please note, by varying the amount of acid, it will be possible to obtain hybrid microgel particles with different magnetic core sizes and architectures.

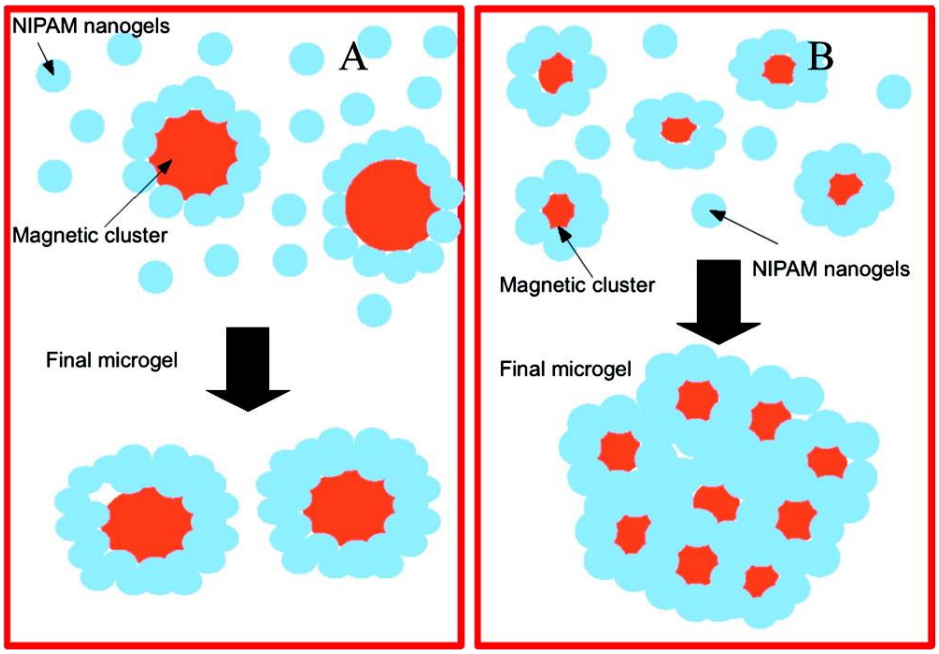

Figure 5.3 Represents the hybrid microgel formation mechanism (a) for magnetic cluster bigger than the nanogels and (b) for magnet cluster smaller than the nanogels. Adapted from [222].

To quantify the hybrid colloids, we then plan to use the thermogravimetry analysis (TGA) to determine the incorporated amount of the inorganic content. Next, typical emulsion batches will be composed following the previously describe methods. Potential findings from the proposed work will provide insightful information focusing on the link between microgel interfacial adsorption and responsive emulsion properties at the fluid interface.

REFERENCES

[1] A. Fernandez-Barbero, I.J. Suarez, B. Sierra-Martin, A. Fernandez-Nieves, F.J. de Las Nieves, M. Marquez, J. Rubio-Retama, E. Lopez-Cabarcos, Gels and microgels for nanotechnological applications, Adv Colloid Interface Sci, 147-148 (2009) 88-108.

[2] J.I. Amalvy, E.J. Wanless, Y. Li, V. Michailidou, S.P. Armes, Y. Duccini, Synthesis and characterization of novel pH-responsive microgels based on tertiary amine methacrylates, Langmuir, 20 (2004) 8992-8999.

[3] A. Burmistrova, M. Richter, M. Eisele, C. Üzüm, R. von Klitzing, The Effect of Co-Monomer Content on the Swelling/Shrinking and Mechanical Behaviour of Individually Adsorbed PNIPAM Microgel Particles, Polymers, 3 (2011) 1575-1590.

[4] S. Chai, J. Zhang, T. Yang, J. Yuan, S. Cheng, Thermoresponsive microgel decorated with silica nanoparticles in shell: Biomimetic synthesis and drug release application, Colloids and Surfaces A: Physicochemical and Engineering Aspects, 356 (2010) 32-39.

[5] R. Pelton, Temperature-sensitive aqueous microgels, Advances in Colloid and Interface Science, 85 (2000) 1-33.

[6] A. Fernandez-Nieves, A. Fernandez-Barbero, B. Vincent, F.J. de las Nieves, Osmotic de-swelling of ionic microgel particles, Journal of Chemical Physics, 119 (2003) 10383-10388.

[7] D. Capriles-González, B. Sierra-Martín, A. Fernández-Nieves, A. Fernández-Barbero, Coupled deswelling of multiresponse microgels, The journal of physical chemistry. B, 112 (2008) 12195-12200.

[8] S. Schmidt, P.A.L. Fernandes, B.G. De Geest, M. Delcea, A.G. Skirtach, H. Mohwald, A. Fery, Release Properties of Pressurized Microgel Templated Capsules, Adv Funct Mater, 21 (2011) 1411-1418.

[9] N.P. Singh, R.E. Stephens, Microgel electrophoresis: Sensitivity, mechanisms, and DNA electrostretching, Mutation Research-DNA Repair, 383 (1997) 167-175.

[10] A. Fernández-Nieves, A. Fernández-Barbero, F.J.d.l. Nieves, B. Vincent, Motion of microgel particles under an external electric field, Journal of Physics: Condensed Matter, 12 (2000) 3605-3614.

[11] C. Ménager, O. Sandre, J. Mangili, V. Cabuil, Preparation and swelling of hydrophilic magnetic microgels, Polymer, 45 (2004) 2475-2481.

[12] D. Saatweber, B. Vogt-Birnbrich, Microgels in organic coatings, Progress in Organic Coatings, 28 (1996) 33-41.

[13] J.B. Thorne, G.J. Vine, M.J. Snowden, Microgel applications and commercial considerations, Colloid and Polymer Science, 289 (2011) 625-646.

[14] I. Kaneda, A. Sogabe, H. Nakajima, Water-swellable polyelectrolyte microgels polymerized in an inverse microemulsion using a nonionic surfactant, Journal of Colloid and Interface Science, 275 (2004) 450-457.

[15] M.S. Wolfe, C. Scopazzi, Rheology of swellable microgel dispersions: Influence of crosslink density, Journal of Colloid and Interface Science, 133 (1989) 265-277.

[16] P.F. Kiser, G. Wilson, D. Needham, Lipid-coated microgels for the triggered release of doxorubicin, Journal of controlled release : official journal of the Controlled Release Society, 68 (2000) 9-22.

[17] G. Liu, X. Li, L. Li, S. Xiong, P.K. Chu, S. Wu, Z. Xu, Fluorine-containing thermo-sensitive core/shell microgel particles: Preparation, characterization, and their applications in controlled drug release, Journal of Fluorine Chemistry, 135 (2012) 75-82.

[18] H. ShamsiJazeyi, C.A. Miller, M.S. Wong, J.M. Tour, R. Verduzco, Polymer-coated nanoparticles for enhanced oil recovery, Journal of Applied Polymer Science, 131 (2014) n/a-n/a.

[19] I.C. Chen, C. Yegin, M. Zhang, M. Akbulut, Use of pH-Responsive Amphiphilic Systems as Displacement Fluids in Enhanced Oil Recovery, DOI 10.2118/169904-pa.

[20] A.H. Bornaee, M. Manteghian, A. Rashidi, M. Alaei, M. Ershadi, Oil-in-water Pickering emulsions stabilized with functionalized multi-walled carbon nanotube/silica nanohybrids in the presence of high concentrations of cations in water, Journal of Industrial and Engineering Chemistry, 20 (2014) 1720-1726.

[21] E. Dickinson, Food emulsions and foams: Stabilization by particles, Current Opinion in Colloid & Interface Science, 15 (2010) 40-49.

[22] M. Kargar, K. Fayazmanesh, M. Alavi, F. Spyropoulos, I.T. Norton, Investigation into the potential ability of Pickering emulsions (food-grade particles) to enhance the oxidative stability of oil-in-water emulsions, Journal of Colloid and Interface Science, 366 (2012) 209-215.

[23] A. Timgren, M. Rayner, M. Sjöö, P. Dejmek, Starch particles for food based Pickering emulsions, Procedia Food Science, 1 (2011) 95-103.

[24] J. Frelichowska, M.-A. Bolzinger, J. Pelletier, J.-P. Valour, Y. Chevalier, Topical delivery of lipophilic drugs from o/w Pickering emulsions, International journal of pharmaceutics, 371 (2009) 56-63.

[25] K. Zhang, W. Wu, K. Guo, J.F. Chen, P.Y. Zhang, Magnetic polymer enhanced hybrid capsules prepared from a novel Pickering emulsion polymerization and their application in controlled drug release, Colloids and Surfaces A: Physicochemical and Engineering Aspects, 349 (2009) 110-116.

[26] K. Zhang, W. Wu, K. Guo, J. Chen, P. Zhang, Synthesis of Temperature-Responsive Poly(N-isopropyl acrylamide)/Poly(methyl methacrylate)/Silica Hybrid Capsules from Inverse Pickering Emulsion Polymerization and Their Application in Controlled Drug Release, Langmuir, 26 (2010) 7971-7980.

[27] N.V. Plechkova, K.R. Seddon, Applications of ionic liquids in the chemical industry, Chemical Society Reviews, 37 (2008) 123-150.

[28] B.R. Saunders, B. Vincent, Microgel particles as model colloids: theory, properties and applications, Advances in Colloid and Interface Science, 80 (1999) 1-25.

[29] T. Hoare, R. Pelton, Highly pH and temperature responsive microgels functionalized with vinylacetic acid, Macromolecules, 37 (2004) 2544-2550.

[30] A. Garcia, M. Marquez, T. Cai, R. Rosario, Z. Hu, D. Gust, M. Hayes, S.A. Vail, C.-D. Park, Photo-, thermally, and pH-responsive microgels, Langmuir : the ACS journal of surfaces and colloids, 23 (2007) 224-229.

[31] M. Das, H. Zhang, E. Kumacheva, Microgels: Old materials with new applications, Annu Rev Mater Res, 36 (2006) 117-142.

[32] M. Dadsetan, K.E. Taylor, C. Yong, Z. Bajzer, L. Lu, M.J. Yaszemski, Controlled release of doxorubicin from pH-responsive microgels, Acta biomaterialia, 9 (2013) 5438.

[33] L. Perez-Alvarez, V. Saez-Martinez, E. Hernaez, I. Katime, Novel pH- and Temperature-Responsive Methacrylamide Microgels, Macromolecular Chemistry and Physics, 210 (2009) 1120-1126.

[34] M. Agrawal, R. Rojas-Reyna, A. Eychmüller, M. Stamm, J. Rubio-Retama, N.E. Zafeiropoulos, N. Gaponik, S. Gupta, V. Cimrova, V. Lesnyak, E. López-Cabarcos, S. Tzavalas, Switchable photoluminescence of CdTe nanocrystals by temperature-responsive microgels, Langmuir : the ACS journal of surfaces and colloids, 24 (2008) 9820-9824.

[35] Z. Yuan, Y. Wang, D. Chen, Preparation and characterization of thermo-, pH-, and magnetic-field-responsive organic/inorganic hybrid microgels based on poly(ethylene glycol), Journal of Materials Science, 49 (2014) 3287-3296.

[36] J.E. Wong, A.K. Gaharwar, D. Müller-Schulte, D. Bahadur, W. Richtering, Dual-stimuli responsive PNiPAM microgel achieved via layer-by-layer assembly: Magnetic and thermoresponsive, Journal of Colloid And Interface Science, 324 (2008) 47-54.

[37] S. Nojd, P.S. Mohanty, P. Bagheri, A. Yethiraj, P. Schurtenberger, Electric field driven self-assembly of ionic microgels, Soft Matter, 9 (2013) 9199-9207.

[38] D.R.E. Snoswell, R.K. Brill, B. Vincent, pH-Responsive Microrods Produced by Electric-Field-Induced Aggregation of Colloidal Particles, Advanced Materials, 19 (2007) 1523-1527.

[39] B.R. Saunders, B. Vincent, Thermal and osmotic deswelling of poly(NIPAM) microgel particles, Journal of the Chemical Society, Faraday Transactions, 92 (1996) 3385-3389.

[40] W.O. Baker, Microgel, A New Macromolecule, Industrial & Engineering Chemistry, 41 (1949) 511-520.

[41] R.H. Pelton, P. Chibante, Preparation of Aqueous Lattices with N-Isopropylacrylamide, Colloid Surface, 20 (1986) 247-256.

[42] M. Zhou, Y. He, Z. Ma, P. Wen, J. Gao, F. Xing, M. Ren, Y. Feng, Y. Zhao, H. Qiu, X. Wang, C. Gao, F. Sun, A facile method to assemble PNIPAM-containing microgel photonic crystals, Chemphyschem : a European journal of chemical physics and physical chemistry, 10 (2009) 523-526.

[43] S. Xu, J. Zhang, C. Paquet, Y. Lin, E. Kumacheva, From Hybrid Microgels to Photonic Crystals, Adv Funct Mater, 13 (2003) 468-472.

[44] Y.Q. He, J.Y. Wang, X.D. Wang, Y. Feng, Y.Q. Zhao, X.D. You, PAM-PAA microgel inverse opal photonic crystal and pH response, Chinese Chemical Letters, 18 (2007) 1395-1398.

[45] H. Chen, L.L. Dai, Adsorption and release of active species into and from multifunctional ionic microgel particles, Langmuir, 29 (2013) 11227-11235.

[46] J. Zhang, S. Xu, E. Kumacheva, Photogeneration of Fluorescent Silver Nanoclusters in Polymer Microgels, Advanced Materials, 17 (2005) 2336-2340.

[47] H. Yan, M. Nishino, Y. Tsuboi, N. Kitamura, K. Tsujii, Template-guided synthesis and individual characterization of poly(N-isopropylacrylamide)-based microgels, Langmuir : the ACS journal of surfaces and colloids, 21 (2005) 7076-7079.

[48] D.B. Shenoy, G.B. Sukhorukov, Microgel-based engineered nanostructures and their applicability with template-directed layer-by-layer polyelectrolyte assembly in protein encapsulation, Macromolecular bioscience, 5 (2005) 451-458.

[49] M. Kaliva, M.A. Frysali, C. Flouraki, L. Papoutsakis, M. Vamvakaki, S.H. Anastasiadis, Metallic Nanocatalysts Embedded within pH-Responsive Polymeric Microgels and Deposition onto Solid Substrates, Macromolecular Symposia, 331-332 (2013) 17-25.

[50] S. Berger, R. Singh, J.D. Sudha, H.-J. Adler, A. Pich, Microgel/clay nanohybrids as responsive scavenger systems, Polymer, 51 (2010) 3829-3835.

[51] M. Malmsten, H. Bysell, P. Hansson, u. Uppsala, f. Farmaceutiska, f. Institutionen för, v. Medicinska och farmaceutiska, Biomacromolecules in microgels — Opportunities and challenges for drug delivery, Current Opinion in Colloid & Interface Science, 15 (2010) 435-444.

[52] R. Pelton, T. Hoare, Microgels and Their Synthesis: An Introduction, Microgel Suspensions, Wiley-VCH Verlag GmbH & Co. KGaA2011, pp. 1-32.

[53] O. Okay, W. Funke, Anionic dispersion polymerization of 1,4-divinylbenzene, Macromolecules, 23 (1990) 2623-2628.

[54] M. Frank, W. Burchard, Microgels by intramolecular crosslinking of poly(allylamine) single chains, Die Makromolekulare Chemie, Rapid Communications, 12 (1991) 645-652.

[55] S. Neyret, B. Vincent, The properties of polyampholyte microgel particles prepared by microemulsion polymerization, Polymer, 38 (1997) 6129-6134.

[56] N.I. Prokopov, I.A. Gritskova, O.P. Kiryutina, M. Khaddazh, K. Tauer, S. Kozempel, The mechanism of surfactant-free emulsion polymerization of styrene, Polym. Sci. Ser. B, 52 (2010) 339-345.

[57] S.A. Deshmukh, S.K.R.S. Sankaranarayanan, K. Suthar, D.C. Mancini, Role of Solvation Dynamics and Local Ordering of Water in Inducing Conformational Transitions in Poly(N-isopropylacrylamide) Oligomers through the LCST, The Journal of Physical Chemistry B, 116 (2012) 2651-2663.

[58] M. Heskins, J.E. Guillet, Solution Properties of Poly(N-isopropylacrylamide), Journal of Macromolecular Science: Part A - Chemistry, 2 (1968) 1441-1455.

[59] Y. Zhang, S. Furyk, D.E. Bergbreiter, P.S. Cremer, Specific Ion Effects on the Water Solubility of Macromolecules: PNIPAM and the Hofmeister Series, Journal of the American Chemical Society, 127 (2005) 14505-14510.

[60] E.E. Meyer, K.J. Rosenberg, J. Israelachvili, Recent progress in understanding hydrophobic interactions, Proceedings of the National Academy of Sciences, 103 (2006) 15739-15746.

[61] Z.H. Farooqi, H.U. Khan, S.M. Shah, M. Siddiq, Stability of poly(N-isopropylacrylamide-*co*-acrylic acid) polymer microgels under various conditions of temperature, pH and salt concentration, Arabian Journal of Chemistry, DOI.

[62] M. Wang, Y. Fang, D. Hu, Preparation and properties of chitosan-poly(N-isopropylacrylamide) full-IPN hydrogels, Reactive and Functional Polymers, 48 (2001) 215-221.

[63] C. Wang, N.T. Flynn, R. Langer, Controlled Structure and Properties of Thermoresponsive Nanoparticle–Hydrogel Composites, Advanced Materials, 16 (2004) 1074-1079.

[64] S. Ohya, S. Kidoaki, T. Matsuda, Poly(N-isopropylacrylamide) (PNIPAM)-grafted gelatin hydrogel surfaces: interrelationship between microscopic structure and mechanical property of surface regions and cell adhesiveness, Biomaterials, 26 (2005) 3105-3111.

[65] K. Nakahama, K. Fujimoto, Thermosensitive Two-Dimensional Arrays of Hydrogel Particles, Langmuir, 18 (2002) 10095-10099.

[66] M. Shibayama, T. Tanaka, Volume Phase Transition and Releated Phenomena of Polymer Gels, Advances In Polymer Science, 109 (1993) 1-62.

[67] S.K. Reed, R.E. Westacott, The interface between water and a hydrophobic gas, Physical Chemistry Chemical Physics, 10 (2008) 4614-4622.

[68] J.C. Rodríguez-Cabello, M. Alonso, T. Pérez, M.M. Herguedas, Differential scanning calorimetry study of the hydrophobic hydration of the elastin-based polypentapeptide, poly(VPGVG), from deficiency to excess of water, Biopolymers, 54 (2000) 282-288.

[69] K. Kratz, T. Hellweg, W. Eimer, Influence of charge density on the swelling of colloidal poly(N-isopropylacrylamide-*co*-acrylic acid) microgels, Colloids and Surfaces A - Physicochemical and Engineering Aspects, 170 (2000) 137-149.

[70] A. Fernandez-Nieves, H. Wyss, J. Mattsson, D.A. Weitz, Microgel Suspensions: Fundamentals and Applications, John Wiley & Sons2011.

[71] M. Ilavský, J. Hrouz, Phase transition in swollen gels, Polym. Bull., 8 (1982) 387-394.

[72] I. Alenichev, L. Hanyková, M. Ilavský, Swelling and mechanical behavior of ionized poly(acrylamide-*co*-N,N’-diethylacrylamide) gels in water/acetone mixtures and in water at various temperatures, Polym. Bull., 58 (2007) 575-586.

[73] T. Tanaka, Phase transitions in gels and a single polymer, Polymer, 20 (1979) 1404-1412.

[74] E. Allahyarov, I. D'Amico, H. Löwen, Attraction between Like-Charged Macroions by Coulomb Depletion, Physical Review Letters, 81 (1998) 1334-1337.

[75] B. Beresford-Smith, D.Y.C. Chan, D.J. Mitchell, The electrostatic interaction in colloidal systems with low added electrolyte, Journal of Colloid and Interface Science, 105 (1985) 216-234.

[76] M. Keerl, V. Smirnovas, R. Winter, W. Richtering, Interplay between hydrogen bonding and macromolecular architecture leading to unusual phase behavior in thermosensitive microgels, Angewandte Chemie (International ed. in English), 47 (2008) 338-341.

[77] I. Juurinen, T. Pylkkänen, C.J. Sahle, L. Simonelli, K. Hämäläinen, S. Huotari, M. Hakala, Effect of the Hydrophobic Alcohol Chain Length on the Hydrogen-Bond Network of Water, The Journal of Physical Chemistry B, 118 (2014) 8750-8755.

[78] M.H. Smith, L.A. Lyon, Tunable Encapsulation of Proteins within Charged Microgels, Macromolecules, 44 (2011) 8154-8160.

[79] K.C. Clarke, L.A. Lyon, Modulation of the Deswelling Temperature of Thermoresponsive Microgel Films, Langmuir, 29 (2013) 12852-12857.

[80] G. Li, S. Song, L. Guo, S. Ma, Self-assembly of thermo- and pH-responsive poly(acrylic acid)-b-poly(N-isopropylacrylamide) micelles for drug delivery, Journal of Polymer Science Part A: Polymer Chemistry, 46 (2008) 5028-5035.

[81] S. Zhou, B. Chu, Synthesis and Volume Phase Transition of Poly(methacrylic acid-*co*-N-isopropylacrylamide) Microgel Particles in Water, The Journal of Physical Chemistry B, 102 (1998) 1364-1371.

[82] Y. Wang, G. Wei, F. Wen, X. Zhang, W. Zhang, L. Shi, Synthesis of gold nanoparticles stabilized with poly(N-isopropylacrylamide)-*co*-poly(4-vinyl pyridine) colloid and their application in responsive catalysis, Journal of Molecular Catalysis A: Chemical, 280 (2008) 1-6.

[83] L. Shen, A. Pich, D. Fava, M. Wang, S. Kumar, C. Wu, G.D. Scholes, M.A. Winnik, Loading quantum dots into thermo-responsive microgels by reversible transfer from organic solvents to water, Journal of Materials Chemistry, 18 (2008) 763-770.

[84] J. Bibette, Emulsion science: basic principles : an overview, Springer, New York, 2002.

[85] S.U. Pickering, CXCVI.-Emulsions, Journal of the Chemical Society, Transactions, 91 (1907) 2001-2021.

[86] B.P. Binks, S.O. Lumsdon, Influence of Particle Wettability on the Type and Stability of Surfactant-Free Emulsions†, Langmuir, 16 (2000) 8622-8631.

[87] B.P. Binks, Particles as surfactants—similarities and differences, Current Opinion in Colloid & Interface Science, 7 (2002) 21-41.

[88] R.M. Wiley, Limited coalescence of oil droplets in coarse oil-in-water emulsions, Journal of Colloid Science, 9 (1954) 427-437.

[89] F. Gautier, M. Destribats, R. Perrier-Cornet, J.-F. Dechezelles, J. Giermanska, V. Heroguez, S. Ravaine, F. Leal-Calderon, V. Schmitt, Pickering emulsions with stimulable particles: from highly- to weakly-covered interfaces, Physical Chemistry Chemical Physics, 9 (2007) 6455-6462.

[90] M. Destribats, M. Eyharts, V. Lapeyre, E. Sellier, I. Varga, V. Ravaine, V. Schmitt, Impact of pNIPAM Microgel Size on Its Ability To Stabilize Pickering Emulsions, Langmuir, 30 (2014) 1768-1777.

[91] T. Ngai, S.H. Behrens, H. Auweter, Novel emulsions stabilized by pH and temperature sensitive microgels, Chemical Communications (Cambridge, United Kingdom), DOI (2005) 331-333.

[92] S. Fujii, S.P. Armes, B.P. Binks, R. Murakami, Stimulus-responsive particulate emulsifiers based on lightly cross-linked poly(4-vinylpyridine)-silica nanocomposite microgels, Langmuir : the ACS journal of surfaces and colloids, 22 (2006) 6818-6825.

[93] S. Fujii, E.S. Read, B.P. Binks, S.P. Armes, Stimulus-Responsive Emulsifiers Based on Nanocomposite Microgel Particles, Advanced Materials, 17 (2005) 1014-1018.

[94] S. Tsuji, H. Kawaguchi, Thermosensitive Pickering Emulsion Stabilized by Poly(N-isopropylacrylamide)-Carrying Particles, Langmuir, 24 (2008) 3300-3305.

[95] B. Brugger, W. Richtering, Emulsions Stabilized by Stimuli-Sensitive Poly(N-isopropylacrylamide)-*co*-Methacrylic Acid Polymers: Microgels versus Low Molecular Weight Polymers, Langmuir, 24 (2008) 7769-7777.

[96] S. Lam, E. Blanco, S.K. Smoukov, K.P. Velikov, O.D. Velev, Magnetically Responsive Pickering Foams, Journal of the American Chemical Society, 133 (2011) 13856-13859.

[97] Q.-X. Mao, H. Wang, Y. Shu, X.-W. Chen, J.-H. Wang, A dual-ionic liquid microemulsion system for the selective isolation of hemoglobin, RSC Advances, 4 (2014) 8177-8182.

[98] Z. Du, Y.-L. Yu, J.-H. Wang, Extraction of Proteins from Biological Fluids by Use of an Ionic Liquid/Aqueous Two-Phase System, Chemistry – A European Journal, 13 (2007) 2130-2137.

[99] H. Monteillet, M. Workamp, X. Li, B. Schuur, J.M. Kleijn, F.A.M. Leermakers, J. Sprakel, Multi-responsive ionic liquid emulsions stabilized by microgels, Chemical Communications, 50 (2014) 12197-12200.

[100] C. Zhao, X. Gao, P. He, C. Xiao, X. Zhuang, X. Chen, Facile synthesis of thermo- and pH-responsive biodegradable microgels, Colloid and Polymer Science, 289 (2011) 447-451.

[101] L. Pérez-Álvarez, V. Sáez-Martínez, E. Hernáez, I. Katime, Novel pH- and Temperature-Responsive Methacrylamide Microgels, Macromolecular Chemistry and Physics, 210 (2009) 1120-1126.

[102] A. Pich, S. Bhattacharya, Y. Lu, V. Boyko, H.-J.P. Adler, Temperature-sensitive hybrid microgels with magnetic properties, Langmuir, 20 (2004) 10706-10711.

[103] L. Hu, L.-Y. Chu, M. Yang, H.-D. Wang, C. Hui Niu, Preparation and characterization of novel cationic pH-responsive poly(N , N'-dimethylamino ethyl methacrylate) microgels, Journal of Colloid and Interface Science, 311 (2007) 110-117.

[104] A.M. Lazim, M. Bradley, J. Eastoe, Controlling gold nanoparticle stability with triggerable microgels, Langmuir, 26 (2010) 11779-11783.

[105] H. Masoud, A. Alexeev, Controlled release of nanoparticles and macromolecules from responsive microgel capsules, ACS Nano, 6 (2012) 212-219.

[106] S.J. Tang, Z.B. Hu, B. Zhou, Z.D. Cheng, J.Z. Wu, M. Marquez, Melting kinetics of thermally responsive microgel crystals, Macromolecules, 40 (2007) 9544-9548.

[107] K. Ogawa, B. Wang, E. Kokufuta, Enzyme-regulated microgel collapse for controlled membrane permeability, Langmuir, 17 (2001) 4704-4707.

[108] L. Zhang, J.M.W. Spears, L.A. Lyon, Tunable swelling and rolling of microgel membranes, Langmuir, 30 (2014) 7628-7634.

[109] M.R. Nabid, Y. Bide, M. Niknezhad, Fe3O4–SiO2–P4VP pH-Sensitive Microgel for Immobilization of Nickel Nanoparticles: An Efficient Heterogeneous Catalyst for Nitrile Reduction in Water, ChemCatChem, 6 (2014) 538-546.

[110] S. Wiese, A.C. Spiess, W. Richtering, Microgel-Stabilized Smart Emulsions for Biocatalysis, Angewandte Chemie International Edition, 52 (2013) 576-579.

[111] R. Regmi, S.R. Bhattarai, C. Sudakar, A.S. Wani, R. Cunningham, P.P. Vaishnava, R. Naik, D. Oupicky, G. Lawes, Hyperthermia controlled rapid drug release from thermosensitive magnetic microgels, Journal of Materials Chemistry, 2 (2010) 6158-6163.

[112] D. Sivakumaran, D. Maitland, T. Oszustowicz, T. Hoare, Tuning drug release from smart microgel-hydrogel composites via cross-linking, Journal of Colloid and Interface Science, 392 (2013) 422-430.

[113] T. Hoare, R. Pelton, Impact of microgel morphology on functionalized microgel-drug interactions, Langmuir, 24 (2008) 1005-1012.

[114] M. Karg, I. Pastoriza-Santos, B. Rodriguez-González, R. von Klitzing, S. Wellert, T. Hellweg, Temperature, pH, and ionic strength induced changes of the swelling behavior of PNIPAM-poly(allylacetic acid) copolymer microgels, Langmuir, 24 (2008) 6300-6306.

[115] Z. Meng, M.H. Smith, L.A. Lyon, Temperature-programmed synthesis of micron-sized multi-responsive microgels, Colloid and Polymer Science, 287 (2009) 277-285.

[116] H. Zhang, S. Mardyani, W.C.W. Chan, E. Kumacheva, Design of biocompatible chitosan microgels for targeted pH-mediated intracellular release of cancer therapeutics, Biomacromolecules, 7 (2006) 1568-1572.

[117] G.M. Eichenbaum, P.F. Kiser, A.V. Dobrynin, S.A. Simon, D. Needham, Investigation of the Swelling Response and Loading of Ionic Microgels with Drugs and Proteins: The Dependence on Cross-Link Density, Macromolecules, 32 (1999) 4867-4878.

[118] A. Kondo, H. Fukuda, Preparation of thermo-sensitive magnetic hydrogel microspheres and application to enzyme immobilization, Journal of Fermentation and Bioengineering, 84 (1997) 337-341.

[119] F. Sauzedde, A. Elaïssari, C. Pichot, Hydrophilic magnetic polymer latexes. 1. Adsorption of magnetic iron oxide nanoparticles onto various cationic latexes, Colloid & Polymer Science, 277 (1999) 846-855.

[120] F. Sauzedde, A. Elaïssari, C. Pichot, Hydrophilic magnetic polymer latexes. 2. Encapsulation of adsorbed iron oxide nanoparticles, Colloid & Polymer Science, 277 (1999) 1041-1050.

[121] J. Ge, Y. Hu, T. Zhang, Y. Yin, Superparamagnetic composite colloids with anisotropic structures, Journal of the American Chemical Society, 129 (2007) 8974-8975.

[122] W. Wu, Q. He, C. Jiang, Magnetic Iron Oxide Nanoparticles: Synthesis and Surface Functionalization Strategies, Nanoscale Research Letters, 3 (2008) 397-415.

[123] H. Ma, L.L. Dai, Synthesis of polystyrene-silica composite particles via one-step nanoparticle-stabilized emulsion polymerization, Journal of Colloid and Interface Science, 333 (2009) 807-811.

[124] J. Rubio-Retama, N.E. Zafeiropoulos, C. Serafinelli, R. Rojas-Reyna, B. Voit, E.L. Cabarcos, M. Stamm, Synthesis and characterization of thermosensitive PNIPAM microgels covered with superparamagnetic gamma-Fe2O3 nanoparticles, Langmuir, 23 (2007) 10280-10285.

[125] N. Dhar, S.P. Akhlaghi, K.C. Tam, Biodegradable and biocompatible polyampholyte microgels derived from chitosan, carboxymethyl cellulose and modified methyl cellulose, Carbohydrate Polymers, 87 (2012) 101-109.

[126] C.T. Schwall, I.A. Banerjee, Micro- and Nanoscale Hydrogel Systems for Drug Delivery and Tissue Engineering, Materials, 2 (2009) 577-612.

[127] M. Andersson, S.L. Maunu, Structural studies of poly(N-isopropylacrylamide) microgels: Effect of SDS surfactant concentration in the microgel synthesis, Journal of Polymer Science Part B: Polymer Physics, 44 (2006) 3305-3314.

[128] S. Peng, C. Wu, Surfactant Effect on pH and Temperature Sensitivities of Poly(N-vinylcaprolactam-*co*-sodium acrylate) Microgels, Macromolecules, 34 (2001) 568-571.

[129] M. Bradley, B. Vincent, G. Burnett, Uptake and release of anionic surfactant into and from cationic core-shell microgel particles, Langmuir, 23 (2007) 9237-9241.

[130] M. Bradley, B. Vincent, Poly(vinylpyridine) core/poly(N-isopropylacrylamide) shell microgel particles: their characterization and the uptake and release of an anionic surfactant, Langmuir, 24 (2008) 2421-2425.

[131] G. Wang, R. Pelton, J. Zhang, Sodium dodecyl sulfate binding to poly(N-isopropylacrylamide) microgel latex studied by isothermal titration calorimetry, Colloids Surf. A, 153 (1999) 335-340.

[132] H.L. Ngo, K. LeCompte, L. Hargens, A.B. McEwen, Thermal properties of imidazolium ionic liquids, Thermochimica Acta, 357–358 (2000) 97-102.

[133] J.G. Huddleston, A.E. Visser, W.M. Reichert, H.D. Willauer, G.A. Broker, R.D. Rogers, Characterization and comparison of hydrophilic and hydrophobic room temperature ionic liquids incorporating the imidazolium cation, Green Chemistry, 3 (2001) 156-164.

[134] M.J. Earle, J.M.S.S. Esperanca, M.A. Gilea, J.N. Canongia Lopes, L.P.N. Rebelo, J.W. Magee, K.R. Seddon, J.A. Widegren, The distillation and volatility of ionic liquids, Nature, 439 (2006) 831-834.

[135] C. Maton, N. De Vos, C.V. Stevens, Ionic liquid thermal stabilities: decomposition mechanisms and analysis tools, Chemical Society Reviews, 42 (2013) 5963-5977.

[136] L. Chancelier, A.O. Diallo, C.C. Santini, G. Marlair, T. Gutel, S. Mailley, C. Len, Targeting adequate thermal stability and fire safety in selecting ionic liquid-based electrolytes for energy storage, Physical Chemistry Chemical Physics, 16 (2014) 1967-1976.

[137] D.M. Fox, J.W. Gilman, A.B. Morgan, J.R. Shields, P.H. Maupin, R.E. Lyon, H.C. De Long, P.C. Trulove, Flammability and Thermal Analysis Characterization of Imidazolium-Based Ionic Liquids, Industrial & Engineering Chemistry Research, 47 (2008) 6327-6332.

[138] M. Hayyan, F.S. Mjalli, M.A. Hashim, I.M. AlNashef, T.X. Mei, Investigating the electrochemical windows of ionic liquids, Journal of Industrial and Engineering Chemistry, 19 (2013) 106-112.

[139] A.M. O'Mahony, D.S. Silvester, L. Aldous, C. Hardacre, R.G. Compton, Effect of Water on the Electrochemical Window and Potential Limits of Room-Temperature Ionic Liquids, Journal of Chemical & Engineering Data, 53 (2008) 2884-2891.

[140] F. Heym, J. Haber, W. Korth, B.J.M. Etzold, A. Jess, Vapor Pressure of Water in Mixtures with Hydrophilic Ionic Liquids – A Contribution to the Design of Processes for Drying of Gases by Absorption in Ionic Liquids, Chemical Engineering & Technology, 33 (2010) 1625-1634.

[141] L.P.N. Rebelo, J.N. Canongia Lopes, J.M.S.S. Esperança, E. Filipe, On the Critical Temperature, Normal Boiling Point, and Vapor Pressure of Ionic Liquids, The Journal of Physical Chemistry B, 109 (2005) 6040-6043.

[142] J.-f. Liu, G.-b. Jiang, J.Å. Jönsson, Application of ionic liquids in analytical chemistry, TrAC Trends in Analytical Chemistry, 24 (2005) 20-27.

[143] Q. Zhang, S. Zhang, Y. Deng, Recent advances in ionic liquid catalysis, Green Chemistry, 13 (2011) 2619-2637.

[144] T. Welton, Room-Temperature Ionic Liquids. Solvents for Synthesis and Catalysis, Chemical Reviews, 99 (1999) 2071-2084.

[145] J.F. Brennecke, E.J. Maginn, Ionic liquids: Innovative fluids for chemical processing, AIChE Journal, 47 (2001) 2384-2389.

[146] B.F. Goodrich, J.C. de la Fuente, B.E. Gurkan, Z.K. Lopez, E.A. Price, Y. Huang, J.F. Brennecke, Effect of Water and Temperature on Absorption of CO2 by Amine-Functionalized Anion-Tethered Ionic Liquids, The Journal of Physical Chemistry B, 115 (2011) 9140-9150.

[147] K.M. Gupta, Y. Chen, Z. Hu, J. Jiang, Metal-organic framework supported ionic liquid membranes for CO2 capture: anion effects, Physical Chemistry Chemical Physics, 14 (2012) 5785-5794.

[148] D.J. Tempel, P.B. Henderson, J.R. Brzozowski, R.M. Pearlstein, H. Cheng, High Gas Storage Capacities for Ionic Liquids through Chemical Complexation, Journal of the American Chemical Society, 130 (2008) 400-401.

[149] J.G. Huddleston, H.D. Willauer, R.P. Swatloski, A.E. Visser, R.D. Rogers, Room temperature ionic liquids as novel media for 'clean' liquid-liquid extraction, Chemical Communications, DOI (1998) 1765-1766.

[150] G.-T. Wei, Z. Yang, C.-J. Chen, Room temperature ionic liquid as a novel medium for liquid/liquid extraction of metal ions, Analytica Chimica Acta, 488 (2003) 183-192.

[151] K. Nakashima, F. Kubota, T. Maruyama, M. Goto, Feasibility of Ionic Liquids as Alternative Separation Media for Industrial Solvent Extraction Processes, Industrial & Engineering Chemistry Research, 44 (2005) 4368-4372.

[152] Y. Sun, K. Yan, X. Huang, Formation, characterization and enzyme activity in water-in-hydrophobic ionic liquid microemulsion stabilized by mixed cationic/nonionic surfactants, Colloids and Surfaces B: Biointerfaces, 122 (2014) 66-71.

[153] T. Kakiuchi, Electrochemical Aspects of Ionic-Liquid|Water Two-Phase Systems, Analytical Chemistry, 79 (2007) 6442-6449.

[154] T. Nakashima, N. Kimizuka, Water/Ionic Liquid Interfaces as Fluid Scaffolds for the Two-Dimensional Self-Assembly of Charged Nanospheres, Langmuir, 27 (2011) 1281-1285.

[155] P. Taylor, Ostwald ripening in emulsions, Advances in Colloid and Interface Science, 75 (1998) 107-163.

[156] M.G. Freire, C.M.S.S. Neves, P.J. Carvalho, R.L. Gardas, A.M. Fernandes, I.M. Marrucho, L.M.N.B.F. Santos, J.A.P. Coutinho, Mutual Solubilities of Water and Hydrophobic Ionic Liquids, The Journal of Physical Chemistry B, 111 (2007) 13082-13089.

[157] G. Young, F. Nippgen, S. Titterbrandt, M.J. Cooney, Lipid extraction from biomass using co-solvent mixtures of ionic liquids and polar covalent molecules, Separation and Purification Technology, 72 (2010) 118-121.

[158] Y.-H. Kim, Y.-K. Choi, J. Park, S. Lee, Y.-H. Yang, H.J. Kim, T.-J. Park, Y. Hwan Kim, S.H. Lee, Ionic liquid-mediated extraction of lipids from algal biomass, Bioresource Technology, 109 (2012) 312-315.

[159] H. Zhao, S. Xia, P. Ma, Use of ionic liquids as ‘green’ solvents for extractions, Journal of Chemical Technology & Biotechnology, 80 (2005) 1089-1096.

[160] M. Matsumoto, K. Mochiduki, K. Fukunishi, K. Kondo, Extraction of organic acids using imidazolium-based ionic liquids and their toxicity to Lactobacillus rhamnosus, Separation and Purification Technology, 40 (2004) 97-101.

[161] K.E. Goklen, T.A. Hatton, Liquid-Liquid Extraction of Low Molecular-Weight Proteins by Selective Solubilization in Reversed Micelles, Separation Science and Technology, 22 (1987) 831-841.

[162] Y. Pei, J. Wang, K. Wu, X. Xuan, X. Lu, Ionic liquid-based aqueous two-phase extraction of selected proteins, Separation and Purification Technology, 64 (2009) 288-295.

[163] R.W. Style, L. Isa, E.R. Dufresne, Adsorption of soft particles at fluid interfaces, Soft Matter, 11 (2015) 7412-7419.

[164] K. Geisel, K. Henzler, P. Guttmann, W. Richtering, New Insight into Microgel-Stabilized Emulsions Using Transmission X-ray Microscopy: Nonuniform Deformation and Arrangement of Microgels at Liquid Interfaces, Langmuir, 31 (2015) 83-89.

[165] W. Richtering, Responsive Emulsions Stabilized by Stimuli-Sensitive Microgels: Emulsions with Special Non-Pickering Properties, Langmuir, 28 (2012) 17218-17229.

[166] V. Schmitt, V. Ravaine, Surface compaction versus stretching in Pickering emulsions stabilised by microgels, Current Opinion in Colloid & Interface Science, 18 (2013) 532-541.

[167] T. Ngai, H. Auweter, S.H. Behrens, Environmental Responsiveness of Microgel Particles and Particle-Stabilized Emulsions, Macromolecules, 39 (2006) 8171-8177.

[168] B.P. Binks, R. Murakami, S.P. Armes, S. Fujii, Effects of pH and Salt Concentration on Oil-in-Water Emulsions Stabilized Solely by Nanocomposite Microgel Particles, Langmuir, 22 (2006) 2050-2057.

[169] S.K. Mehta, G. Ram, K.K. Bhasin, Molecular interactions of [alpha],I-alkanediols in pyrrolidin-2-one: Thermophysical and spectroscopic measurements, The Journal of Chemical Thermodynamics, 40 (2008) 498.

[170] M. Constantin, M. Cristea, P. Ascenzi, G. Fundueanu, Lower critical solution temperature versus volume phase transition temperature in thermoresponsive drug delivery systems, Express Polymer Letters, 5 (2011) 839-848.

[171] E. Daly, B.R. Saunders, A study of the effect of electrolyte on the swelling and stability of poly(N-isopropylacrylamide) microgel dispersions, Langmuir, 16 (2000) 5546-5552.

[172] S. Dünnhaupt, J. Barthelmes, J. Hombach, D. Sakloetsakun, V. Arkhipova, A. Bernkop-Schnürch, Distribution of thiolated mucoadhesive nanoparticles on intestinal mucosa, International journal of pharmaceutics, 408 (2011) 191-199.

[173] J.E. Berlier, C.-Y. Cheung, W. Chang, J.D. Hirsch, J.M. Beechem, R.P. Haugland, R.P. Haugland, A. Rothe, G. Buller, J. Bradford, D.R. Gray, B.J. Filanoski, W.G. Telford, S. Yue, J. Liu, Quantitative comparison of long-wavelength Alexa Fluor dyes to Cy dyes: fluorescence of the dyes and their bioconjugates, The journal of histochemistry and cytochemistry : official journal of the Histochemistry Society, 51 (2003) 1699-1712.

[174] R.K. Mishra, K. Ramasamy, A.B.A. Majeed, pH-responsive poly(DMAPMA-*co*-HEMA) based hydrogels for prolonged release of 5-fluorouracil, Journal of Applied Polymer Science, 126 (2012) E98-E107.

[175] R.K. Mishra, A.R. Ray, Synthesis and characterization of poly{N-[3-(dimethylamino) propyl] methacrylamide-*co*-itaconic acid} hydrogels for drug delivery, Journal of Applied Polymer Science, 119 (2011) 3199-3206.

[176] J.M.D. Heijl, F.E. Du Prez, Fast, multi-responsive microgels based on photo-crosslinkable poly(2-(dimethylamino)ethyl methacrylate), Polymer, 45 (2004) 6771-6778.

[177] X. Pang, L. Zhao, C. Feng, Z. Lin, Novel Amphiphilic Multiarm, Starlike Coil–Rod Diblock Copolymers via a Combination of Click Chemistry with Living Polymerization, Macromolecules, 44 (2011) 7176-7183.

[178] X. Pang, L. Zhao, W. Han, X. Xin, Z. Lin, A general and robust strategy for the synthesis of nearly monodisperse colloidal nanocrystals, Nat Nano, 8 (2013) 426-431.

[179] M.E. Arnold, K. Nagai, R.J. Spontak, B.D. Freeman, D. Leroux, D.E. Betts, J.M. DeSimone, F.A. DiGiano, C.K. Stebbins, R.W. Linton, Microphase-Separated Block Copolymers Comprising Low Surface Energy Fluorinated Blocks and Hydrophilic Blocks: Synthesis and Characterization, Macromolecules, 35 (2002) 3697-3707.

[180] Y. Liu, S. Wang, C. Zhang, X. Su, S. Huang, M. Zhao, Enhancing the Selectivity of Enzyme Detection by Using Tailor-Made Nanoparticles, Analytical Chemistry, 85 (2013) 4853-4857.

[181] K.C.C. Johnson, F. Mendez, M.J. Serpe, Detecting solution pH changes using poly (N-isopropylacrylamide)-*co*-acrylic acid microgel-based etalon modified quartz crystal microbalances, Analytica Chimica Acta, 739 (2012) 83-88.

[182] S. Ito, K. Ogawa, H. Suzuki, B. Wang, R. Yoshida, E. Kokufuta, Preparation of Thermosensitive Submicrometer Gel Particles with Anionic and Cationic Charges†, Langmuir, 15 (1999) 4289-4294.

[183] K. Ogawa, A. Nakayama, E. Kokufuta, Preparation and Characterization of Thermosensitive Polyampholyte Nanogels, Langmuir, 19 (2003) 3178-3184.

[184] W.N. Charman, D.P. Christy, E.P. Geunin, D.C. Monkhouse, Interaction between calcium, a model divalent cation, and a range of poly (Acrylic Acid) resins as a function of solution pH, Drug Development and Industrial Pharmacy, 17 (1991) 271-280.

[185] H. Chen, M. Kelley, C. Guo, J.L. Yarger, L.L. Dai, Adsorption and release of surfactant into and from multifunctional zwitterionic poly(NIPAm-*co*-DMAPMA-*co*-AAc) microgel particles, Journal of Colloid and Interface Science, 449 (2015) 332-340.

[186] M.J. Snowden, B.Z. Chowdhry, B. Vincent, G.E. Morris, Colloidal copolymer microgels of N-isopropylacrylamide and acrylic acid: pH, ionic strength and temperature effects, Journal of the Chemical Society, Faraday Transactions, 92 (1996) 5013-5016.

[187] Z.H. Farooqi, H.U. Khan, S.M. Shah, M. Siddiq, Stability of poly(N-isopropylacrylamide-*co*-acrylic acid) polymer microgels under various conditions of temperature, pH and salt concentration, Arabian Journal of Chemistry, DOI.

[188] I. Dreissig, S. Machill, R. Salzer, C. Krafft, Quantification of brain lipids by FTIR spectroscopy and partial least squares regression, Spectrochimica Acta Part A: Molecular and Biomolecular Spectroscopy, 71 (2009) 2069-2075.

[189] T.A. Istarova, M.G. Semenova, G.M. Sorokoumova, A.A. Selishcheva, L.E. Belyakova, Y.N. Polikarpov, M.S. Anokhina, Effect of pH on the interactions of sodium caseinate with soy phospholipids in relation to the foaming ability of their mixtures, Food Hydrocolloids, 19 (2005) 429-440.

[190] A. Watanabe, A. Fujii, Y. Sakamori, K. Higashitsuji, H. Tamai, Studies on the behaviour of phospholipids at oil-water interfaces, Colloid & Polymer Science, 243 (1971) 42-47.

[191] M. Bradley, B. Vincent, G. Burnett, Uptake and release of surfactants from polyampholyte microgel particles, Colloid and Polymer Science, 287 (2009) 345-350.

[192] D. Platikanov, D. Exerowa, Highlights in Colloid Science, John Wiley & Sons2009.

[193] D. Steffy, A. Nichols, G. Kiplagat, Investigating the effectiveness of the surfactant dioctyl sodium sulfosuccinate to disperse oil in a changing marine environment, Ocean Sci. J., 46 (2011) 299-305.

[194] A. Chatterjee, S.P. Moulik, S.K. Sanyal, B.K. Mishra, P.M. Puri, Thermodynamics of Micelle Formation of Ionic Surfactants: A Critical Assessment for Sodium Dodecyl Sulfate, Cetyl Pyridinium Chloride and Dioctyl Sulfosuccinate (Na Salt) by Microcalorimetric, Conductometric, and Tensiometric Measurements, The Journal of Physical Chemistry B, 105 (2001) 12823-12831.

[195] C. Akbay, N. Wilmot, R.A. Agbaria, I.M. Warner, Characterization and application of sodium di(2-ethylhexyl) sulfosuccinate and sodium di(2-ethylhexyl) phosphate surfactants as pseudostationary phases in micellar electrokinetic chromatography, Journal of Chromatography A, 1061 (2004) 105-111.

[196] N. Jain, S. Trabelsi, S. Guillot, D. McLoughlin, D. Langevin, P. Letellier, M. Turmine, Critical Aggregation Concentration in Mixed Solutions of Anionic Polyelectrolytes and Cationic Surfactants, Langmuir, 20 (2004) 8496-8503.

[197] M.L. Stahla, B. Baruah, D.M. James, M.D. Johnson, N.E. Levinger, D.C. Crans, 1H NMR Studies of Aerosol-OT Reverse Micelles with Alkali and Magnesium Counterions: Preparation and Analysis of MAOTs, Langmuir, 24 (2008) 6027-6035.

[198] S. Bereswill, T. Vey, M. Kist, Susceptibility in vitro of Helicobacter pylori to cetylpyridinium chloride, FEMS Immunology & Medical Microbiology, 24 (1999) 189-192.

[199] S. Yunoki, M. Kohta, Y. Ohyabu, M. Sekiguchi, T. Kubo, T. Iwasaki, Electrostatic immobilization of cetylpyridinium chloride to poly(vinyl alcohol) hydrogels for the simple fabrication of wound dressings with the suppressed release of antibacterial agents, Journal of Applied Polymer Science, 131 (2014).

[200] M. Chiarini, C.A. Bunton, Oxidation of Thioanisole by Peroxomolybdate in Alcohol-Modified Micelles of Cetylpyridinium Chloride, Langmuir, 18 (2002) 8806-8812.

[201] D. Koley, A.J. Bard, Triton X-100 concentration effects on membrane permeability of a single HeLa cell by scanning electrochemical microscopy (SECM), Proceedings of the National Academy of Sciences of the United States of America, 107 (2010) 16783-16787.

[202] L.A. Lyon, A. Fernandez-Nieves, The Polymer/Colloid Duality of Microgel Suspensions, Annual Review of Physical Chemistry, 63 (2012) 25-43.

[203] S. Park, J.-Y. Wang, B. Kim, J. Xu, T.P. Russell, A Simple Route to Highly Oriented and Ordered Nanoporous Block Copolymer Templates, ACS Nano, 2 (2008) 766-772.

[204] R.A. Segalman, A. Hexemer, R.C. Hayward, E.J. Kramer, Ordering and Melting of Block Copolymer Spherical Domains in 2 and 3 Dimensions, Macromolecules, 36 (2003) 3272-3288.

[205] F. Aurenhammer, Voronoi diagrams—a survey of a fundamental geometric data structure, ACM Comput. Surv., 23 (1991) 345-405.

[206] A. Libál, C. Reichhardt, C.J.O. Reichhardt, Point-defect dynamics in two-dimensional colloidal crystals, Physical Review E - Statistical, Nonlinear, and Soft Matter Physics, 75 (2007) 011403.

[207] L.L. Dai, S. Tarimala, C.-y. Wu, S. Guttula, J. Wu, The Structure and Dynamics of Microparticles at Pickering Emulsion Interfaces, Scanning, 30 (2008) 87-95.

[208] H. Ma, L.L. Dai, Structure of Multi-Component Colloidal Lattices at Oil−Water Interfaces, Langmuir, 25 (2009) 11210-11215.

[209] K. Geisel, L. Isa, W. Richtering, The Compressibility of pH-Sensitive Microgels at the Oil–Water Interface: Higher Charge Leads to Less Repulsion, Angewandte Chemie, 126 (2014) 5005-5009.

[210] F. Pinaud, K. Geisel, P. Masse, B. Catargi, L. Isa, W. Richtering, V. Ravaine, V. Schmitt, Adsorption of microgels at an oil-water interface: correlation between packing and 2D elasticity, Soft Matter, 10 (2014) 6963-6974.

[211] Z. Li, T. Ming, J. Wang, T. Ngai, High Internal Phase Emulsions Stabilized Solely by Microgel Particles, Angewandte Chemie International Edition, 48 (2009) 8490-8493.

[212] M. Destribats, M. Wolfs, F. Pinaud, V. Lapeyre, E. Sellier, V. Schmitt, V. Ravaine, Pickering Emulsions Stabilized by Soft Microgels: Influence of the Emulsification Process on Particle Interfacial Organization and Emulsion Properties, Langmuir, 29 (2013) 12367-12374.

[213] Z. Li, D. Harbottle, E. Pensini, T. Ngai, W. Richtering, Z. Xu, Fundamental Study of Emulsions Stabilized by Soft and Rigid Particles, Langmuir, 31 (2015) 6282-6288.

[214] P. Massé, E. Sellier, V. Schmitt, V. Ravaine, Impact of Electrostatics on the Adsorption of Microgels at the Interface of Pickering Emulsions, Langmuir, 30 (2014) 14745-14756.

[215] M. Destribats, V. Lapeyre, M. Wolfs, E. Sellier, F. Leal-Calderon, V. Ravaine, V. Schmitt, Soft microgels as Pickering emulsion stabilisers: role of particle deformability, Soft Matter, 7 (2011) 7689-7698.

[216] M. Destribats, V. Lapeyre, E. Sellier, F. Leal-Calderon, V. Ravaine, V. Schmitt, Origin and Control of Adhesion between Emulsion Drops Stabilized by Thermally Sensitive Soft Colloidal Particles, Langmuir, 28 (2012) 3744-3755.

[217] T.A. Vilgis, M. Stapper, Microgels and fractal structures at interfaces and surfaces, Eur. Phys. J. B, 2 (1998) 69-74.

[218] D.S. Frost, J.J. Schoepf, E.M. Nofen, L.L. Dai, Understanding droplet bridging in ionic liquid-based Pickering emulsions, Journal of Colloid and Interface Science, 383 (2012) 103-109.

[219] Z. Chen, H. Ji, C. Zhao, E. Ju, J. Ren, X. Qu, Individual Surface-Engineered Microorganisms as Robust Pickering Interfacial Biocatalysts for Resistance-Minimized Phase-Transfer Bioconversion, Angewandte Chemie International Edition, 54 (2015) 4904-4908.

[220] Z. Chen, H. Ji, C. Zhao, E. Ju, J. Ren, X. Qu, Individual Surface-Engineered Microorganisms as Robust Pickering Interfacial Biocatalysts for Resistance-Minimized Phase-Transfer Bioconversion, Angewandte Chemie, 127 (2015) 4986-4990.

[221] Y. Yu, L. Fu, F. Zhang, T. Zhou, H. Yang, Pickering-Emulsion Inversion Strategy for Separating and Recycling Nanoparticle Catalysts, ChemPhysChem, 15 (2014) 841-848.

[222] M. Laurenti, P. Guardia, R. Contreras-Cáceres, J. Pérez-Juste, A. Fernandez-Barbero, E. Lopez-Cabarcos, J. Rubio-Retama, Synthesis of Thermosensitive Microgels with a Tunable Magnetic Core, Langmuir, 27 (2011) 10484-10491.

[223] J.-P. Belieres, C.A. Angell, Protic ionic liquids: Preparation, characterization, and proton free energy level representation, Journal of Physical Chemistry B, 111 (2007) 4926-4937.

[224] J. Lu, F. Yan, J. Texter, Advanced applications of ionic liquids in polymer science, Progress in Polymer Science, 34 (2009) 431-448.

[225] P. Kubisa, Application of ionic liquids as solvents for polymerization processes, Progress in Polymer Science, 29 (2004) 3-12.

[226] X. Han, D.W. Armstrong, Ionic liquids in separations, Accounts of Chemical Research, 40 (2007) 1079-1086.

[227] Z. Yang, Y.-J. Yue, M. Xing, Effect of ionic liquids on enzyme catalysis, Journal of Biotechnology, 136 (2008) S394-S395.

[228] A. Lewandowski, A. Świderska-Mocek, Ionic liquids as electrolytes for Li-ion batteries—An overview of electrochemical studies, Journal of Power Sources, 194 (2009) 601-609.

[229] D. Wakeham, G.G. Warr, R. Atkin, Surfactant adsorption at the surface of mixed ionic liquids and ionic liquid water mixtures, Langmuir, 28 (2012) 13224-13231.

[230] Y. Wang, L. Wei, K. Li, Y. Ma, N. Ma, S. Ding, L. Wang, D. Zhao, B. Yan, W. Wan, Q. Zhang, X. Wang, J. Wang, H. Li, Lignin dissolution in dialkylimidazolium-based ionic liquid-water mixtures, Bioresource technology, 170 (2014) 499-505.

[231] L.S. Sciarini, A. Rolland-Sabate, S. Guilois, P. Decaen, E. Leroy, P. Le Bail, Understanding the destructuration of starch in water-ionic liquid mixtures, Green Chemistry, 17 (2015) 291-299.

[232] A. Brandt, M.J. Ray, T.Q. To, D.J. Leak, R.J. Murphy, T. Welton, Ionic liquid pretreatment of lignocellulosic biomass with ionic liquid-water mixtures, Green Chemistry, 13 (2011) 2489-2499.

[233] J. Jeon, H. Kim, r.W.A. Goddard, T.A. Pascal, G.-I. Lee, J.K. Kang, The Role of Confined Water in Ionic Liquid Electrolytes for Dye-Sensitized Solar Cells, The Journal of Physical Chemistry Letters, 3 (2012) 556.

[234] Z. Liu, S.Z.E. Abedin, F. Endres, Electrodeposition of zinc films from ionic liquids and ionic liquid/water mixtures, Electrochimica Acta, 89 (2013) 635-643.

[235] C.E. Woodward, K.R. Harris, A lattice-hole theory for conductivity in ionic liquid mixtures: Application to ionic liquid + water mixtures, Physical Chemistry Chemical Physics, 12 (2010) 1172-1176.

[236] A. Efimova, G. Hubrig, P. Schmidt, Thermal stability and crystallization behavior of imidazolium halide ionic liquids, Thermochimica Acta, 573 (2013) 162-169.

[237] Y. Zhao, L. Wang, H.R. Byon, High-performance rechargeable lithium-iodine batteries using triiodide/iodide redox couples in an aqueous cathode, Nature Communications, 4 (2013) 1896.

[238] H. Huang, V. Agafonov, H. Yu, Molecular electric transducers as motion sensors: A review, Sensors (Switzerland), 13 (2013) 4581-4597.

[239] G. García, S. Aparicio, R. Ullah, M. Atilhan, Deep eutectic solvents: Physicochemical properties and gas separation applications, Energy and Fuels, 29 (2015) 2616-2644.

[240] P. Wang, S.M. Zakeeruddin, J.-E. Moser, M. Grätzel, A new ionic liquid electrolyte enhances the conversion efficiency of dye-sensitized solar cells, Journal of Physical Chemistry B, 107 (2003) 13280-13285.

[241] K.A. Maerzke, G.S. Goff, W.H. Runde, W.F. Schneider, E.J. Maginn, Structure and dynamics of Uranyl cations in ionic liquid/water mixtures via molecular dynamics simulations, Journal of Physical Chemistry B, 117 (2013) 10852.

[242] W. Jiang, Y. Wang, G.A. Voth, Molecular dynamics simulation of nanostructural organization in ionic liquid/water mixtures, The Journal of Physical Chemistry. B, 111 (2007) 4812.

[243] Z. Wojnarowska, K. Grzybowska, L. Hawelek, A. Swiety-Pospiech, E. Masiewicz, M. Paluch, W. Sawicki, A. Chmielewska, P. Bujak, J. Markowski, Molecular dynamics studies on the water mixtures of pharmaceutically important ionic liquid lidocaine HCl, Molecular Pharmaceutics, 9 (2012) 1250-1261.

[244] C.G. Hanke, R.M. Lynden-Bell, A simulation study of water-dialkylimidazolium ionic liquid mixtures, Journal of Physical Chemistry B, 107 (2003) 10873-10878.

[245] H.J.C. Berendsen, D. van der Spoel, R. van Drunen, GROMACS: A message-passing parallel molecular dynamics implementation, Computer Physics Communications, 91 (1995) 43-56.

[246] E. Lindahl, B. Hess, D. van der Spoel, u. Uppsala, b. Institutionen för naturvetenskaplig, s. Biologiska, m. Institutionen för cell- och, s. Kemiska, v. Teknisk-naturvetenskapliga, GROMACS 3.0: a package for molecular simulation and trajectory analysis, Journal of Molecular Modeling, 7 (2001) 306-317.

[247] D. Van Der Spoel, E. Lindahl, B. Hess, G. Groenhof, A.E. Mark, H.J.C. Berendsen, GROMACS: Fast, flexible, and free, Journal of Computational Chemistry, 26 (2005) 1701-1718.

[248] H.J.C. Berendsen, J.R. Grigera, T.P. Straatsma, The missing term in effective pair potentials, Journal of Physical Chemistry, 91 (1987) 6269-6271.

[249] J.N. Canongia Lopes, J. Deschamps, A.A.H. Pádua, Modeling Ionic Liquids Using a Systematic All-Atom Force Field, Journal of Physical Chemistry B, 108 (2004) 2038-2047.

[250] B. Bhargava, S. Balasubramanian, Refined potential model for atomistic simulations of ionic liquid [bmim] [P F 6], Journal of Chemical Physics, 127 (2007) 114510-114510-114516.

[251] B.L. Bhargava, S. Balasubramanian, Insights into the structure and dynamics of a room-temperature ionic liquid: Ab initio molecular dynamics simulation studies of 1-n-butyl-3- methylimidazolium hexafluorophosphate ([bmim][PF6]) and the [bmim][PF6]-CO2 mixture, Journal of Physical Chemistry B, 111 (2007) 4477-4487.

[252] B. Hess, P-LINCS: A parallel linear constraint solver for molecular simulation, Journal of Chemical Theory and Computation, 4 (2008) 116-122.

[253] B. Hess, H. Bekker, H.J.C. Berendsen, J.G.E.M. Fraaije, LINCS: A Linear Constraint Solver for molecular simulations, Journal of Computational Chemistry, 18 (1997) 1463-1472.

[254] W.L. Jorgensen, J.D. Madura, C.J. Swenson, Optimized intermolecular potential functions for liquid hydrocarbons, Journal of the American Chemical Society, 106 (1984) 6638-6646.

[255] M. Bühl, A. Chaumont, R. Schurhammer, G. Wipff, Ab initio molecular dynamics of liquid 1,3-dimethylimidazolium chloride, Journal of Physical Chemistry B, 109 (2005) 18591-18599.

[256] T.I. Morrow, E.J. Maginn, Molecular dynamics study of the ionic liquid 1-n-butyl-3-methylimidazolium hexafluorophosphate, Journal of Physical Chemistry B, 106 (2002) 12807-12813.

[257] N. Sieffert, G. Wipff, The [BMI][Tf2N] ionic liquid/water binary system: A molecular dynamics study of phase separation and of the liquid-liquid interface, Journal of Physical Chemistry B, 110 (2006) 13076-13085.

[258] D.S. Frost, M. Machas, B. Perea, L.L. Dai, Nonconvective mixing of miscible ionic liquids, Langmuir, 29 (2013) 10159-10165.

[259] T.G.A. Youngs, C. Hardacre, Application of static charge transfer within an ionic-liquid force field and its effect on structure and dynamics, ChemPhysChem, 9 (2008) 1548-1558.

[260] E. Maginn, H. Liu, A molecular dynamics investigation of the structural and dynamic properties of the ionic liquid 1-n-butyl-3-methylimidazolium bis(trifluoromethanesulfonyl)imide, Journal of Chemical Physics, 135 (2011) 124507-124507-124516.

[261] H.J.C. Berendsen, J.P.M. Postma, W.F. Van Gunsteren, A. Dinola, J.R. Haak, Molecular dynamics with coupling to an external bath, The Journal of Chemical Physics, 81 (1984) 3684-3690.

[262] M. Parrinello, Polymorphic transitions in single crystals: A new molecular dynamics method, Journal of Applied Physics, 52 (1981) 7182.

[263] G. Yu, D. Zhao, L. Wen, S. Yang, X. Chen, Viscosity of ionic liquids: Database, observation, and quantitative structure-property relationship analysis, AIChE Journal, 58 (2012) 2885-2899.

[264] U. Domanska, M. Krolikowska, Density and Viscosity of Binary Mixtures of Thiocyanate Ionic Liquids plus Water as a Function of Temperature, Journal of Solution Chemistry, 41 (2012) 1422-1445.

[265] H. Rodríguez, J.F. Brennecke, Temperature and composition dependence of the density and viscosity of binary mixtures of water + ionic liquid, Journal of Chemical and Engineering Data, 51 (2006) 2145-2155.

[266] O. Redlich, A.T. Kister, Algebraic Representation of Thermodynamic Properties and the Classification of Solutions, Industrial & Engineering Chemistry, 40 (1948) 345-348.

[267] B. Mokhtarani, A. Sharifi, H.R. Mortaheb, M. Mirzaei, M. Mafi, F. Sadeghian, Density and viscosity of pyridinium-based ionic liquids and their binary mixtures with water at several temperatures, The Journal of Chemical Thermodynamics, 41 (2009) 323-329.

APPENDIX A

A COMBINED EXPERIMENTAL AND MOLECULAR DYNAMICS STUDY OF IODIDE-BASED IONIC LIQUID

INTRODUCTION

As discussed in Chapter 2, Ionic liquids (ILs) are salts that remain liquid at or below 100 °C, and often at or below room temperature. They remain liquid at such unusually low temperatures due to bulky, asymmetric constituent ions, which resist crystalline packing [223]. As they are liquids made up entirely of ions, ILs have unusual properties that make them potentially useful for a variety of applications including polymerization [224, 225], gas separation [226], enzymatic reactions [227], and batteries [228]. One intriguing aspect of ILs is their tunability—because each ionic liquid consists of a cation and an anion, cations and anions can be mixed and matched to obtain desired properties [229]. The properties of ILs can be further tuned by mixing them with other liquids such as water.

Water/IL mixtures have been explored for use in bio-engineering applications such as dissolving biopolymers [230], destructuring starch [231], and pretreating biomass for use in fuels [232]. These mixtures have also found important use in electrical applications, serving as electrolytes for dye-sensitized solar cells [233] and the electrodeposition of zinc films [234]. Adding water to ionic liquids is particularly useful in electrical applications because many ionic liquids, while they can function as charge carriers, are highly viscous. This high viscosity limits the diffusion of charge carriers, thus limiting conductivity. Adding a low-viscosity solvent like water, therefore, has been found to greatly improve electrical performance [235]. The most common electrochemical application utilizing iodide ionic liquids, dye-sensitized solar cells, works most effectively with a low water content (about 10% by mole) [233]. However, the triiodide/iodide redox couple has been used in other electrochemical devices, many of

which do not have the same limits in regards to water content as cells containing dyes [236, 237]. Some of these applications, such as molecular electric transducer (MET) based sensors [238] currently use water-based electrolytes, but their usefulness could be limited by the working temperature range of water. Furthermore, water can act as a hydrogen bond donor with halide salts such as ILs to greatly lower the mixture transition temperature [239], potentially creating mixtures with an unusually wide operating temperature. Hopefully, the study of iodide IL/water mixtures will pave the way for the use of ILs in a wider variety of electrochemical devices.

This paper examines mixtures of water with 1-butyl-3-methylimidazolium iodide ([BMIM][I]). While pure alkyl-imidazolium iodide ILs have been widely employed as iodide sources in electrolytes for dye-sensitized solar cells [240], their usefulness is limited by their particularly high viscosity. Thus, we set out to overcome this limitation by adding water to lower the viscosity of [BMIM][I]. The properties of such mixtures have not been systematically studied or even reported. Here, we combine an experimental study with molecular dynamics (MD) simulations to explore the properties of [BMIM][I]/water mixtures.

In the experimental study, density, melting point, viscosity, and ionic conductivity were reported for a range of concentrations of water in the IL. Trends in these properties were identified. The density measurements were used to tune an all-atom molecular dynamics model describing [BMIM][I], which was then used in MD simulations of the same [BMIM][I]/water mixtures. Similar simulations have been used to study mixtures of other ILs with water [241-244] and allow description of the molecular structure and fundamental physics of these mixtures. In this study, the results of MD simulations were

directly compared to the experimentally measured properties, relating molecular-level physics and structure to the macroscopic behavior of the mixtures. This study does not only provide a greater theoretical understanding of ionic liquids and their mixtures - also allows researchers to tune mixtures for desired properties such as conductivity and viscosity. We also hope that researchers might consider the usefulness of iodide-containing ionic liquids and their mixtures for a wider variety of applications in the future.

METHODOLOGY

Materials and Mixing

The ionic liquid 1-butyl-3-methylimidazolium iodide ([BMIM][I]) was purchased from Ionic Liquids Technologies Inc. and the water was HPLC grade from Fisher Scientific. Both were used as received, without further purification. The ionic liquid/water mixtures were prepared by ultrasonic agitation for 1 minute with a Sonics VibraCell 500W in an ice water bath at an amplitude of 21%. The mixtures were observed to be homogenous and fully miscible by visual inspection.

Density

Density values were obtained by using a 2 mL specific gravity bottle at room temperature, following calibration of the bottle with pure HPLC water.

Melting Point

The melting points of the mixtures were measured using a TA Instruments Q20 differential scanning calorimeter (DSC). A cooling scan was performed from 20 to -90 °C at a rate of 2 °C per min followed by a heating scan from -90 to 20 °C, also at 2 °C per min, and the melting point was determined with the TA Universal Analysis software at

the large spike in the heat flow signifying the heat of fusion. T_{zero} pans with lids were used to contain all samples, with air used as the reference.

Viscosity

A TA Instruments AR-G2 rheometer equipped with a 60 mm, 1° cone was used to measure the viscosity via a flow procedure, with the temperature kept at 25°C via a water cooled/heated Peltier plate. A strain rate sweep was performed from 0.1 to 100 s^{-1}. The IL/water mixtures were generally Newtonian fluids with a constant viscosity across sheer rates, and so the viscosity at a sheer rate of 1 s^{-1} was taken to be the viscosity of each mixture.

Conductivity

Conductivity measurements were determined via Oakton PC 700 pH/mV/Conductivity bench top meter. The instrument conductivity ranges from 0 to 200.00 mS. The instrument has a full scale resolution of 0.5% and an accuracy of ±1%. Throughout the experiment, the sample was placed in a constant temperature water bath kept at 300.0 ± 0.5 K. Each measurement was repeated three times and the average values were evaluated. In addition, prior to each measurement, the instrument was calibrated with corresponding KCl conductivity standard solutions.

Computational Section

Simulations were performed using the GROMACS 4.6 package [245-247]. Simulation systems were designed to mirror the same [BMIM][I]/water mixture proportions studied in the experimental section. The total number of molecules in each system was chosen to give a simulation box of approximately 5x5x5 nm^3. The number of [BMIM][I] pairs and water molecules in each system is shown in Table A1. In each

system, molecules were placed in a simulation box randomly and then allowed to equilibrate for 1 ns.

Table A1 Compositions of simulation systems.

	Pure	**Mole % Water**					
	[BMIM][I]	**10%**	**20%**	**30%**	**50%**	**70%**	**90%**
[BMIM][I] (# ion pairs)	450	450	440	420	400	360	300
Water (# molecules)	0	50	110	180	400	840	2700

Water was described with the extended simple point charge (SPC/E) model [248]. The BMIM molecule was described by the all-atom force field developed by Lopes, et al. [249], and refined by Bhargava and Balasubramanian [250, 251]. In keeping with this force field, h-bonds within the BMIM molecule were constrained by the LINCS algorithm [252, 253]. The Leonard-Jones parameters for iodide were taken from the optimized intermolecular potentials for liquid simulations (OPLS) force field [254]. For both BMIM and iodide, we scaled the partial atomic charges to give total molecular charges of ±0.5. The technique of scaling charges in this manner has been extensively used to capture the effect of charge transfer between cation and anion in ionic liquids when using a non-polarizable force field [250, 255-258]. Models with scaled charges have been found to simulate density and diffusivity of ionic liquids better than models using charges of ±1 [250, 259, 260]. In this case, the charges were scaled to fit the simulated densities of [BMIM][I]/water mixtures to the densities measured by experiment. With molecular charges of ±0.5, densities of each simulation were within 1.6% of the experimental density (as seen in Table A4 in the results section below).

After the initial boxes were generated, 1,000 energy minimization steps were performed using the steepest descent method. Initial atomic velocities were generated with a Maxwellian distribution at an absolute temperature of 300 K. Newton's equation of motion was integrated using the leap-frog algorithm with a time step of 0.002 ps. All simulations were carried out under the NPT ensemble using the Berendsen-thermostat [261] to maintain temperature at 300K and the Parinello-Rahman barostat [262] to maintain pressure at 1 bar. The Particle-Mesh Ewald (PME) method was used to account for long-range electrostatic interactions. The cut off distance for Lennard-Jones forces was chosen as r = 1.2 nm to match the cut-off used by the developers of the BMIM forcefield [249, 250]. After the simulation, densities, radial distribution functions, and diffusion coefficients were calculated using GROMACS analysis tools and the simulation systems were visualized using visual molecular dynamics (VMD).

RESULTS AND DISCUSSION

Densities and Melting Points of [BMIM][I]/Water Mixtures

Density and melting point for each mixture were measured, as each of these properties is related to the internal structure and molecular interactions of ionic liquids and their mixtures. The values of each for [BMIM][I]/water mixtures containing various percentages of water are shown in Figure A1. The density of the mixture decreases only slightly (staying almost steady) between 0 and 50% water. From 50 to 100% water, density decreases exponentially with increasing water. The trend in melting points is similar, with one major difference – between 10 and 50% water, adding more water actually *decreases* the melting point, the opposite trend from that which might be expected given the relatively high melting point of water. This unusual trend in particular

calls for study of the mixtures on a molecular level, and will be discussed further below. As more water is added past 50% the melting point increases rapidly.

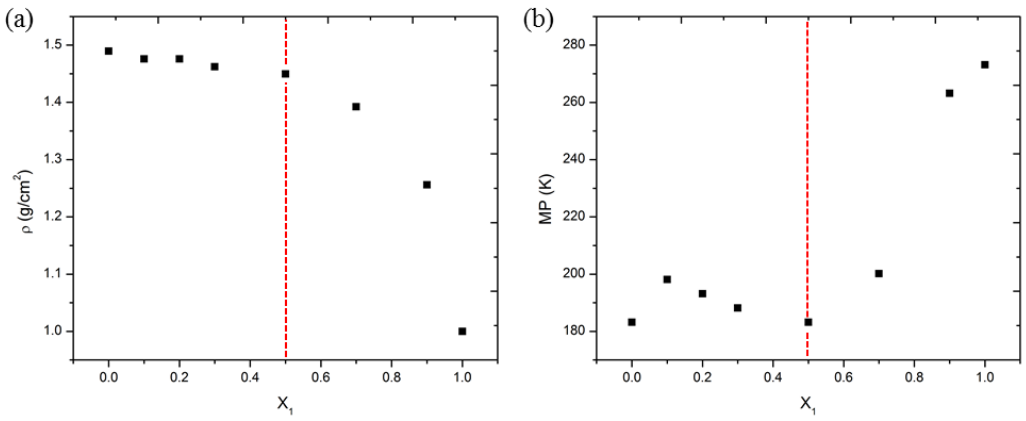

Figure A1 (a) Density and (b) melting point of binary water/[BMIM][I] mixtures by mole fraction water (X_1). The vertical line at X_1=0.5 for each chart is provided for guidance.

From these results, it is clear that there are two distinct regions within the range of [BMIM][I]/water mixtures—one encompassing all mixtures up to 50% water by mole, and one encompassing all mixtures from 50% to pure water. Both properties shown above – density and melting point – are related to molecular-level ordering within the liquid. Density depends on the packing-together of molecules, while ionic liquids have unusually low melting points because their bulky structures prevent the formation of crystal structures. Therefore, it is likely that the two regions of IL/water mixtures (above and below 50% water) have different structures on the molecular scale. To explore this phenomenon, we employed molecular dynamics simulations performed in parallel to the experimental measurements.

The densities calculated from MD simulations of the [BMIM][I]/water mixtures were compared to experimental densities, as seen in Table A2. The difference between

the simulated and experimental densities ranges from -1.6% to 0.3%, indicating that the model is adequate to describe the interaction between water and [BMIM][I] molecules.

Table A2 Simulated vs. experimental mixture density at 300 K**.**

X_1 (mole fraction water)	Density Simulation (g/cm^3)	Density Experiment (g/cm^3)	% Difference
0	1.465	1.489	-1.6%
0.1	1.462	1.476	-0.9%
0.2	1.459	1.476	-1.1%
0.3	1.454	1.462	-0.6%
0.5	1.437	1.450	-0.8%
0.7	1.398	1.392	0.4%
0.9	1.259	1.259	0.3%

Figure A2 shows representative snapshots of the simulation system for each of the mixtures. From viewing the system visually, it is possible to make qualitative judgments about the molecular ordering within the mixtures. At low water concentrations, individual water molecules are suspended within [BMIM][I]. Each water molecule is paired with at least one iodide atom, and most have attracted two. This may explain the trend in melting points between 10 and 50% water as seen in Figure A1. The water molecules draw the iodide atoms away from the BMIM molecules, making the mixture less ordered and preventing crystallization.

At 50% water, the water molecules are beginning to form chains of water-iodide-water. After this point, the overall structure changes drastically with additional water. By 70% water, chains of water reach across the simulation box, and not every water molecule is matched by an iodide atom, though nearly every iodide is attached to a water

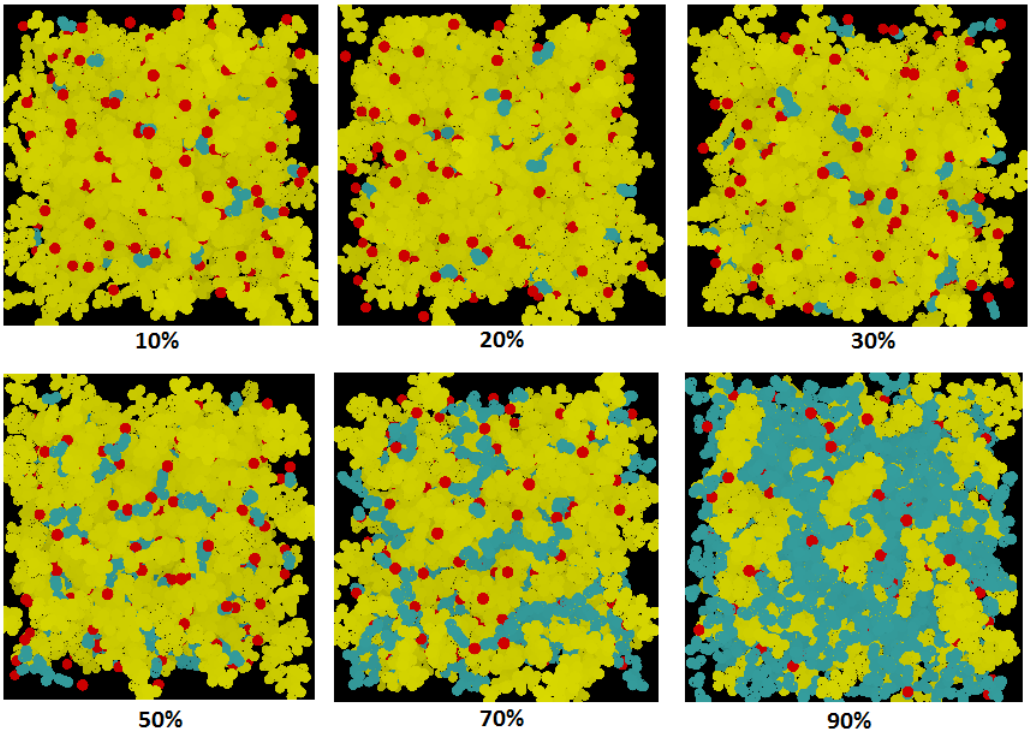

Figure A2 Representative snapshots of MD simulation boxes for mole percentages of water ranging from 10-90%. Each dot is an atom, with yellow representing [BMIM], red [I], and blue water.

chain. At 90% water, the system resembles water with [BMIM][I] dissolved in it more than it does [BMIM][I] with chains of water snaking through. This may explain the rapid change in density at concentrations of water over 50%. It may also explain the change in the trend of melting points in this composition region. As the water molecules aggregate, it becomes easier for the water molecules to crystallize and the [BMIM][I] molecules become less of a barrier to crystallization.

Viscosities and Conductivities of [BMIM][I]/Water Mixtures

Viscosity and ionic conductivity were measured as both properties are highly relevant to potential electrochemical applications of [BMIM][I]/water mixtures. These properties are shown in Figure A3.

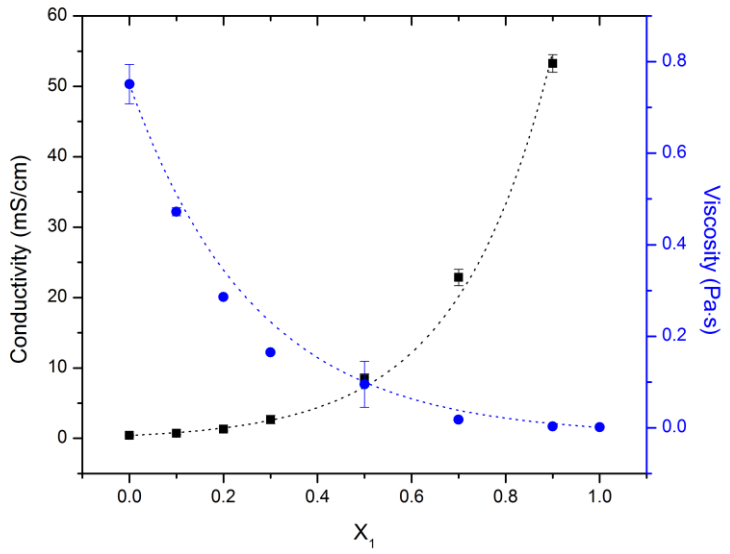

Figure A3 comparison of the conductivity (black squares) and average viscosity (blue circles) of binary water/[BMIM][I] mixtures by mole fraction water (X_1).

Viscosity and conductivity are generally related, as high viscosity impedes the movement of ions. Figure A3 confirms this relationship, showing that conductivity increases exponentially as viscosity decreases with a similar trend.

As hydrogen bonding is one of the most significant factors effecting the viscosity of ionic liquids [263], it is not surprising that water content strongly effects viscosity: as water is added to [BMIM][I], the viscosity drops sharply. However, this effect seems to be more powerful for [BMIM][I]/water mixtures than for aqueous mixtures of other imidazolium ionic liquids. For example, neither [BMIM][SCN] [264], [EMIM][$EtSO_4$]

[265], [EMIM][OTf] [265], nor [EMIM][TFA] [265] show such a steep drop in viscosity at compositions below 50% water. The viscosities of all of these ionic liquids decrease with added water, but more slowly. From this observation, it was hypothesized that the interaction between iodide and water accounts for the dramatic drop in viscosity with increasing water content and is important to the behavior of these mixtures. The MD

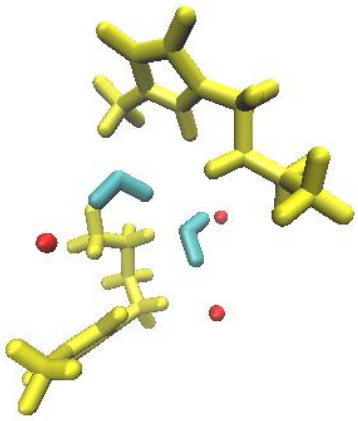

Figure A4 BMIM (yellow), iodide (red), and water (blue) from simulation, showing hydrogen bonds.

simulations bear out this hypothesis. Figure A4 shows a representative picture of the arrangement of BMIM, iodide, and water from the simulation, making it clear that iodide forms hydrogen bonds with the water. The pattern shown here reoccurs throughout the simulation, with water and iodide effectively forming chains of hydrogen-bonded molecules.

The intermolecular interactions within the mixtures are further illustrated by the viscosity deviation – a measure of how the mixture viscosity differs from the viscosity of an ideal mixture. Viscosity deviation is calculated by the equation [266]:

$$\Delta\eta = \eta - x_1\eta_1 - x_2\eta_2 \qquad \text{(A.1)}$$

where η is the mixture viscosity as measured by experiment, x_n is mole fraction, η_n is the viscosity of the pure components, and n = 1 for water and 2 for [BMIM][I]. It is shown in Figure A5. In an ideal mixture, each component behaves as if it were in a pure liquid, so the viscosity deviation represents the interaction of the components in so far as those interactions affect viscosity. In this case, the viscosity deviation is negative for all mole fractions of water – the interactions between water and [BMIM][I] reduce viscosity. This is similar to other ionic liquid/water mixtures [264, 265, 267]. However, the magnitude of the deviation is much greater than that of these other mixtures, indicating that the interactions between [BMIM][I] and water must be unusual in some way although the detailed mechanisms of this interaction are unclear. This reinforces the observation made above that small amounts of water decrease the viscosity of [BMIM][I] more than similar ionic liquids with different anions.

As can be seen in Figure A5, the viscosity deviation curve is also skewed toward the left with a minimum at about 30% water. This means that a small amount of water effects the viscosity of [BMIM][I] more than a small amount of [BMIM][I] effects the viscosity of water.

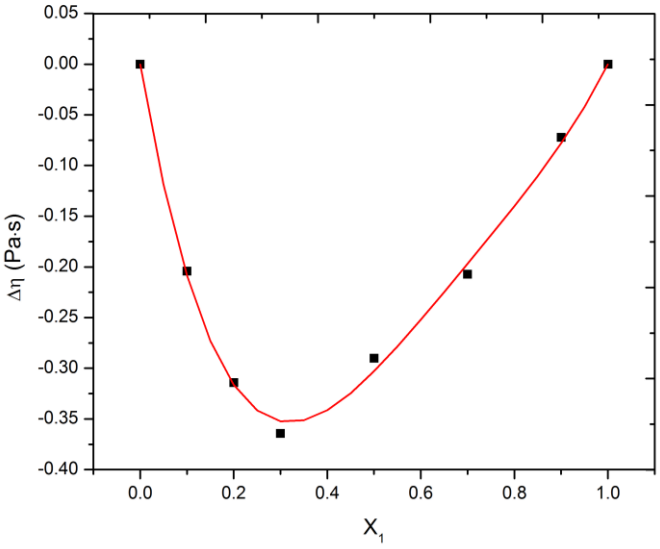

Figure A5 Viscosity deviation vs. mole fraction water (X_1). The line is a Redlich-Kister polynomial [263] fit to the data by least-squares regression. Redlich-Kister polynomials describe excess molar quantities such as excess molar volume and viscosity deviation. It is the form $\mathbf{Q_{ij} = x_i x_j \sum_{k=0}^{m} B_k (x_i - x_j)^k}$ where i and j are any two components, B_k are parameters fit by regression, and m is the degree of the polynomial expansion. In this case a third order polynomial was used.

Radial Distribution Functions and Self-Diffusion Coefficients for [BMIM][I]/Water Mixtures

To give a more quantitative picture of the structure of these mixtures, radial distribution functions (rdfs) were calculated from the MD simulations. Figure A6 shows rdfs centered around the imidazolium ring within BMIM. (Each cation molecule consists of a hydrophilic imidazolium ring, the "head," and a hydrophobic hydrocarbon chain, the "tail.") Adding any water at all changes the molecular ordering of [BMIM][I]. Even 10% water pushes the BMIM tail closer to the head. The water inserts itself into the ordered structure of the ionic liquid as it is pulled close to iodide through hydrogen bonds. The pattern is similar for all rdfs up to 50% water, when this ordering begins to break down. Between 50 and 90% water, the ordered spacing of iodide anions around the cation head

becomes less distinct until the rdf shows one broad, messy peak rather than several sharp ones. The water no longer has a small peak on either side of the iodide peak. By 90% water, the water is not inserted into the [BMIM][I] structure at all, and there is no apparent ordering of water around the cation head.

These rdfs provide further evidence of two distinct behavior regimes below and above 50% water. They may also show why the viscosity deviation plot in Figure A5 is skewed to the left – even a small amount of water inserts itself into the ordering of [BMIM][I], disrupting the intermolecular interactions that account for the IL's unusually high viscosity.

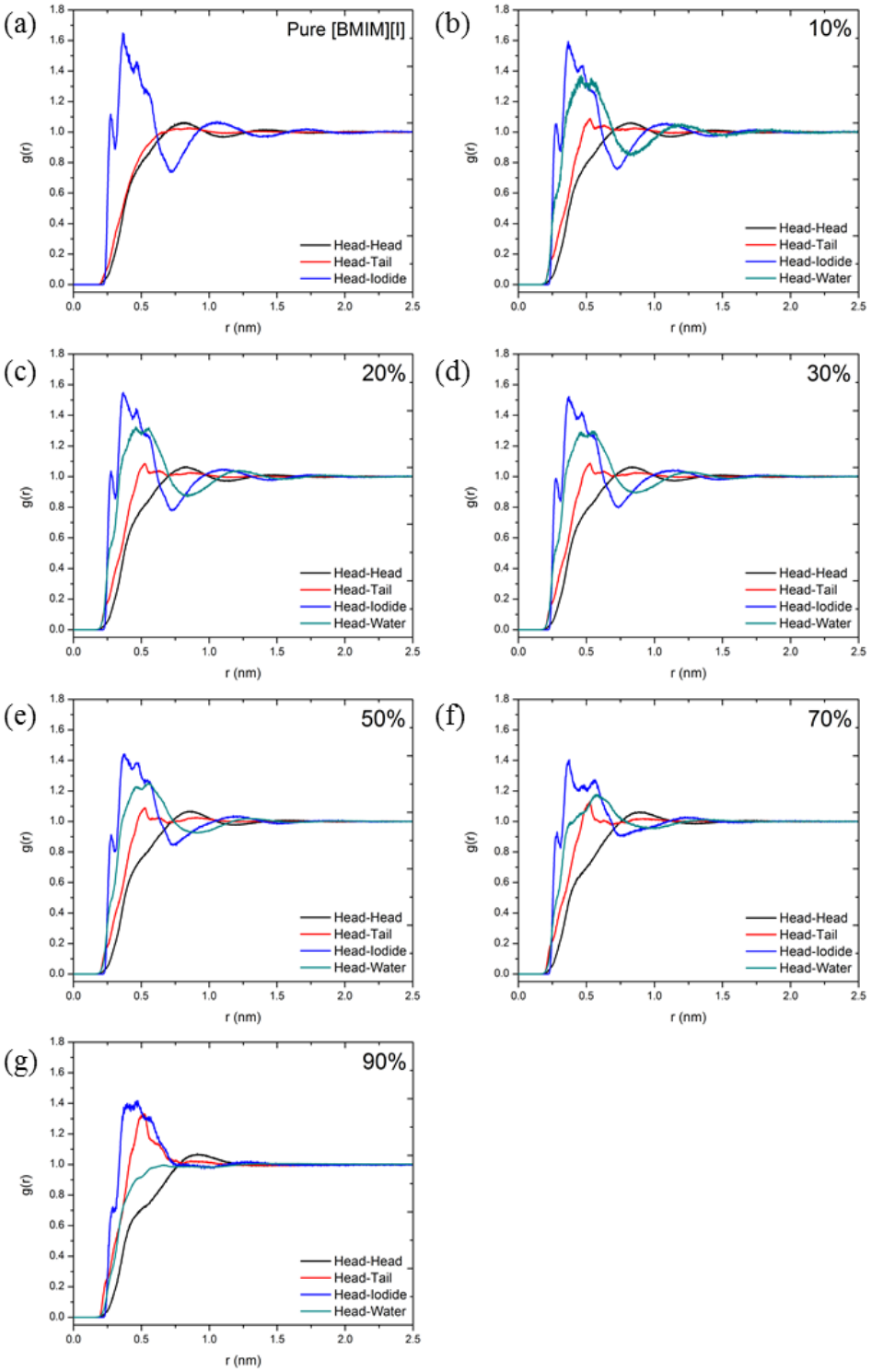

Figure A6 Radial distribution functions around the cation head. "Head" refers to the imidazolium ring within BMIM while "tail" refers to the butyl chain.

Since iodide-water hydrogen bonding has been shown to important for the behavior of these mixtures, rdfs were also calculated for iodide and water surrounding the iodide anion. These are shown in Figure A7. Water arranges itself around iodide in two peaks which probably represent two hydrogen atoms drawn to the iodide by hydrogen bonds. Please note, the magnitude of these peaks decrease as the water content increases. This is because, in low water content mixtures, every single water molecule is drawn close to an iodide atom. As more water is added, some of the water molecules are close to other water molecules instead. Since the rdf is normalized against the all the water in the system, the size of the peaks around iodide decrease. More interesting is the radial distribution function of iodide around itself. At low concentrations of water, there is a broad peak indicating that iodide molecules tend to stay at a similar distance from each other, but only somewhat. As more water is added, another peak appears closer to the center iodide as the water molecules draw the iodide atoms closer together than they would otherwise arrange themselves. This peak becomes distinct at 50% water (the divide between the two composition regions identified above) and only becomes more so as the water concentration rises to 90% and every single iodide is hydrogen-bonded to water (the reverse of what happens at low water concentrations).

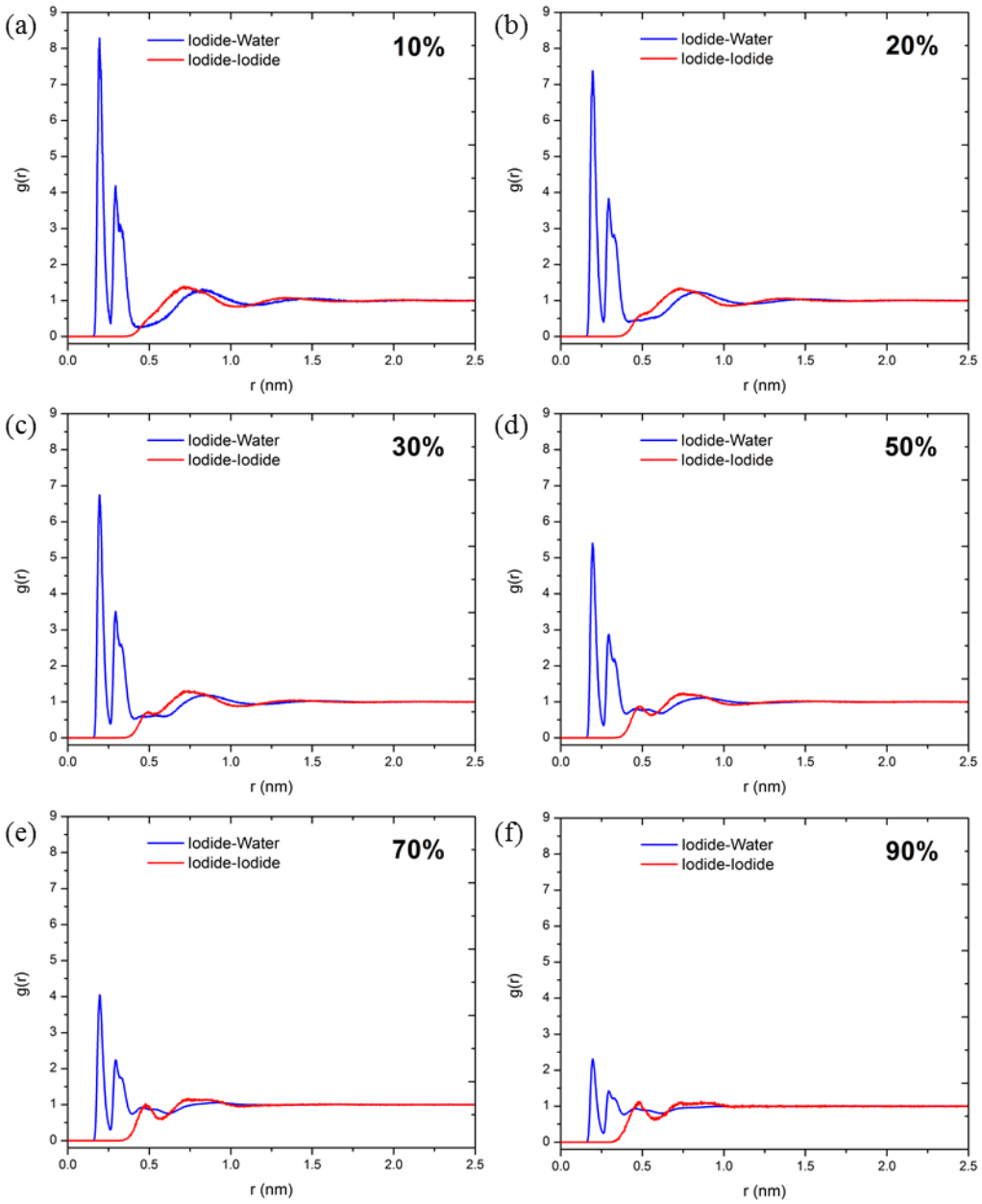

Figure A7 Radial distribution functions of iodide and water around the iodide anion.

Finally, in order to examine the dynamics of the MD simulation systems, self-diffusion coefficients were calculated for the cation, anion, and water. These are shown in Figure A8.

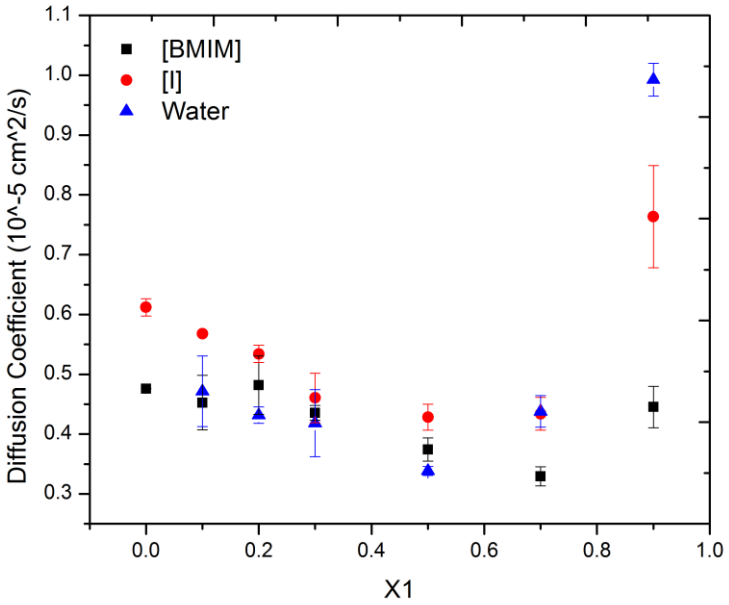

Figure A8 Self-diffusion coefficients versus mole fraction water (X_1).

In the 0-50% water region, increased water concentration decreases the mobility of all species (though the diffusion coefficient of BMIM does rise slightly at $X_1 = 0.2$). Like the melting points shown in Figure A1, this is the opposite of the expected trend. At higher water concentrations, the diffusion coefficient for BMIM dips even lower before rising to a value slightly below that for pure [BMIM][I]. The diffusion coefficients for water and iodide, on the other hand, rise as water aggregates into a bulk phase, allowing for high mobility. At 90% water, iodide anions move much more freely than the cations they are paired with as they are pulled along by their strong attraction to water. This complements the experimental measurement of ionic conductivity, which found that

increasing amounts of water dramatically increased conductivity, particular at concentrations greater than 50%.

CONCLUSIONS

Density, melting point, viscosity, and ionic conductivity were measured for [BMIM][I]/water mixtures with various concentrations of water. Density was found to change little at water concentrations below 50 mol. %, but drop dramatically with additional water at concentrations above 50%. Melting point was found to increase with the addition of any water (compared to pure [BMIM][I]) but to decrease slightly with more water up to 50%, after which it increases rapidly. Viscosity was found to decrease exponentially with added water, while conductivity (a related property) was found to increase exponentially. Viscosity deviation was calculated and found to be negative and to skew toward lower water compositions. This indicates that the interactions between [BMIM][I] and water were disproportionately strong at small water concentrations.

Molecular dynamics simulations showed ordering within the IL/water mixtures. At low concentrations, water molecules were found to insert themselves into the ordered cation/anion structure. However, at 50 mol% water this complicated ordering began to break down until, at high concentrations of water, the mixtures resemble water with regions of [BMIM][I] dissolved within. This distinction—between low and high water concentration regions – may explain the observed trends in density and melting point of these mixtures. Hydrogen bonding between water and iodide were found to be strong and important for understanding mixture behavior, particularly the dramatic increase in conductivity at higher water concentrations.

This paper is the first systematic study of [BMIM][I]/water mixtures, either experimentally or through simulations. It begins the work of understanding these mixtures so that they may be better tuned for future applications.